STUDY OF

3D AUXETIC TEXTILE REINFORCED COMPOSITES

ZHOU LIN

M.Phil

The Hong Kong Polytechnic University

2018

THE HONG KONG POLYTECHNIC UNIVERSITY
INSTITUTE OF TEXTILES AND CLOTHING

STUDY OF

3D AUXETIC TEXTILE REINFORCED

COMPOSITES

ZHOU LIN

A thesis submitted in partial fulfillment of the requirements for

the degree of Master of Philosophy

August 2017

CERTIFICATE OF ORIGINALITY

I hereby declare that this thesis is my own work and that, to the best of my knowledge and belief, it reproduces no material previously published or written, nor material that has been accepted for the award of any other degree or diploma, except where due acknowledgement has been made in the text.

______________________ (Signed)

______ZHOU Lin______ (Name of student)

ABSTRACT

Auxetic materials are a novel type of materials with negative Poisson's ratio (NPR), which explore a new direction to improve mechanical properties and mechanisms of materials. Due to their unique performance, auxetic materials have shown enormous suitable applications in various industries. Auxetic composites are an important category of auxetic materials, which have been proven to have many enhanced properties compared with non-auxetic composites, such as enhanced impact resistance, increased energy absorption ability and improved mechanical indentation resistance. These properties have led to many interesting applications of auxetic composites including protective protection, aerospace industry and biomedical area. Although the auxetic laminates have been designed and developed in recent years, some limitations and gaps still exist. The concept of auxetic effect in composites is only studied in two-dimensional space. In addition, the developed 3D auxetic textile structure for composites reinforcement is still at a primary stage and has not further produced composites. So far systematic manufacture and investigations on the 3D auxetic textile reinforced composites are still missing.

In this study, a three-dimensional (3D) auxetic textile structure previously developed was used as reinforcement to fabricate auxetic composites with conventional polyurethane (PU) foam. Both the deformation behaviors and mechanical properties of the auxetic composites under compression were analyzed and compared with those of the pure PU foam and non-auxetic composites made with the same materials and

structural parameters but with different yarn arrangement. The results showed that the negative Poisson's ratio of composites could be obtained when suitable yarn arrangement in a 3D textile structure is adopted. The results also showed that the auxetic composites and non-auxetic composites have different mechanical behaviors due to different yarn arrangements in 3D textile structure. While the auxetic composites behave more like damping material with lower compression stress, the non-auxetic composite behaves more like stiffer material with higher compression stress.

A further study on their mechanical properties under low velocity impact is presented. Both single-time and repeating impact tests were conducted under different impact energy levels ranging from 12.7 J to 25.5 J. Results showed that the 3D auxetic textile composite has better impact protective performance than the 3D non-auxetic textile composite because of better transmitted force reduction and higher energy absorption capacity under single-time impact and higher structural stability under repeating impacts. Moreover, the stress hardening effect under impact was observed for the auxetic composite, which could enhance its impact protection properties with increasing of impact velocity.

This study systematically investigated 3D auxetic textile reinforced composite. The results of this study deepen the understanding of 3D auxetic textile reinforced composites against with non-auxetic ones under compression and impact loading, which will assist in the development of applications for 3D auxetic textile composites. This work has shown further potential applications for auxetic composites to be applied under low-velocity impact. In summary, this study brings a deeper understanding of 3D auxetic textile reinforced composites based on the previous study and provides a guidance for making 3D auxetic composites using non-auxetic materials. Overall, it is expected that this study could pave a way to the development of innovative 3D auxetic textile composites for different potential applications such as impact protection.

LIST OF PUBLICATIONS

Journal paper

1. **Lin Zhou**, Lili Jiang, Hong Hu, Auxetic composites made of 3D textile structure and polyurethane foam, Physica status solidi (b), 253(7), 1331-1341.
2. **Lin Zhou**, Jifang Zeng, Lili Jiang, Hong Hu, Low Velocity Impact Properties of 3D Auxetic Textile Composite, Journal of Material Science, submitted.
3. Jifang Zeng, Hong Hu, **Lin Zhou**, A study on negative Poisson's ratio effect of 3D auxetic orthogonal textile composites under compression, Smart Materials and Structures 26.6 (2017): 065014.

Conference

1. **Lin Zhou,** Hong Hu, Composite Made of 3D Auxetic Textile Structure and PU Foam, Auxetics 2015, 14-17 Sept. 2015, Malta, invited talk.
2. **Lin Zhou**, Hong Hu, A Study of 3D Auxetic Textile Reinforced Composite, The Fiber Society 2017 Spring Conference, 17-19 May 2017, Aachen, Germany
3. Hong Hu, Lili Jiang, **Lin Zhou**, Kun Xu, Three-dimensional textile structural composites with negative Poisson's ratio, 17th European Conference on Composite Materials, 26-30 June, 2016 at Munich, Germany.

ACKNOWLEDGEMENTS

I registered to be a research student two years ago. During this period, I cannot persist until today without supports and assistances from many others. I would like to take this opportunity to express my sincere appreciation.

First, I would like to express my great and sincere appreciation to my Chief supervisor, Prof. Hu Hong, Professor of Institute of Textiles and Clothing, The Hong Kong Polytechnic University. He is not only an excellent supervisor in academic, but also a wonderful supervisor in spirit. I am very thankful for his great patience and tolerance to guide, instruct and support me during my study. Without his advice, guidance and instruction, I will not be brave enough to finish my study.

I also would like to appreciate my friends and my team members Dr. Zeng Jifang, Dr Jiang Lili, Ms Ng Wingsum, who afford me a lot of assistances and friendship. Moreover, I would like to express my special appreciation to my family. Without their encouragement and great support, I could not stick to my study until now.

Finally, the present study is financially supported by the Research Grants Council of Hong Kong Special Administrative Region Government (grant number PolyU 515812), which is gratefully acknowledged.

Thanks so much to all of you!

TABLE OF CONTENTS

LIST OF FIGURES

LIST OF TABLES

CHAPTER 1 INTRODUCTION

1.1 Motivation of the research

Poisson's ratio (PR) is clearly characterized as the negative ratio of the transverse strain to the longitudinal strain on the physical condition of being stretched or compressed. Most conventional materials, which show positive Poisson's ratio (PPR), become thinner when stretched, as shown in Figure 1-1(a). Auxetic materials are seen as a particular type of materials that display negative Poisson's ratio (NPR), which are laterally bulge if extended or contract when compressed [3] , as shown in Figure 1-1(b).

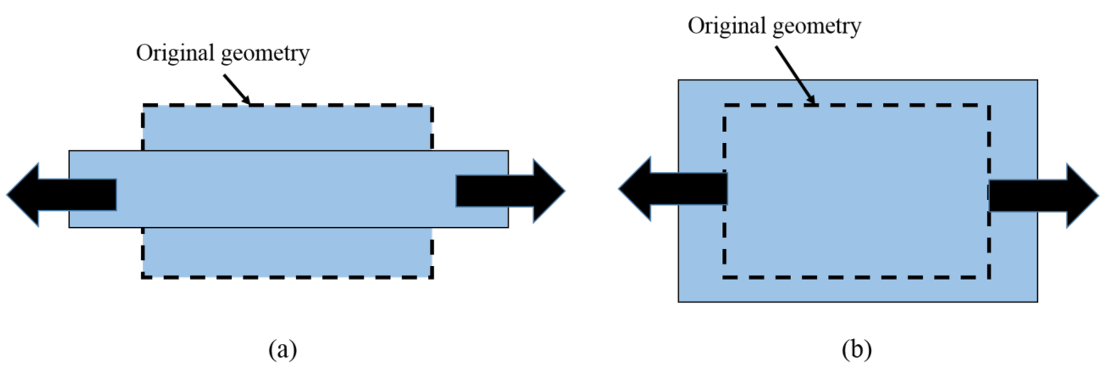

Figure 1- 1 Deformation of material when stretched (a) Conventional; (b) Auxetic

One method of achieving NPR in materials is by using a re-entrant structure [4]. Although Lakes first produced isotropic PU foam materials with a PR value of -0.7 by using a non-auxetic open-cell structure through volumetric compression and heating process in 1987 [5, 6], some theoretical works on NPR had been undertaken before[6, 7]. Since then, more efforts have been made to discover, propose, predict, and develop new auxetic structures and materials based on different material scales. In recent years, auxetic materials continue to gain increasing research interests due to their counter-intuitive behaviors [8]. With such unique behaviors, auxetic materials have been shown to provide some remarkable benefits, including fracture toughness, synclastic curvature, enhanced energy absorption ability, and indentation resistance, which make them considerably outperform non-auxetic materials with various potential applications [9, 10].

Presently, there are mainly two methods for fabricating auxetic composites, either from conventional components via specially designed configurations [11-13] or from auxetic components [14]. The conventional manufacturing method is to utilize unidirectional planes of carbon fiber reinforced epoxy well-stacked in specific sequences [15] exhibiting in-plane [16] or out of plane NPRs [12, 17]. A further method of fabricating auxetic composites is to make an auxetic structure by using non-auxetic fibers. In 1992, Evans et al. [18] successfully modelled auxetic effect in network-embedded composites. Alderson et al. [1] proposed that utilizing auxetic fibers as reinforced component exhibit better mechanical properties than other auxetic composites, because enhancing the interface strength of the matrix and fibers enables composites to bear more than twice the maximum load. Miller et al.[19] reported the fabrication of auxetic composites by making use of woven auxetic fabrics manufactured from auxetic yarns. Recently, auxetic textile structures have also been developed for composite reinforcement. One of the examples is a 3D auxetic textile structure developed by Ge and Hu et al.[20-22] from 3D woven fabric structure by reducing warp yarns in one aspect of the fabric structure in a regular manner. This innovative 3D auxetic textile structure has similar mechanism to the nodule fibril mechanism used to explain auxetic effect in microporous polymers studied by Alderson et al. [23]. Both types of structures could result in strain-dependent PPR and NPR when compressed. By removing the stitching yarn in the textile structure invented by Ge and Hu et al., Jiang, Hu et al. [24] recently proposed a new process to fabricate auxetic composite using multilayer orthogonal auxetic structures with ABS tubes as inner reinforced component and polyurethane (PU) foam as matrix. Based on the results, it is found that the auxetic composites easily exhibited NPR under static compression test. However, as the stitch yarns were not applied to the inner auxetic textile structures, the delamination of composite structure may happen under impact load.

Although some auxetic composites have been developed, some problems still exist: first, most of auxetic textile structures for composite reinforcement are only studied in a two-dimensional space and the concept of auxetic effect is hardly used in three-dimensional space. Second, although the previous research work by Ge and Hu is related to 3D auxetic textile structure [20, 21, 25] for composite reinforcement and the technique proposed by them is innovative, the development is still at a primary stage and has not put into real application for manufacturing 3D auxetic textile reinforced composites. Moreover, the developed 3D auxetic textile structure is relatively unstable and cannot be repeatedly used. Third, a competent auxetic composites should be able to produce auxetic effect of inner textile structure; should be recyclable with dimensional stability. In this regard, a novel type of auxetic composites using 3D auxetic textile structure as reinforcement and conventional PU foam as matrix need to be developed and manufactured. Then the composites need to be investigated and tested under quasi-static compression and impact loading to assess their deformation behaviors and mechanical properties. It is expected that this study could pave a way to the development of innovative 3D auxetic textile composites for different potential applications such as impact protection.

1.2 Objectives

The study aims at a systematic research related to the design, fabrication and evaluation of 3D auxetic textile composites with the following specific objectives:

(1) To design 3D auxetic reinforced textile structures by studying the existing 3D auxetic structures in depth.

(2) To fabricate 3D textile reinforced auxetic composites by using polyurethane foams as matrix.

(3) To carry out quasi-static compression experiments in order to determine negative Poison's ratio effect and effect of boundary conditions on auxetic effect of 3D textile reinforced auxetic composites.

(4) To carry out impact tests to investigate the impact compressive behaviors of the 3D textile reinforced auxetic composites.

With the successful completion of this study, a 3D auxetic textile reinforced composite with stable auxetic effect can be developed and investigated, and the principle of 3D auxetic textile reinforced composite can be revealed. It is helpful to guide the design, production of 3D auxetic textile reinforced composite with desired auxetic effect for specific application.

1.3 Methodology

The main aim of this study is to develop a novel 3D textile structure and fabrication methods for producing 3D auxetic composites, to discover the parameters which affect NPR of auxetic materials under quasi-static compression experiment, and to investigate the performance under impact tests. The research methodology adopted to achieve the purposes of this study is explained briefly as follows:

(1) Design and fabricate 3D auxetic textile reinforced structures.

The 3D textile reinforced auxetic structures will be designed and fabricated by using a novel prototype which had been specially proposed at the ITC, The Hong Kong Polytechnic University. The work in this stage includes selecting the appropriate yarns in three directions of the 3D auxetic textile structure. The warp yarns used are braided ropes, and the weft yarns are made of cotton. The stitch polyester yarns are used for binding the warp yarns and weft yarns together, which will make the textile structure more stable.

(2) Fabricate 3D textile reinforced auxetic composites by using customized molds.

Both auxetic and conventional composites were fabricated using the 3D textile structures above fabricated as reinforced components and PU foam as matrix through a filling and foaming procedure.

(3) Carry out quasi-static compression experiments.

The pure PU foam and composites with NPR and PPR above produced were subjected to static compression tests with the use of a high-resolution camera to capture photograph in order to assess their deformation behaviors and mechanical properties. Thus, PR-deformation curves are generated. Experimental data in the form of force-displacement signals were recorded and transferred to a computer for post-processing for illustrating stress-strain curves.

(4) Carry out dynamic impact experiments

For the dynamic impact tests, we used a low-velocity impact tester to evaluate the energy absorption ability of produced auxetic and non-auxetic composites. It is expected that the impact test could help us to better understand the impact properties of the auxetic textile composites in order to promote their application for impact protection.

1.4 Significance and Value

First, this study will bring advancement in 3D auxetic textile reinforced composites, through analysing their deformation behaviors and compression properties. Based on previous research work, we will combine the 3D auxetic textile structures with conventional PU foams, which will provide a deep understanding of the properties of 3D auxetic textile reinforced composites and may overcome the limitations of the inner textile structures.

Plus, we will investigate the structural parameters, including the diameters of warp yarns, the density arrangement of weft yarns and the proportion of PU foams, which may affect the compression behaviors of 3D auxetic textile reinforced composites. In addition, the factors, which possibly affect auxetic effects, will be highlighted so that we can achieve the optimum auxetic effects for textile based on composite applications in the future.

1.5 Thesis Outline

This report includes five chapters:

Chapter 1 introduces the background knowledge of the topic and then gives the objectives of this research project. Its significances and values are pointed out.

Chapter 2 reviews the previous research works to have deeper understanding of the auxetic composites and structures. The research gaps of the previous works are discovered and described.

Chapter 3 introduces design and manufacture of 3D auxetic and non-auxetic structures. The fabrication processes of auxetic and non-auxetic composites are also included. Chapter 3 also summarizes the produced samples prepared for the quasi-static compression tests.

Chapter 4 describes an experimental research work of the deformation behaviors and the compression properties of the pure PU foams, 3D auxetic and non-auxetic textile composites. Moreover, the experiment conditions setting of static state compression test and repeated compression test are also introduced in this chapter respectively. Chapter 4 investigates the compression test results by analysing the deformation behaviors and compression behaviors of produced samples and making comparisons between pure PU foams, 3D auxetic and non-auxetic composites.

Chapter 5 presents the mechanical properties under low velocity impact of produced 3D auxetic and non-auxetic textile composites. Both single-time and repeating impact tests were conducted under different impact energy ranging from 12.7J to 25.5J.

Chapter 6 concludes the research findings, conclusions, and recommendations for future work.

CHAPTER 2 LITERATURE REVIEW

2.1 Introduction

Chapter 2 lays a foundation for deeply understanding auxetic materials, structures and their related properties and applications, as well as providing a rationale for the choice of 3D auxetic composites in the present study. The chapter initially outlines the auxetic materials, followed by a discussion on their properties and applications. Secondly, the auxetic geometric structures are reviewed. After that, the previous works on 3D textile structures and auxetic composites are studied, specifically those related to auxetic foams and composites. Lastly, the research gaps of this study are found.

2.2 Auxetic Cellular Structures

To date, auxetic materials could be classified by deformation mechanism or microstructure [26], including re-entrant structures, rotating units, nodule and fibril structure and so on. This section provides background and knowledge for evaluating and explaining auxetic behaviors. All the micromechanical models exhibit auxetic effect.

2.2.1 Re-entrant Structure

2.2.1.1 2D Re-entrant Structure

Re-entrant structure is one of the basic structures having NPR. It rises from the combination of geometric feature in the microstructure of auxetic materials and the deformation mechanism. Figure 2-1 shows the traditional re-entrant structure. It deformed by hinging of the ribs under tensile along horizontal direction, causing the ribs in another direction to bugle, resulting in auxetic effect [27]. In early 1980s, Gibson et.al [28] proposed the earliest 2D cellular re-entrant honeycomb structure which deformed by flexure of the ribs. Then, Evans et al.[3] proposed auxetic reflexyne molecular networks that were designed to mimic the 2D dove-shaped re-entrant unit, as illustrated in Figure 2-2. Followed by Masters and Evans [29] who identified three deformation mechanisms of honeycombs, namely flexure, hinging and stretching of the ribs. When subjected to external loading, the ribs move apart and the whole structure bulges in the other direction, imparting auxetic behaviors. Theocaris et al.[30] reported a star-shaped honeycomb and numerically analyzed NPR in composite with star-shaped inclusions, as shown in Figure 2-3.

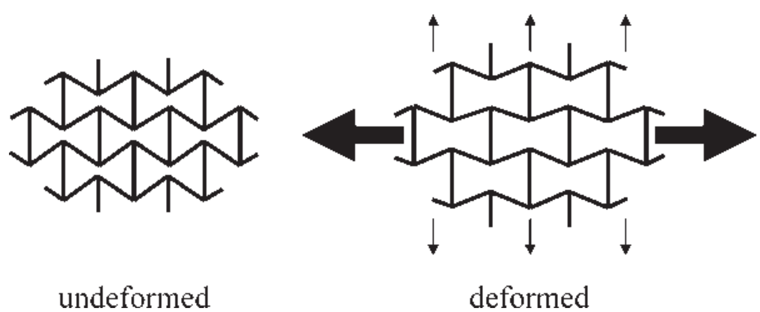

Figure 2- 1 Deformation of re-entrant hexagonal honeycomb [27]

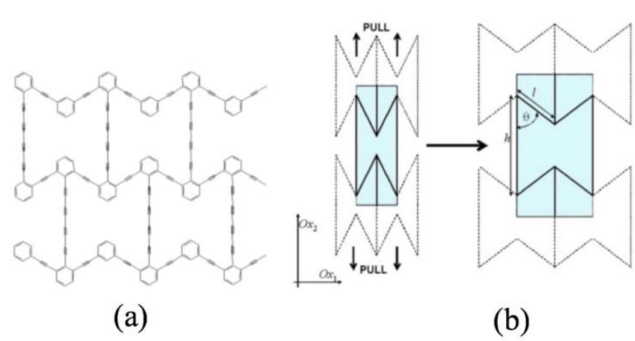

Figure 2- 2 (a) Auxetic reflexyne molecular system; (b) The idealized re-entrant structure [3, 31]

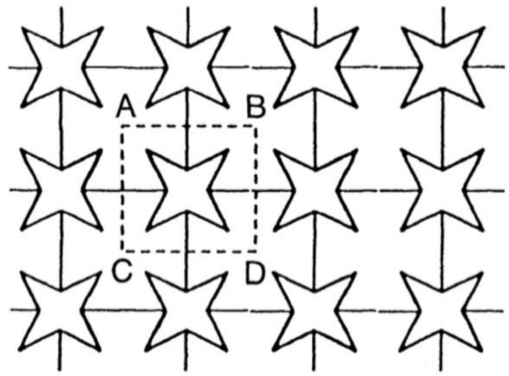

Figure 2- 3 Microstructure of star honeycomb [30]

Subramani et al. [32] developed a novel kind of auxetic structures in macro scales and evaluated their mechanism properties. The developed auxetic structures that are based on re-entrant hexagon exhibit NPR with maximum value of -9. There are two factors found to affect auxetic behaviors: structural angle and straight elements. Among different fibers evaluated by the researchers, carbon based auxetic structures are found to have the highest work of rupture, and then is basalt followed by glass. The results also show that the composite material can be beneficial for civil engineering applications.

2.2.1.2 3D Re-entrant Structure

In recent years, more research works emphasis on extension of 2D auxetic models towards 3D models. Development of 3D re-entrant structure was started with Almgren's analysis of 3D isotropic structure (Figure 2-4) deforming from rods, hinges, and springs which maintains its aspect ratios in 3D, exhibiting NPR ν=-1[6]. Then auxetic foams with NPR -0.7 were developed [5] in which auxetic effect was achieved by volumetric compression on conventional foams, resulting in micro-buckling of the cell ribs. Another early attempts on 3D re-entrant structure has been proposed by Wei [33]. Wei theoretically evaluated effective PRs of polymeric networks with special microstructures. Researchers took into account two critical deformation mechanisms, that is, stretching and bending. Chan et al.[34] manufactured auxetic foams by using a re-entrant cell structure because some features of re-entrant structure could be controlled by processing techniques such as cell shapes. The re-entrant model is described in Figure 2-5(a).

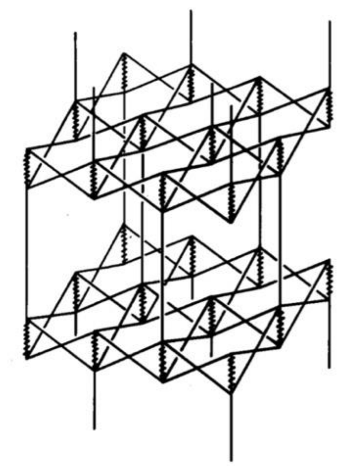

Figure 2- 4 Three-dimensional structures with ν= -1[6]

Inspired by the previous analytical results, Rad et al. [35] proposed a more complicated re-entrant structure by using brick element. Figure 2-5(b) and (c) show the developed 3D re-entrant structure. In addition, Rad et al. [35] also developed and analyzed the 3D versions of 2D re-entrant structure, consisting of six elastic beams. The 3D re-entrant structures are obtained by aligning the two 2D re-entrant structures perpendicular to each other, as illustrated in Figure 2-6.

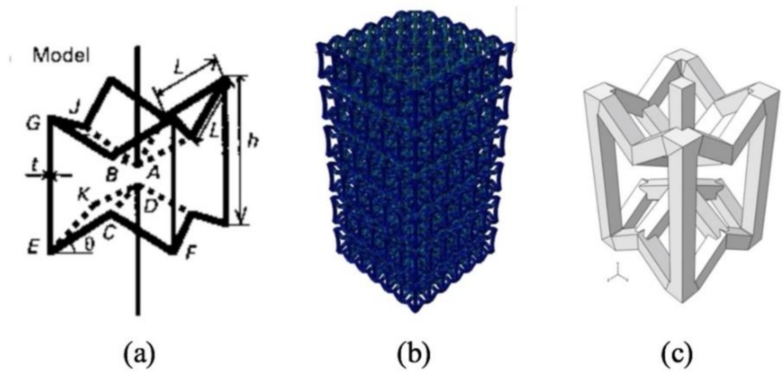

Figure 2- 5 3D re-entrant structure (a) The model [34]; (b) The structure; (c) The unit cell [35]

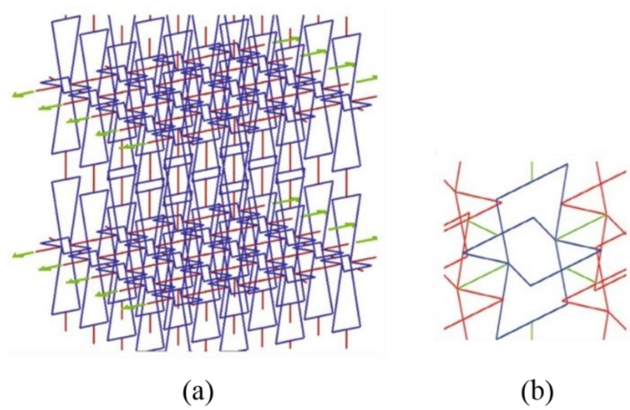

Figure 2- 6 (a) The microstructure; (b) The unit cell of 3D re-entrant structure [35]

Yang et al.[36-38] modeled a 3D auxetic re-entrant honeycomb structure in all three orthogonal directions, as illustrated in Figure 2-7. Experimental studies were conducted with Ti6Al4V samples fabricated by the electron beam melting process and compared with theoretical modeling. The lowest recorded NPR value could reach -0.57.

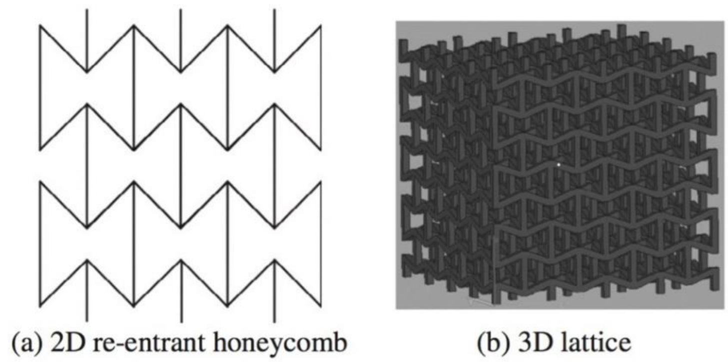

Figure 2- 7 3D re-entrant honeycomb structure with auxetic effect [36, 37]

2.2.2 Rotating Structure

2.2.2.1 2D Rotating Structure

The auxetic behaviors of the rotating structures was analysed and developed with 2D models including rotating rectangles [31, 39], the triangles [40] and semi-rigid [41]. Grima et al. [40, 42] presented new auxetic rotating geometries based on an arrangement involving rigid squares or equilateral triangular cells connected through simple hinges. Auxetic behaviors arises from rotation of connected squares and triangles, as illustrated in Figure 2-8. Several factors affect PR including the aspect ratio of triangles or rectangles, angles, and loading directions [39]. These kinds of structures result in in-plane analytical NPR value of -1[43]. Grima et al.[42] developed more general structures on the ‘rotating squares’ geometry (Figure 2-9), like hinging parallelograms and structures built with different sized units.

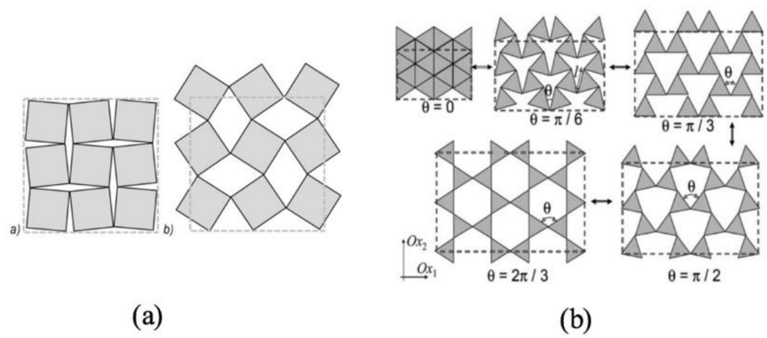

Figure 2- 8 (a) ‘Rotating squares’ auxetic structures; (b) ‘Rotating triangle’ auxetic structure [40, 42]

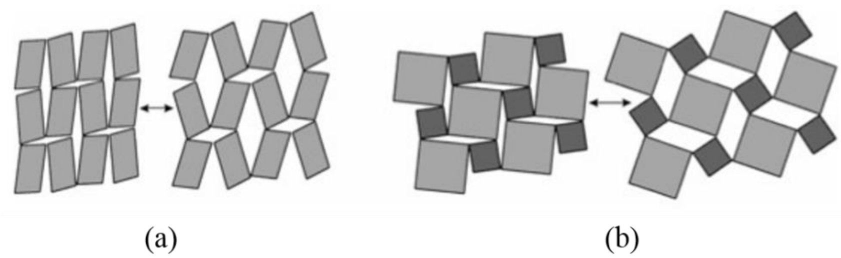

Figure 2- 9 Variation on the ‘rotating square’ geometry: (a) A more general rotating parallelogram auxetic structure; (b) A ‘rotating square’ built from different sized units [42]

2.2.2.2 3D Rotating Structure

Alderson et al. [44, 45] developed a 3D tetrahedral framework structures which was extended from the 2D rotating squares and triangles structures developed by Grima and Evans [40, 42], as shown in Figure 2-10. The auxetic behaviors of this 3D network is observed because of ‘rotation (RTM)’, ‘dilatation (DTM)’, and ‘concurrent rotation and dilatation (CTM)’, with all ν= -1. The strain-dependent positive and NPR are possible in the CTM which combines the RTM and the DTM. This 3D model was proposed to better evaluate deformation mechanism of α-cristobalite [46], a NPR form of silicon dioxide.

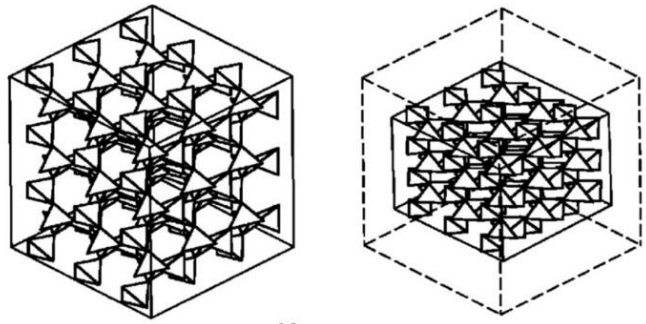

Figure 2- 10 Tetrahedral rotation deformation mechanism: fully-expanded and fully-densified [44]

Bückmann et al.[47] presented a dilational 3D cubic auxetic structure based on 2D rotating rigid unit with an ultimate PR value of -1. As shown in Figure 2-11, the cell consists of a checkboard arrangement of a motif made of squares and triangles. Researchers studied the 3D structure numerically and the sample was produced by 3D printing technology.

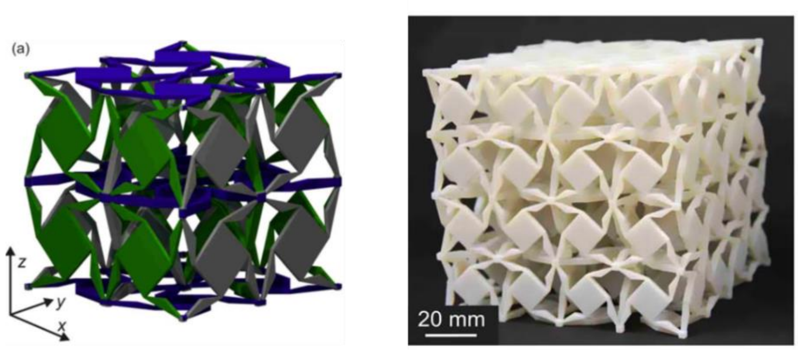

(a) (b)

Figure 2- 11 (a) Unit cell of 3D dilational metamaterial (b) Prototype made by 3D printer[47]

2.2.3 Chiral Structure

2.2.3.1 2D Chiral Structure

In recent years, chiral structures have been developed for auxetic honeycomb. Prall and

Lakes [48] theoretically and experimentally tested and evaluated 2D chiral honeycomb which displays NPR of -1 for deformations in-plane, essentially independent of strain. The deformation of the 2D chiral structure is illustrated in Figure 2-12. The ligaments coil around the circular nodes when undeformed. And the NPR of the structure generates by unwrapping the ligaments under compression.

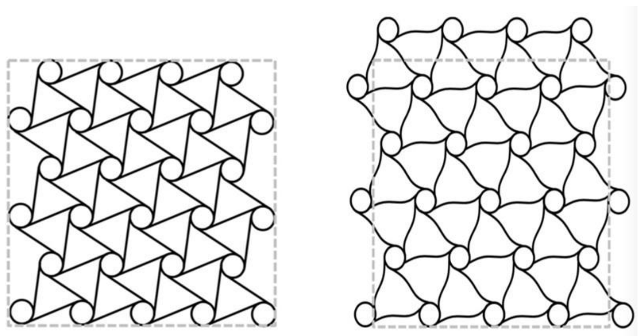

(a) (b)

Figure 2- 12 2D chiral honeycomb structure: (a) Undeformed and (b) Deformed [49]

In the last decade, the hexagonal chiral system has attracted considerable attention. Wojciechowski [50] has presented a concept of hexamer structure. Due to lack of the mirror symmetry of the structure, the auxetic phase of hexamer structure is chiral, as illustrated in Figure 2-13. Later, Grima et al. [51] have developed a 'meta-chiral' system having six, four and three ribs attached to each node. As shown in Figure 2-14, this structure is deformed by connecting the symmetric blocks in which the node in each chiral building bloc is in shape of rectangle[8]. The structures exhibit both positive and NPRs which can diverge to extremely large magnitudes. Spadoni et al.[52, 53] designed a 2D structural lattice with an in-plane NPR, known as chiral lattice. The developed NPR structure involves rings linked with tangent ligaments. The researchers evaluated the photonic properties and elasto-static micropolar behaviors. Pozniak and

Wojciechowski [54] developed a novel kind of anti-chiral structure which contains rotating hexamers and trimers (Figure 2-15) and investigated its influence of structural disorder with rectangular symmetry on their PR. The lowest auxetic values of ν_{xy} could reach -2.3.

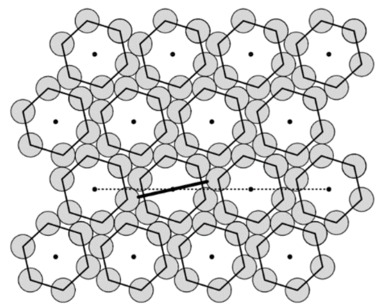

Figure 2- 13 Geometry of hard cyclic hexamers structure [50]

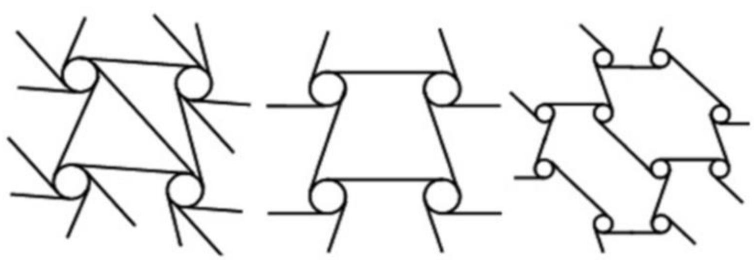

(a) (b) (c)

Figure 2- 14 Meta-chiral systems having (a) Six; (b) Four; (c) Three ribs attached to each node [51]

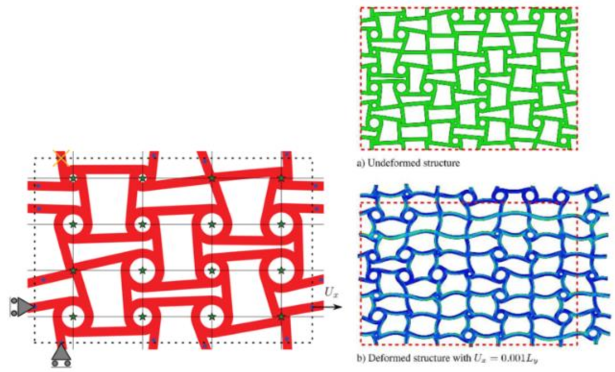

Figure 2- 15 Anti-chiral structure (a) Unit cell; (b) Deformation (stretched along x axis) [54]

2.2.3.2 3D Chiral Structure

Ha et al.[55] recently developed a 3D chiral structure consisting of rigid cubical nodules and multiple deformable ribs, as illustrated in Figure 2-16. The lattices show geometry dependent PR that could be tuned to negative. The designed 3D chiral structure also exhibits PR that tends to zero when relative rib slenderness increases. In addition, Lu et al.[56] presented two novel 3D cross auxetic chiral structures (structure 1 and structure 2) , as presented in Figure 2-17. It can be found that structure 1 can be evolved into structure 2 by adding a star structure. Compared to structure 1, structure 2 can help significantly improve the Young's modulus. All the NPR value can be designed up to -1. The presented structures have potential applications as auxetic matrix for composites.

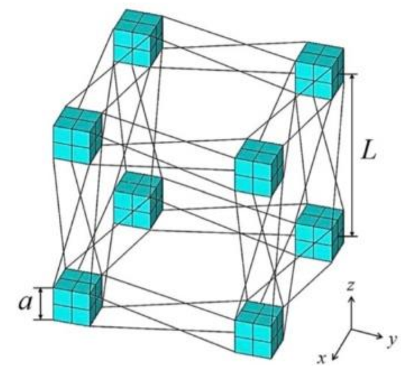

Figure 2- 16 The developed 3D chiral lattice structure [55]

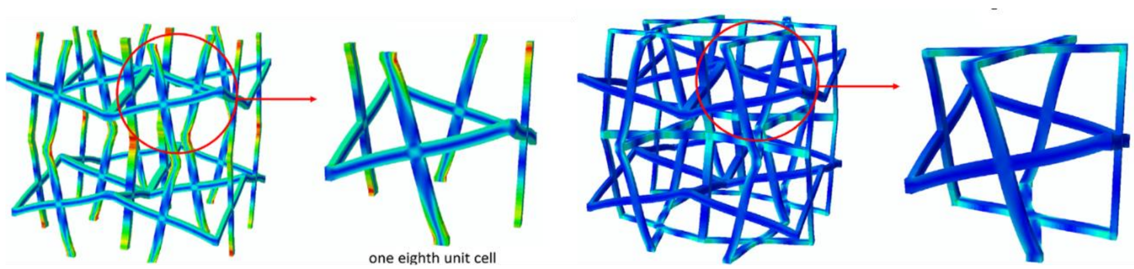

Figure 2- 17 3D view and unite cell of (a) structure 1; (b) structure 2 [56]

2.2.4 Nodule Fibril Structure

2.2.4.1 2D Nodule Fibril Structure

Geometric node-fibril (NF) model has been developed by Alderson and Evans [23]. As shown in Figure 2-18, NF structure is deformed by hinging of the fibrils when applied load and can lead to NPR, depending on geometry of the structure [23, 57]. Alderson have proposed to explain how the microstructure of auxetic material reacts to indention by using of NF geometric models. And it takes place by the local densification of the nodules caused by the fibrils under indenter and by the closing up of the pores in the materials [58]. Lim and Acharya [59] developed a hexangular series of four-fold interrelated hexagonal nodules that is similar to sphere-like nodules for the performance evaluation and prediction of PP films and fibers. The researchers also found that for the hexagonal NF models, the ones in 3D form exhibited a lower NPR than the equivalent 2D ones.

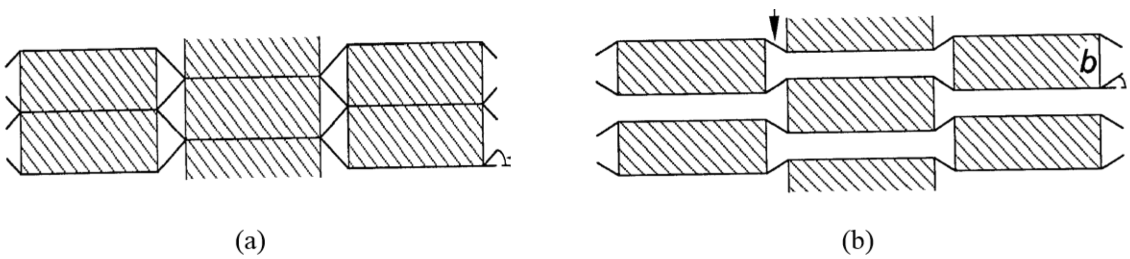

Figure 2- 18 NF model structure (a) undeformed; (b) deformed [23]

2.2.4.2 3D Nodule Fibril Structure

The 2D NF microstructures was developed into 3D models by Gaspar [60], as shown in Figure 2-19. The 3D structure containing corner-linked cubical is based on 2D corresponding fibril hinging and stretching model which can be applied to microporous expanded polymers including 'e-PTFE', 'e-UHMWPE', porous materials with body-centered cubic foams.

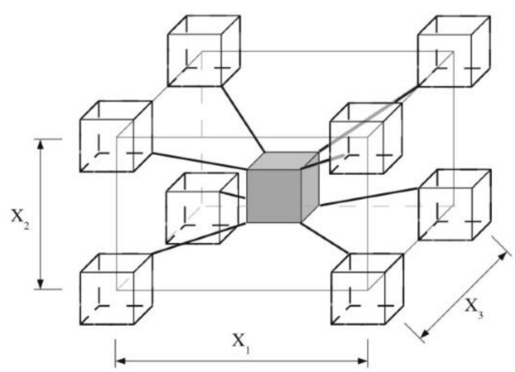

Figure 2- 19 The microstructures of 3D nodule fibril structures [60]

2.2.5 Double Arrowhead Structures

2.2.5.1 2D Double Arrowhead Structures

Based on mechanics of re-entrant structures, arrow-head honeycomb was presented by Larsen et al. [61], as shown in Figure 2-20(a). The structures will collapse and contract in vertical direction when compressed, exhibiting NPR effect. The achieved NPR material (Figure 2-20(b)) was fabricated by silicon surface micromachining in thin-film materials.

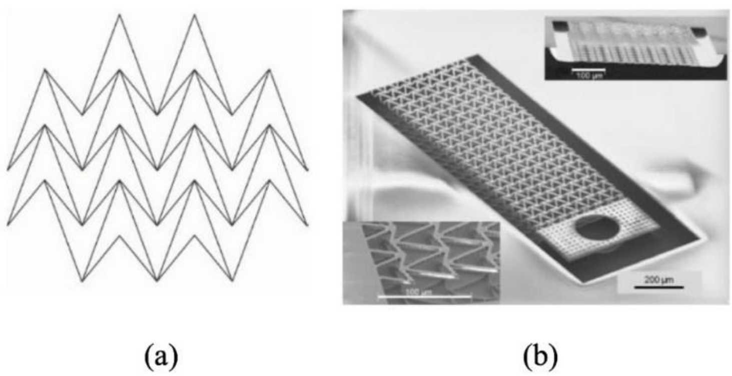

Figure 2- 20 (a) Double arrow-head structure; (b) Fabricated NPR material [61]

2.2.5.2 3D Double Arrowhead Structures

Ma et al. [62] developed an innovative 3D auxetic double arrowhead structural material for army application. Figure 2-21(a) illustrates the 3D NPR double arrowhead structure. The effective NPR of designed structure achieved is as low as -77 by controlling the two design variables (at θ_1 =40°and θ_2=50°). The 3D NPR structure could be made into prototype by using stainless steel, as presented in Figure 2-21(b). Moreover, Zhang et al. [63] studied the nonlinear compressive response and deformation of 3D double arrowhead structure theoretically and experimentally. Figure 2-22 shows the 3D view and deformation of produced structure. It is found that the structure with lower relative density of auxetic cell may have better energy absorption ability. The double arrowhead structure with 3*3 unit cell could reach -11.97 effective PR value under quasi-static compression test. Recently, Lim [64] introduced a 3D auxetic linkage structures by developing the double arrowhead honeycomb to an intersecting ones in the out-of-plane direction. It is found that this 3D model can be conveniently tailored by 3D printing and it can control the extent of auxeticity in terms of the relative linkage lengths or half angles. The microstructure of the 3D auxetic intersecting double arrowhead is illustrated in Figure 2-23.

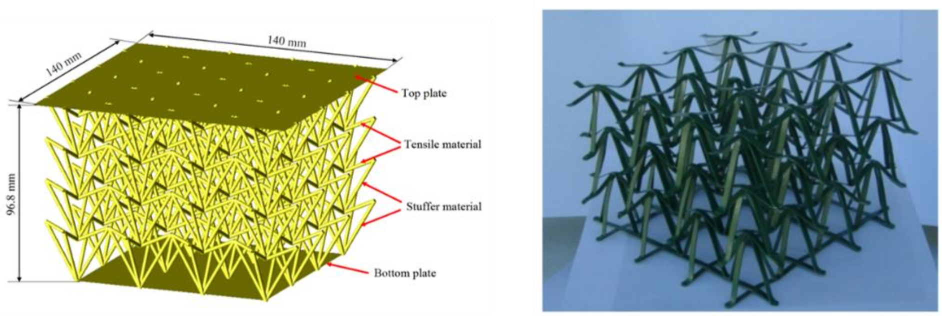

(a) (b)

Figure 2- 21 (a) 3D view of 3D NPR double arrowhead structure; (b) Prototype of 3D NPR material [62]

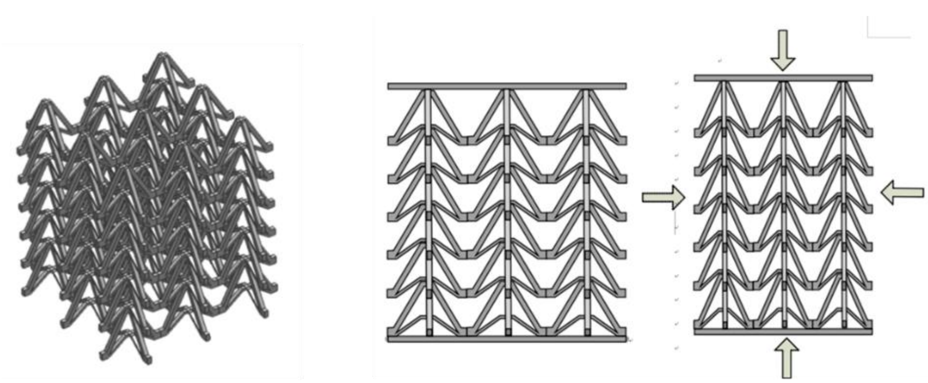

(a) (b)

Figure 2- 22 3D double arrowhead structure (a) 3D view; (b) Deformation

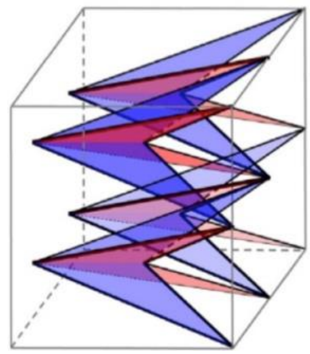

Figure 2- 23 Microstructure of the 3D auxetic intersecting double arrowhead [64]

2.2.6 Other Structures

2.2.6.1 2D Other Structures

Missing rib structure is extended from conventional honeycombs where cutting selective ribs from hexagonal structures without changing internal angles, resulting in auxetic behaviors [65]. Figure 2-24 illustrates the deformation of missing rib structure. And Gaspar et al.[66] experimentally tested two different conventional structure named Sample 1 and 2 and missing rib structures named Sample 3 and 4, as shown in Figure 2-25. Sample 1 and 2 exhibit a PPR, while Sample 3 and 4 demonstrate a NPR. The results show that the PR does not change rapidly with deformation strain, which is similar to the predictions models by Smith et al.[65]. The researchers used microscopic information about the mesh including internal angles and rib length to predict PR and deformation strain. Subramani et al.[67] developed auxetic structures (Figure 2-26) from composite materials and evaluated their mechanical performance, which were used polyester multifilament yarns and produced by vertical braiding machine. The produced auxetic structures showed PPR from -0.3 to -5.2 under tensile testing.

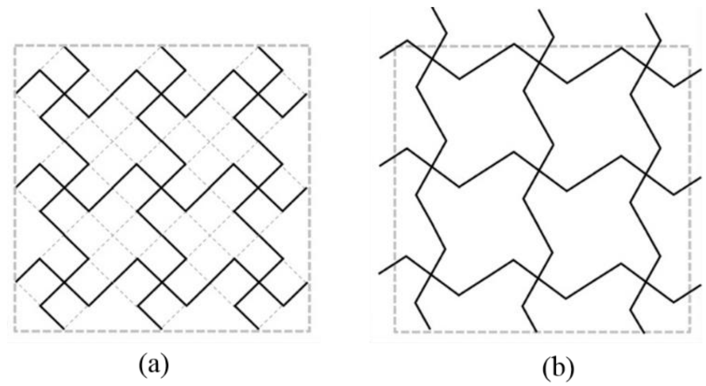

Figure 2- 24 Missing rib structure (a) Undeformed; (b) Deformed [49]

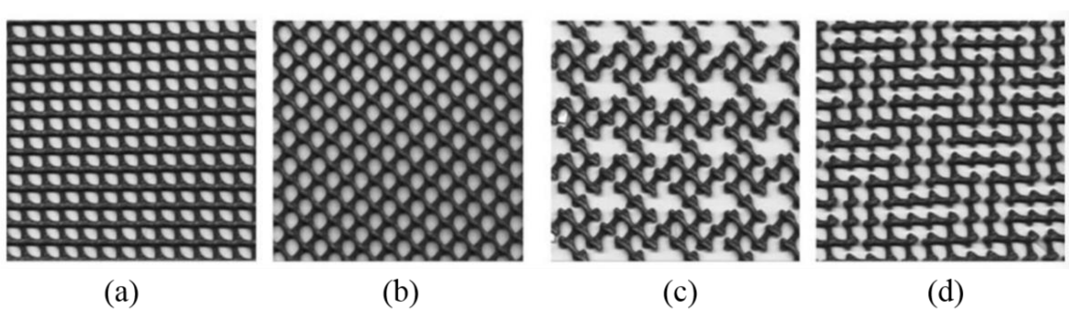

Figure 2- 25 Conventional and missing rib foams (a) and (b) conventional; (c) and (d) auxetic [66]

Figure 2- 26 Developed auxetic structures by Subramani et al. [67]

He and Liu[68, 69] presented a novel kind of site-connectivity driven rod reorientation molecular model, as illustrated in Figure 2-27. Under tensile stress, the inter-chain distance would increase if the laterally attached rods are long enough, which may result in an expansion in the orthogonal direction. The researchers also experimentally evaluated and reported the critical molecular parameters to achieve NPR by the X-ray scattering method [68, 69]. Bertoldi et al.[70-72] proposed a novel kind of 2D auxetic structure that is a series of circular holes in an elastomeric matrix (Figure 2-28). The deformation of the structure is that, when applied uniaxial strain, the geometric reorganization is both reversible and repeatable. Motivated by previous structure, researchers have developed a 3D structure – the 'Buckliball' (Figure 2-29). It has a spherical shell with a range of circular voids laid out orderly. The deformation of the 'Buckliball' undergoes a structural transformation induced by buckling under compression [73].

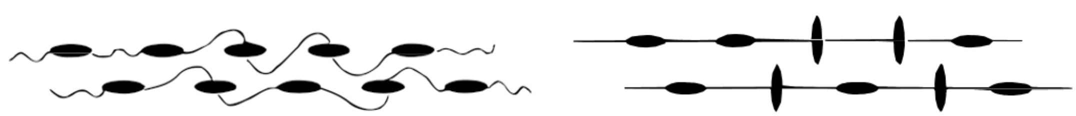

(a) (b)

Figure 2- 27 Site-connectivity driven rod reorientation molecular model (a) Undeformed; (b) Deformed [69]

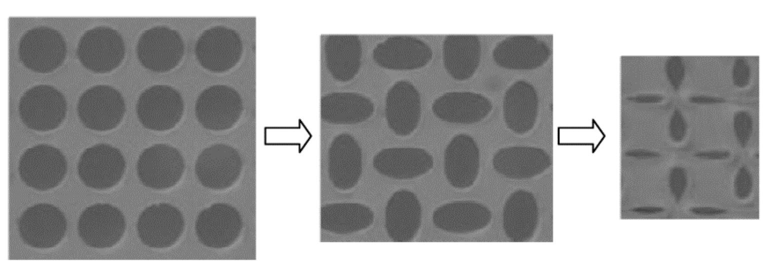

Figure 2- 28 2D circle holes structure under compression [71]

Figure 2- 29 Geometry of Buckliball [73]

2.2.6.2 3D Other Structures

Liu et al. [74] proposed a 3D structure formed with parallelogram planes which are connected edge to edge in a way of zigzag. The NPR of the structure can be achieved by each parallelogram changing its inclined position related to the surface plane, resulting in an opening of the whole structure by expanding its dimensions in each direction when stretched, as illustrated in Figure 2-30.

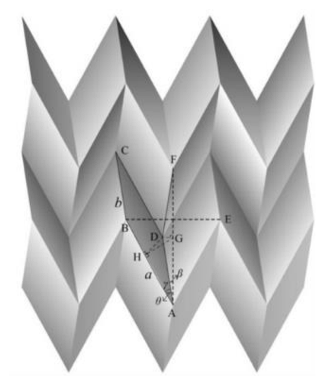

Figure 2- 30 Geometrical structure of 3D parallelogram planes [74]

Schwerdtfeger et al.[75] presented self-designed 3D auxetic structures (Figure 2-31) through selective electron-beam melting (SEBM) technique and determine its mechanical properties by compression testing. The measured NPR on different faces are ranging from -0.2 to -0.4 depending on orientations except the faces resembling a wavy honeycomb structures which shows positive value of ν in the range between 0.45 and 0.5. By using SEBM manufacturing technique, it allows for a high degree of control over the mechanical properties of auxetic cellular geometry.

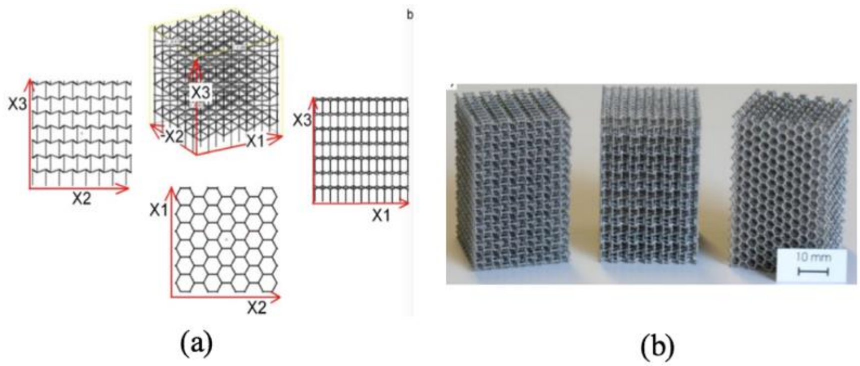

Figure 2- 31 (a) CAD model of 3D auxetic structures; (b) The actual samples (three different directions) [75]

2.3 Auxetic Textile Structures

Presently, 3D textile structures gain increasingly research attention due to their unique and advanced performance. In this section, three types of 3D textile structures are reviewed including 3D woven structures, 3D braided structures and 3D knitted structures. Some 3D advanced auxetic textile structures are also included. Different techniques have been applied to develop auxetic structures including thermal processing, wrapping, knitting, reinforcement arrangements, filling and foaming process [76].

2.3.1 Auxetic Woven Structures

Ge et al. [20-22] developed a 3D auxetic textile structure which is designed to reinforce composite (Figure 2-32). The 3D auxetic textile structure is developed from a kind of 3D woven fabric structure by reducing warp yarns of the textile structure in a regular manner. Under quasi-static compression, the produced 3D auxetic structure can concentrate itself, which makes it suitable for composite reinforcement. The highest

NPR value is -0.16. The researchers found that the ratio between diameters of warp and weft yarns have a significant influence on auxetic effect. It is suggested that high yarn diameter ratio is required for achieving higher auxetic effect.

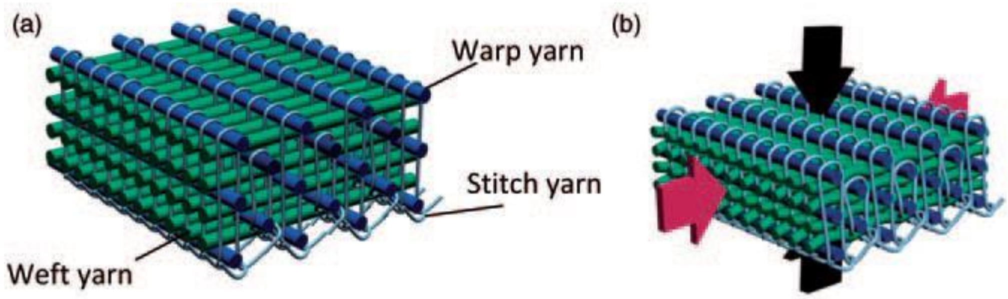

Figure 2- 32 3D NPR textile structure (a) Undeformed; (b) Deformed [20]

Recently, Liaqat et al.[76] proposed a novel 3D auxetic woven structure with improved impact resistance that has a modified four layer through the thickness. Three sets of yarns were interlaced with each other in three dimensions, as shown in Figure 2-33. The fabric was made of plain weave for the four layers, and two binding threads were used for stitching in the fabric thickness direction. The 3D woven fabrics can be used as reinforcement in composite, which will help to gain high impact resistance than conventional composite.

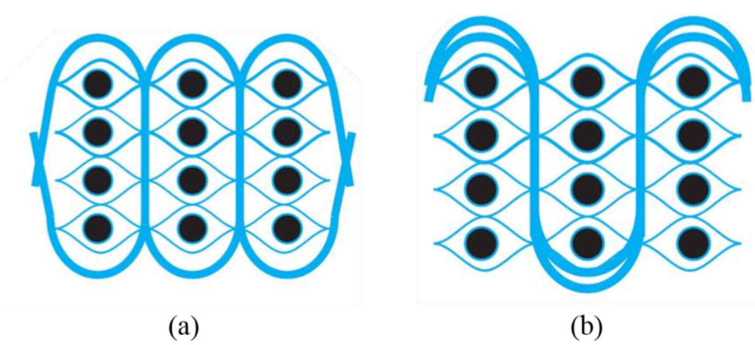

Figure 2- 33 (a) Standard and (b) Modified four layers 3D woven fabric structure [76]

2.3.2 Auxetic Knitted Structures

Knitted fabrics usually produced by either the weft knitting technology or warp knitting process. Knitted fabrics may have a great shape-fitting ability that make them attractive for some applications like protection industry.

Liu and Hu [74] designed the auxetic folded weft-knitted fabrics which were manufactured by flat-knitting technique. From Figure 2-34, the NPR generates from the opening of the folded structures in both orthogonal directions under tension. In addition, the researchers find that the main structural parameter that affecting NPR of the fabric is the opening angle when undeformed. The fabric with a smaller opening angle in its structure will achieve lower PR value.

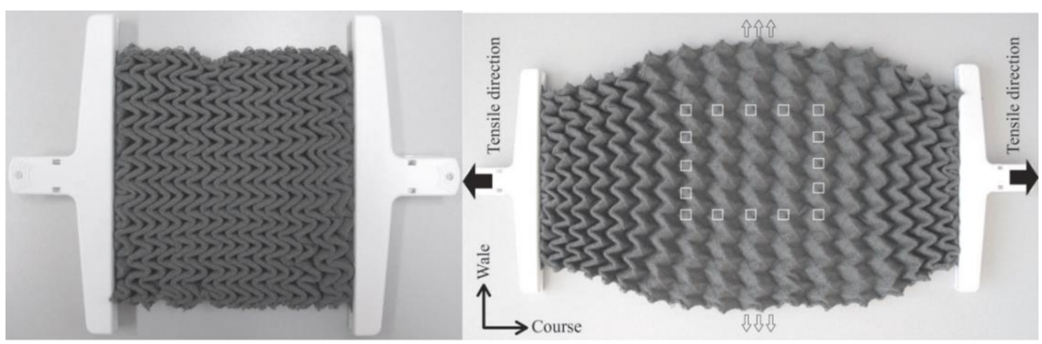

(a) (b)

Figure 2- 34 3D auxetic folded knitted structures (a) Undeformed; (b) Deformed state [74]

Ugbolue et al. [77] designed and analyzed the auxetic and non-auxetic hexagonal knit structures (Figure 2-35). The non-auxetic knitted fabrics with polyester yarn show PPR with average value of 0.54. Moreover, the auxetic knitted fabrics made of polyest ground and inlay Spandex show NPR (average value of -0.21). The researcher also identified the factors that influence PR including yarn type, number of chain courses and strain level. The researchers [78, 79] summarized that yarn type is the most critical factor to determine the PR value.

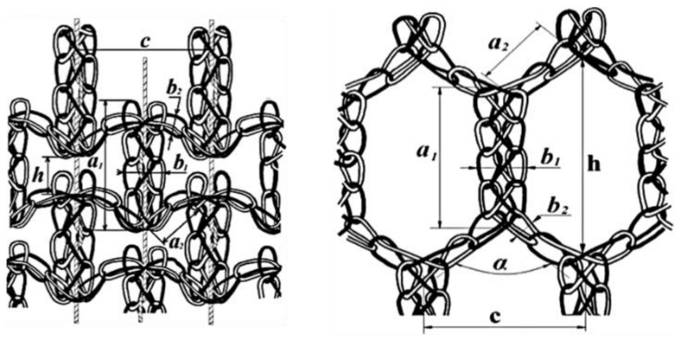

(a) (b)

Figure 2- 35 Knitted structure (a) Auxetic; (b) Non-auxetic [77]

Hu et al.[80] developed auxetic fabric using flat knitting machines based on different geometrical structures including foldable structure, rotating rectangle and reentrant hexagon, as shown in Figure 2-36. As shown in Figure 2-36(a), the fabric was knitted with lamb wool yarn. The NPR achieved only in one principal direction is because of the extension of the folded fabric in the course direction that can result in the expansion of the fabric in the wale direction. The highest NPR value obtained could reach -0.14. As illustrated in Figure 2-36(b), another knitted fabric is the arrangement of the face and reverse loops in horizontal and vertical stripes with mercerized wool yarn. This structure can achieve auxetic effect in course and wale direction with the highest NPR value -0.41 and -0.19 respectively. Figure 2-36(c) shows the knitted fabric with rotating rectangles made by partial knitting and binding-off technique. The fabric only achieves auxetic effect in the course direction with the highest NPR -0.5 measured. As shown in Figure 2-36(d), the knitted fabric consists of re-entrant hexagonal structure with acrylic yarn that achieved the highest NPR value of around -0.6 only in the wale direction. The NPR value vary with the tensile strain for all the above fabrics except the folded fabric of which the auxetic value increases firstly and then declines with the increasing strain. Hu et al.[80] also theoretically analyzed the developed knitted fabric. However, the prediction of auxetic effects was relatively higher than the measured value due to the yarn slippage effect and loop shape deformation.

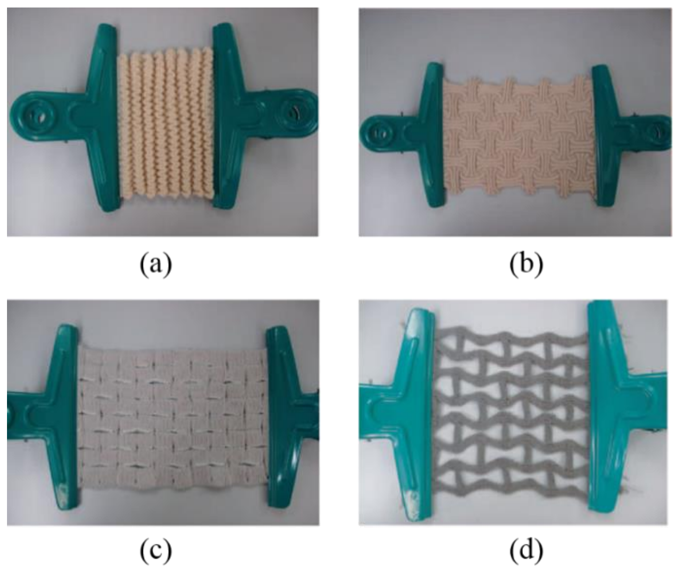

Figure 2- 36 Auxetic fabric formed with (a) Folded structure; (b) The face loops in horizontal and vertical stripes; (c) Rotating structure; (d) Re-entrant hexagonal structure [80]

Wang et al.[81, 82] reported and evaluated the deformation behaviors of a 3D auxetic knitted spacer fabric produced from a wrap-knitted spacer structure generated from a particular geometrical structure with NPR[83], as shown in Figure 2-37. This novel kind of auxetic fabrics exhibit auxetic effect in both orthogonal directions within large deformation strain. It also has great shape-fitting property that makes the fabrics attractive for different potential applications including sports, protection and even fashion industry.

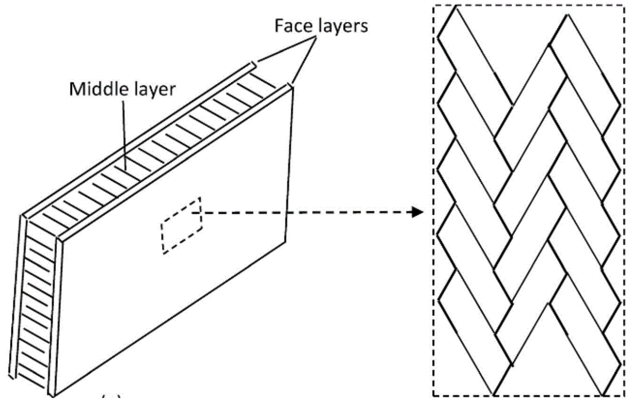

Figure 2- 37 Auxetic spacer fabric and its geometrical structure [81]

2.4 Auxetic Foams

Generally, non-auxetic materials exhibit PPR, becoming thinner when stretched. The opposite effect exists in materials with NPR, known as auxetic materials. Foams materials usually exhibit PPR unless processed by manufacturing methods that gives them auxetic properties. Figure 2-38 shows the idealized unit cell of conventional and auxetic foam. Many researchers have investigated the methods of improving the mechanical properties of conventional foams. In theory, there are mainly two ways, either by changing the chemical properties of the solid struts or by altering the cell geometry [84].

In the late 1980s, Lakes [85] first developed a route to convert conventional polymeric foam with re-entrant cell structure into the 3D auxetic foam through a process involving ‘tri-compression’ and ‘heating’. The NPR value measured was -0.7. Lakes’ work gave the impetus for the interest in auxetic materials. Friis et al. [86] successfully obtained re-entrant auxetic foam with a minimum NPR of -0.39 and a volumetric compression ratio of 3.4 by transforming conventional copper foams which exhibited PR of +0.42. The researchers reported three transformation methods that are tri-axial compression followed by heat treatment and during foaming procedure for thermoplastic polymer foams and successive plastic compression in 3D for metal foams. Choi and Lakes [87] also used the similar transformation method which apply sequential permanent compressions to transform into re-entrant foams. The achieved NPR was as small as -0.8. Most of the difference between conventional and re-entrant materials is the changes in cell shapes.

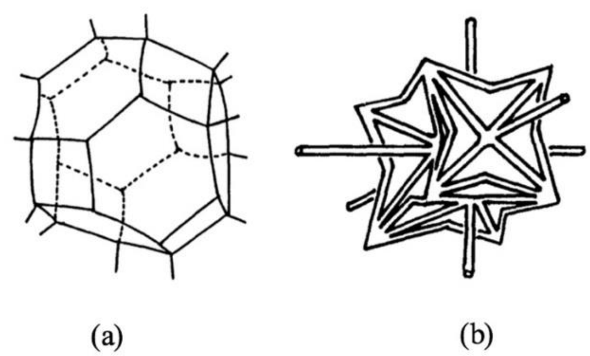

Figure 2- 38 Idealized unit cell of (a) Conventional foam; (b) Auxetic foam [86]

Then, close-cell polyethylene foam was successfully converted to an auxetic foam by Lakes [88] in 1996. Chan and Evans [89] proposed the improved multi-stage processing method for auxetic foams to develop to larger specimen. The multi-stage processing method divided tri-compression into several stages, resulting in minimizing the risk of surface creasing and improving the homogeneity and stability of auxetic foams. The highest NPR value as large as -0.82 was obtained. Chan and Evans [84] also found that by changing the geometry of the repeated unit, PR can be produced positive or negative values with mechanical properties which are isotropic or anisotropic.

Smith et al.[90] converted 30 ppi polyester polyurethane with +0.85 PR for loading in the 'rise direction' to auxetic foams that shows NPR of -0.6. The process includes volumetric compression, heated at 200°C and then cooling whilst being compressed. Then, Brandel et al.[91] successfully transformed large cell foams into re-entrant microstructures exhibiting NPR. The polyurethane foams were subjected to thermos-mechanical processing and the NPR values ranged from -0.14 to -0.32 under the conditions ranging from 100°C for 12 minutes to 120°C for 5 minutes, respectively. Moreover, Scarpa et al.[92, 93] evaluated the static and dynamic compressive performance of auxetic compliant flexible PU foams and make comparisons with conventional foams. The results shows that auxetic foams have enhanced damping decrease factor of 20% in comparison with the non-auxetic ones and increased crashworthiness qualities.

More recently, Grima et al.[94] achieved NPR in cellular foams with a 'rotation of rigid units' mechanism. The new model is not required to modify any inner structure at the joints of the cell or rib-breakage. Bezazi et al[95] investigated and compared the static and repeated compressive properties of auxetic, non-auxetic iso-density and conventional PU foams under compressive repeated loading, the obtained highest NPR values is -0.185, 0 and +0.25, respectively. The results show that the auxetic foams keep the advanced energy absorption ability over a large extent of repeated loading over conventional and iso-density foams that is up to 10 Hz and 12.5% of offset with 5% of compression strain.

To date, one novel way of producing highly idealized geometries with auxetic behavior is through the application of 3D printing technology. Critchley [96] developed two types of repeatable pliable auxetic foam structure and evaluated the PR of structures experimentally and theoretically. The lowest PR recorded was -1.18 when stretched. The microstructure of 3D printed auxetic foams is shown in Figure 2-39.

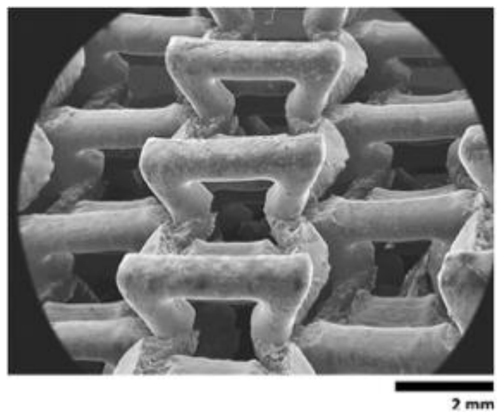

Figure 2- 39 Microstructure of auxetic foams by 3D printing [96]

2.5 Auxetic Microporous Polymer

Material microstructures have been proposed and developed producing NPR which are based on different deformation mechanism including flexural deformation elements [5] or tensile deformation mechanisms and topological constraints [97]. The auxetic microporous polymer material identified was firstly proposed by Evans and Caddock[98, 99] in 1989. The polymer was a form of polytetrafluoroethylene (PTFE) with a high anisotropic NPR of -12 by means of its complex microstructure consisting of NF structure, as shown in Figure. Deformation of the NF structure can show NPR behaviors, depending on the geometry of the structure [23, 57].

A similar microstructure has subsequently been fabricated by using ultra-high molecular weight polyethylene (UHMWPE) by Alderson and Evans [100]. The auxetic UHMWPE could reach NPR as low as -19 by this novel thermal process which consists of 'compaction, sintering and extrusion' of the non-auxetic UHMWPE. Alderson and Evans [101] developed a geometric network from material microstructure to apply to expand UHMWPE. When stretched, as shown in Figure 2-40, the fibrils cause lateral nodule translation, resulting in strain-dependent auxetic behaviors. The model shows that the key determining factor for the measured PR is the interconnectivity of the microstructure. More recently, Alderson et al.[102-104] invented a new method to manufacture auxetic form of UHMWPE by using the powder processing techniques. This new route consists of compaction process followed by double sintering treatments, resulting in a strain dependent NPR as low as -0.32. The researchers [103] also examined the mechanical properties of the produced auxetic UHMWPE that was shown to be 2.5 time that of conventional UHMWPE at low loads.

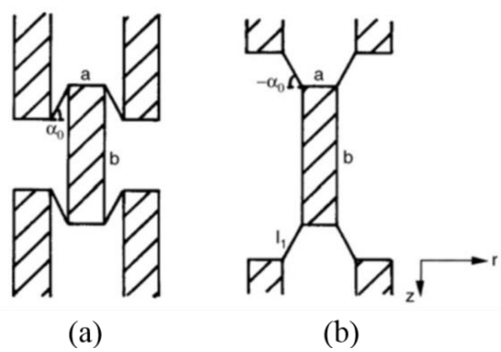

Figure 2- 40 Microstructure of auxetic polymer (a) Undeformed; (b) Deformed [104]

2.6 Auxetic Composites

Auxetic composites are an important category of auxetic materials, which have been proven to have a number of enhanced properties compared with non-auxetic composites, such as enhanced impact resistance[1, 2] ,increased energy absorption ability[105, 106] and improved mechanical indentation resistance[107]. These properties have led to many interesting applications of auxetic composites including protective protection [108] . Up to date, auxetic composites can be fabricated by using conventional components like off-the-shelf prepregs via specially designed configurations[11-13] or by embedding non-auxetic fibers into a conventional matrix material to form so called network-embedded composites[18]. In 1992, Milton [109] firstly proposed the possibility of producing composite laminates with a predicted PR closed to -1.

2.6.1 Auxetic Composites with Auxetic Inclusions

Wei and Edwards [110] theoretically evaluated the PR and Young's modulus of the composites made with auxetic inclusions of different forms including discs, spheres, blades and disks. And the disk-like inclusion produced a composite with the highest value of NPR.

More recently, Hou et al.[111] developed a 2D composite structure with the isotropic NPR (Figure 2-41). The structure is embedded re-entrant squares and triangles with random orientations and locations into a matrix. In addition, they numerically evaluated compression behaviors of four different composite structures inner embedded with inclusions of 20, 40, 60 and 80. The composite structure with 80 inclusions achieved highest NPR value ν=-0.434. The researchers suggested that the similar concept could be broadened to the 3D composite structures making use of re-entrant tetrahedron inclusions.

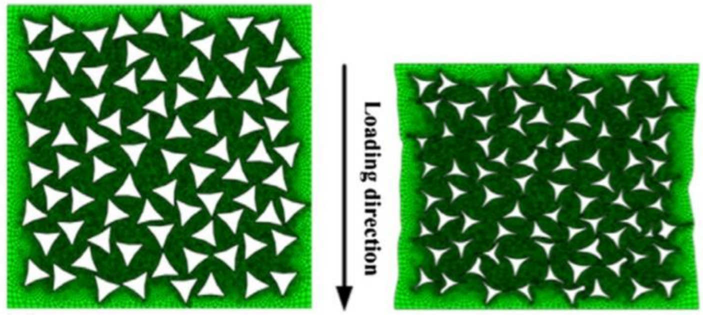

Figure 2- 41 Undeformed and deformed models with 80 inclusions [111]

2.6.2 Auxetic Fiber Reinforced Composites (FRCs)

A further method of fabricating auxetic composites is to make an auxetic structure by using non-auxetic fibers embedded in a conventional matrix material, which is also called network-embedded composites [18].

2.6.2.1 Auxetic FRCs Made from Auxetic Components

Another fabrication method is using intrinsically NPR component, alternatively either the reinforcement or the matrix. The inner interface between matrix and reinforced component is the weakest position for auxetic FRCs, as shown in Figure 2-42. And fiber pull-out is a main failure factors in FRCs. After evaluating auxetic fiber[112] and conventional fiber specimens through the designed single fiber pull-out tests using auxetic filaments embedded in a softened expoxy resin, Simkins et al.[113] found that auxetic fibers have been shown to increase fiber pull-out resistance over conventional ones that enable the auxetic specimens to carry more than twice the maximum load. As shown in Figure 2.39, for the conventional composite materials, it will go through transverse shrinkage of both matrix and fibers when compressed. In contrast, if auxetic fibers are applied, it could delay the fibers pull-out and help to withstand crack extension. Due to fiber expansion during pull-out, it help to maintain the interface by matching the PR of matrix and fiber [113]. Alderson et al.[104, 114] also proposed to use standard fabrication procedure and commercially materials to embed auxetic fibers in composite so that to improve pull-out resistance of materials [13].

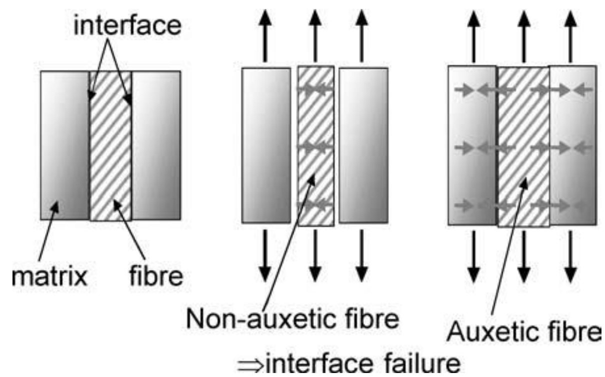

Figure 2- 42 Fiber pull-out in composites [113]

Auxetic fiber for composite reinforcement

The study of auxetic textiles has gained significant attentions in recent years, especially auxetic yarns and fibers. Auxetic fibers have many potential applications, including reinforced in composite materials, protective clothing, bio-medical materials and so on [115]. Auxetic fibers with diameters ranging from 0.14mm to 1mm[116] were manufactured by using a partial melt spinning technique including polypropylene(PP) [112], polyester[115], and nylon[117]. Alderson et al.[112] proposed the PP fiber with NPR using a novel thermal partial melt extrusion method. The obtained NPR value was -0.6.

Auxetic yarns for composite reinforcement

Miller et al.[19, 118] developed a low modulus composite using a woven auxetic fabric based on double helix yarn (DHY) reinforcements. As shown in Figure 2-43(a), the auxetic helix yarn was produced using polyurethane fiber as core and ultra-high molecular weight polyethylene fiber as wrap by a dual fiber spinning technique. The produced yarn wraps two conventional filaments with different stiffness together in the way that the stiffer filament is wrapped around the softer core filaments, in tension the stiff yarn tends to straighten and force the softer one to be wrapped around itself. The maximum value of NPR achieved for reinforced yarn is -2.1[19]. The produced woven auxetic composite (Figure 2-43(b)) is auxetic fabric as reinforcements and silicone rubber gel as matrix materials. The NPR of double layer composites was approximately -0.1, which indicated that a minimum of two layers are required to generate NPR. And Miller et al. [118] fabricated the HAY using nylon fiber as the core yarns and carbon fiber as the wrap in different wrap angles (10°, 20° and 30°), the NPR of which exhibited -5.8, -2.3 and -1.1 respectively. Sloan et al.[119] also proposed to use helical auxetic yarns (HAYs) in a simple weave pattern to manufacture a low-modulus composites. They suggested using polyurethane as core fiber and polyamide as wrap fiber. Moreover, they have investigated tensile properties of HAY by using finite element analysis. The result shows that NPR for HAY is as low as -2.7 for the yarn with 13° of wrap angle and it exhibits nonlinear behaviors.

Later, Bhattacharya et al.[120] explored the effect of a core-indentation phenomenon on the performance of the HAY. The produced HAY is PET as core fiber and UHMWPE as wrap fiber. The test results shows that the HAY has a large NPR of -13.52 at the strain of 0.02, which indicated that selecting an appropriate wrap fiber is essential to optimise NPR of the auxetic yarns.

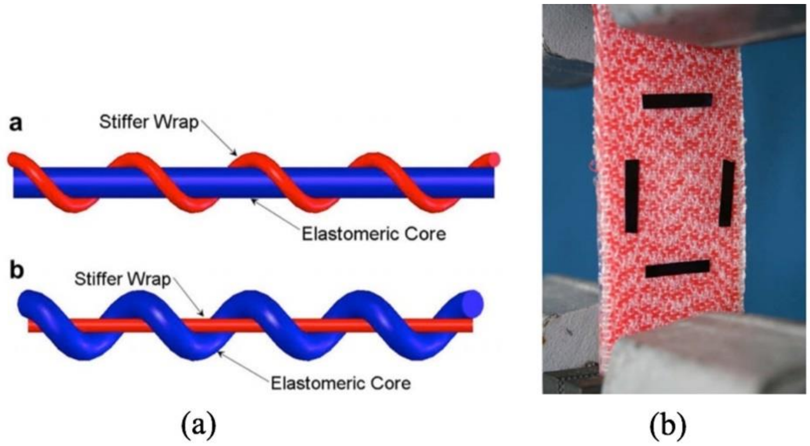

Figure 2- 43 HAY yarn (a) at undeformed and deformed state; (b) produced woven auxetic composite [19]

Recently, Ge et al.[121] proposed auxetic plied yarn structure using conventional fibers, as show in Figure 2-44. This novel plied yarn structure has better twist regularity than the existing ones. The auxetic plied yarn structure has obvious auxetic effect when stretched and the achieved highest NPR value is -4.4.

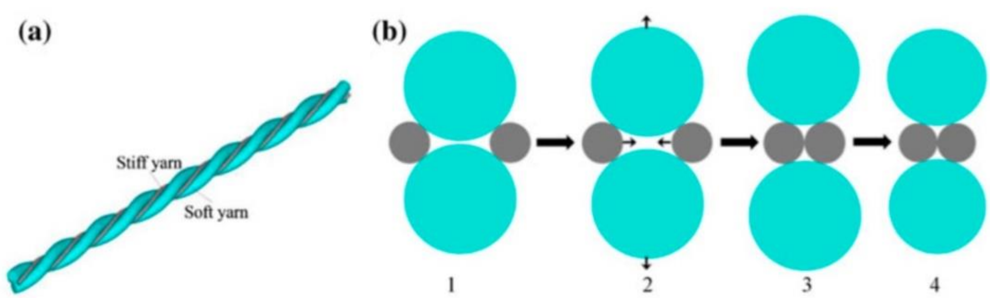

Figure 2- 44 View of auxetic plied yarn structure (a) 3D; (b) Cross-section [121]

Composites with auxetic matrix

On the other hand, researchers have developed auxetic foam composites. Chen and Lakes [14] developed auxetic composites with re-entrant NPR copper foam as a matrix and high-loss-filler materials including viscoelastic elastomer, solder and indium for composite reinforcement.

2.6.2.2 Auxetic FRCs made from non-auxetic components

Laminated angle-ply auxetic composite

One of manufacturing conventional materials method is using special stacking sequence [1] which could be applied to produce NPR angle-ply laminates. The advantage is their structural simplicity and deformation mechanism that make them be produced more easily by normal fabrication techniques and common commercial materials [111].

Almgren [6] proposed a rod-and-hinge structures (Figure 2-45(a)), in which the reentrant units fold inwards and cause the width shrink when compression. But one of the limitation is the structure cannot bear lateral shears [109]. A kind of multiscale laminate material were developed by Milton used soft phase laytered with the rigid phase through dilations as the modes of deformation, as illustrated in Figure 2-45(b). Then, Milton proposed a new rod-and hinge model (Figure 2-45(c)). When these models are laid together vertically, it shows NPR and simplizes the previous laminate but with similar structure and behaviors. And the parallelogram cells provide the inevitable shear resistance[109].

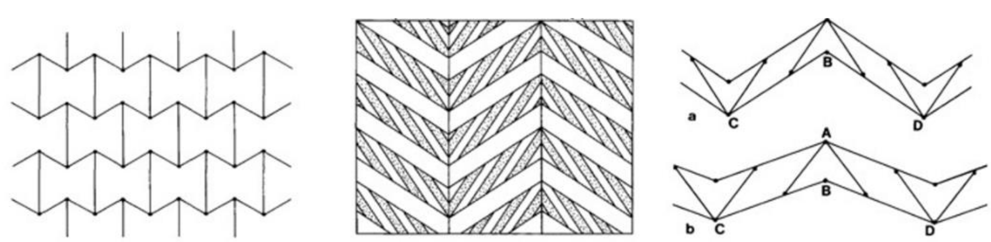

(a) (b) (c)

Figure 2- 45 (a) Rod-and-hinge structure; (b) Multiscale laminate material; (c) Model of

auxetic [109]

In 1984, Herakovich[12] designed the graphite-epoxy composite laminate to show that the through-the-thickness PR can be achieved for angle ply composite ranging from -0.21 to 0.49. The conventional manufacture of laminate composites is to use off-the-shelf pre-preg material and vacuum bagging techniques. Several researchers have subsequently shown that it is possible to design and engineer composite laminates in order to have in-plane [16] or through thickness[12, 17, 122] NPR by utilize unidirectional planes of carbon fiber reinforced epoxy laid in a particular manner[15]. Zhang and Yeh et al. [15] found that it may be more appropriate to design auxetic composites with higher NPR by using carbon fiber rather than glass fiber and Kevlar composites [16, 123]. The reason for this is that the individual ply materials are required to be highly anisotropic for auxetic composites [1]. The NPR of composites produced with this method is between -0.21 and -0.37 when the angle of laminates ranges from ±15° to ±30° [124]. And more researchers have concentrated on verify ν values of fibrous composites using carbon fiber[17, 125, 126] and have made some inroads into the indentation resistance [126] and low velocity impact resistance[1] of carbon fiber laminates. Alderson et al.[1] produced a single fiber composite by using auxetic PP fibers embedded in a softened expoxy resin. The tests were used to assess energy absorption and the pull-out performance from a specially designed matrix. Sharmila et al.[124] developed auxetic FRCs by embedding an auxetic fibrous network in a polymer matrix. Panels of three different porosities including 60%, 70% and 80% were investigated and found to have NPR in the out-of-plane direction. The mat samples with 60% porosity has the highest NPR ν=-18.6.

Auxetic textile fiber reinforced laminates

By removing the stitching yarns of the 3D auxetic textile reinforced structures [20-22], Jiang, Hu et al. [24] recently proposed a new process to fabricate auxetic composite using multilayer orthogonal auxetic reinforced structure and PU foam as matrix, as shown in Figure 2-46. In addition, the NPR values and mechanical properties of produced auxetic composite, non-auxetic composite and PU foam under compression were conducted and evaluated. It is apparent from result that auxetic composite displays NPR and shows more like a kind of damping material with a large deformation of compression strain. The highest obtained NPR value is -0.105 with the deformation strain reaches around 50%. The non-auxetic composite fails with 18% of compression strain due to misalignment of the embedded multilayer orthogonal structure. More recently, Jiang et al. [127] evaluated the energy absorption and impact resistance of the produced multilayer orthogonal structural auxetic composites and compared with mechanical properties of polymeric foams and non-auxetic composites. Due to different deformation and damage mechanism, the composites with NPR and PPR show different mechanical responses under impact energies ranging from 7.25J to 65.25J. And it is concluded that the auxetic composites show improved energy absorption performance in medium strain range.

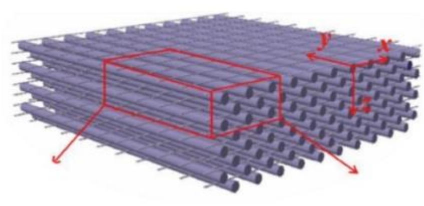

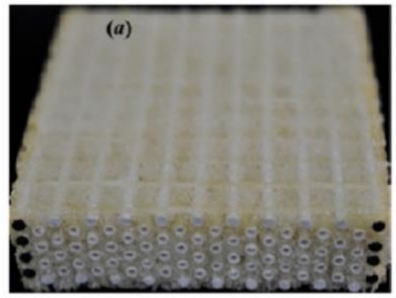

(a) (b)

Figure 2- 46 (a) 3D view of multilayer orthogonal auxetic structure; (b) Produced auxetic composite [24]

3D auxetic textile fiber reinforced composites

3D auxetic composites are made by the 3D auxetic preform using the textile processes of weaving, braiding, stitching and knitting. 3D textile composites significantly outperform 3D laminates especially in the thickness direction due to their improved properties including delamination resistance and impact damage resistance [128-130].

Recently, auxetic textile structures have also been developed for composite reinforcement. One of the examples is a novel kind of 3D auxetic textile fabric structure used for reinforcing composite (Figure 2-32) developed by Ge et al.[20-22] . This innovative 3D auxetic textile structure has similar mechanism to the nodule fibril mechanism used to explain auxetic effect in microporous polymers studied by Alderson and Evans [23]. Both types of structures could result in strain-dependent PPR and NPR when compressed. By eliminating the stitching yarns in this 3D auxetic textile structure. Based on the compression testing results, they found that the auxetic composite had an obvious NPR under compression. However, as the stitch yarns were not used in the auxetic multi-plane orthogonal structure, the delamination of composite structure could happen under impact load. Recently, Liaqat et al.[76] proposed a novel 3D auxetic woven structure with improved impact resistance that has a modified four layer through the thickness, as shown in Figure 2-47. The 3D woven fabrics were transformed into composites by Vacuum-assisted resin Transfer Moulding. The highest achieved NPR was warp wise -2.08. The energy absorption ability of 3D auxetic woven composites was found to be 6.7% higher than the non-auxetic composite.

(a) (b)

Figure 2- 47 3D auxetic woven composites (a) Weft wise (b) Warp wise [76]

2.7 Properties and Application of Auxetic Materials

In recent years, because of the unique counter-intuitive behaviors, more research works related to auxetic are developed [8]. In addition, auxetic materials have shown some remarkable benefits, including fracture toughness, enhanced energy absorption ability, and indentation resistance. The various properties make auxetic materials considerably outperform non-auxetic ones with applications in different industries [9, 10].

2.7.1 Compressive Strength and Shear Stiffness

A unique property of auxetic materials is better resistance to shear strain, undergoing twisting or tearing forces [131]. And NPR can play a critical role in tailoring the mechanical performance of the structures to enhance their performance. Usually, the auxetic foams have lower Young's modulus than that of non-auxetic ones. However, the shear modulus of auxetic foams is higher than that of non-auxetic foams [132, 133]. Four constants are usually used to explain the material's shear properties: the Young's moduli (E), the shear moduli (G), the bulk moduli (K) and the PR (ν). For isotropic material, the relations are: $E = 2G (1+ \nu) = 3K (1-2 \nu)$. The majority of auxetic materials are needed to have a higher G than K. If the microstructure of a material is changed in a way that E remains constant but PR alters, it will change the values of K and G. [134, 135].

2.7.2 Fracture Toughness

Fracture toughness is a non-linear mechanical property of auxetic materials. Choi and Lakes [136] have investigated and analysed fracture toughness properties of auxetic re-entrant foam materials. The results show that both re-entrant auxetic foams and conventional foams are observed to have facture toughness. For re-entrant auxetic foams, the increase in toughness is accompanied by an increase in compliance. Although the re-entrant foams have a small Young's modulus, the fracture toughness of auxetic re-entrant foams is greater than that of non-auxetic ones. Compared to that of non-auxetic foams, the toughness is increased by factors of 1.4, 1.5 and 1.7 with increases of compression ratio of 2.0, 2.5, 3.0, respectively [87].

2.7.3 Synclastic Curvature

Auxetic materials have a common deformation mechanism that is synclastic curvature. Due to the synclastic curvature property, auxetic materials are formed into doubly curved or domed shapes when they are subjected to a bending force, as illustrated in

Figure 2-48(a). However, for conventional materials, they display a saddle shape that the perpendicular direction has different trend with the bending direction due to the edges curl upwards (Figure 2-48(b)) [27]. Unlike auxetic materials, it is required for the non-auxetic materials to take up the desired shape by use of expensive and damaging techniques [108]. Auxetic materials have many potential applications with the synclastic curvature such as aircraft nose-cones, which eliminating the use of expensive and damaging techniques required for non-auxetic materials.

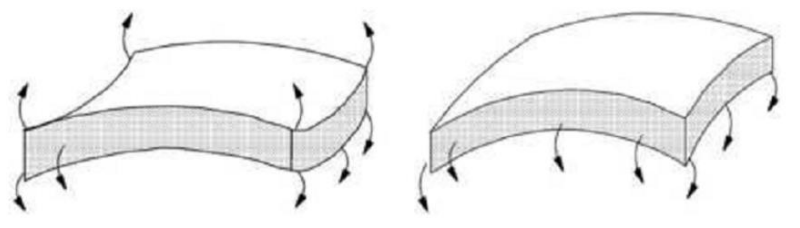

(a) (b)

Figure 2- 48 Synclastic curvature (a) Non-auxetic materials (b) Auxetic materials [8]

2.7.4 Indentation Resistance

Compared with conventional materials, auxetic materials have better indentation behaviors. As illustrated in Figure 2-49, the non-auxetic materials will flows away in the lateral direction when impacted with an object; the force compresses the material, while the auxetic materials behave in opposite way that flows into the vicinity of the impact position. Due to the auxetic effect, the material turns to be denser at the impact point, which is more resistant to indentation. From classical elasticity theory, elastic indentation behaviors are predicted to be enhanced [58].

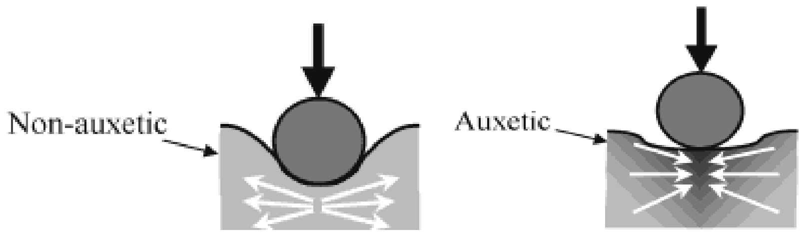

Figure 2- 49 Indentation resistance ability of conventional and auxetic materials **[108]**

2.7.5 Energy Absorption

Compared with conventional materials, auxetic materials shows better energy absorption capacity, including ultrasonic, acoustic and damping [8]. In a NPR's material, the energy dissipation abilities could be up to 15 times higher than in PPR's material and 5 to 6 times higher with high density [137]. Lakes and Elms [4] found that auxetic copper foams have greater energy absorption for impact than conventional ones. Scarpa et al. [93, 138] conducted high strain rate compression test on both non-auxetic and auxetic materials. And the results showed that auxetic foams have greater energy absorption capacity and dynamic crushing properties.

The experimental researches of the dynamic impact properties of auxetic composites could be generally divided into high-velocity and low-velocity impact tests [139]. One important type of low velocity impact tester is drop weight tester that could measure the impact performance of a completed structure under out-of-plane impact loading. Moreover, the drop weight tester can be adapted to different testing conditions including the shape of impactor, boundary conditions and impact energy. The impact energy is defined as the total amount of energy introduced to the composite which equals to the potential energy released from the impact striker from the initial impact height [140].

2.7.6 Applications of Auxetic Materials

Auxetic materials explore a new direction to improve mechanical properties and mechanisms of materials. Due to their unique performance, auxetic materials have shown enormous suitable applications in various industries. Generally, applications of auxetic materials are mainly three aspects: first is the unusual PR; second is based on some superior properties like fracture toughness, resilience and shear resistance; last is acoustic properties associated with the vibration of ribs in NPR materials [131].

In the textile industry, auxetic materials are suitable for functional fabrics [20, 80, 82, 141, 142], auxetic fibers [112, 113], and colour-change straps or fabric [143]. For example, due to pull-out performance, auxetic fibers can be used for composite reinforcement [113]. For protection area like military industry or sports application, due to their better impact and energy absorption property, auxetic materials can be used for safety equipment such as helmets and body armour [99], personal protective clothing like bullet proof vest, knee pad or glove [8].

Another important application of auxetic materials can be applied in aerospace industry like thermal protection [144], aircraft nose-cones [135], wing panel [26], vanes for gas turbine engines [145], etc. Moreover, auxetic materials can also be applied to biomedical area and artificial blood vessel is a typical example [108]. If the auxetic blood vessel is applied, its wall thickness tends to increase when a pulse of blood flows through it. More potential applications include auxetic spinal implants [146], auxetic annuloplasty prosthesis [147].

2.8 Conclusions

This chapter summarized the previous research work on auxetic materials, 3D textile structures and auxetic composites. Although different types of auxetic composites have been developed, some research gaps are still identified. The limitation is that most of auxetic structures for composite reinforcement are only studied in a two-dimensional space and the concept of auxetic effect is hardly used in 3D space. Although our previous research work is advanced, but the development for 3D composite is still at an initial phase and is not put into real application for making 3D auxetic composites. Due to the limitations of the auxetic foams like low structural stability and low impact recovery, the use of 3D auxetic textile structures can enhance their properties. Therefore, the main objective of this work is to adopt new 3D textile auxetic structures developed in the previous research work to reinforce foams. In the next chapter, the design and manufacture of 3D auxetic composites is first introduced.

CHAPTER 3 DESIGN AND MANUFACTURE OF 3D AUXETIC AND NON-AUXETIC COMPOSITES

3.1 Introduction

Chapter 3 reports the design and the manufacture of 3D auxetic textile structural composite samples for the quasi-static compression tests. The process includes two steps. The first step is to produce 3D textile structure reinforcement and the second step is to produce the composites by using customized moulds made of stainless steel and PTFE respectively. During the design and manufacturing process, three structural parameters are considered and summarized in this chapter, namely the diameter of warp yarns, the arrangement of weft yarns and the proportions of A/B PU foams

3.2 Design and Fabrication of 3D Auxetic and Non-auxetic Textile Structures

3.2.1 3D Auxetic Textile Structure Design

3D auxetic textile structure used in this study was designed based on the modification of the 3D woven textile structure by reducing warp yarns in a regular manner in the same fabric direction [20, 25]. As shown in Figure 3-1(a), the structure includes three yarn systems: weft yarns in X axis, warp yarns in Y axis and stitch yarns in the Z-axis. The warp yarns and weft yarns are set as reinforcing yarns. They are alternately arranged in each layer in x-y fabric plane and are bound together by the stitching yarns in the direction of Z axis to form an integrated 3D textile structure. Another objective of using the stitch yarns is to avoid the possible delamination of the structure. The cross-sections of the structure in x-y plane, x-z plane and y-z plane are illustrated in Figure 3-1(b), (c) and (d), respectively. A small part of amplified structure is also shown in Figure 3-1(c) to get a better view. In the original situation, both the warp yarns and weft yarns are in a straight status. To achieve auxetic effect in the x-z plane, as illustrated in Figure 3-1(c), the warp yarns are regularly eliminated in each warp yarn layer to create void spaces. As shown in Figure 3-2(a), because of the empty room created by elimination of the warp yarns, the weft yarns will shrink by action of the warp yarns when vertically compressed, resulting in shrinking of the fabric network in the x-z plane. Finally, NPR effect is obtained. Unlike the arrangement of warp yarns, the weft yarns are arranged in each and every weft yarn layer without any elimination. In this situation, the warp yarns can remain straight state when compressed due to support of the weft yarns. Therefore, the 3D auxetic structure will have NPR in the x-z plane and zero PR in the y-z plane for loading in the Z direction.

As the 3D auxetic textile structure is designed for reinforcing composite, selecting the appropriate yarns in three directions is important. To easily achieve NPR of the auxetic structure, rigid braided yarns made of polyamide fiber were chosen as the warp yarn, and braided cotton yarn was used as the weft yarn. Polyester multifilament was used as stitching yarn to bind the warp yarns and weft yarns together. The yarn components and structural parameters are presented in Table 3-1.

To make the comparisons, 3D textile structures with different warp yarn arrangement is also included in this study. As illustrated in Figure 3-2(b), as the warp yarns are arranged vertically in the loading direction and the distance between two adjacent warp yarns S_x

are kept unchanged, the weft yarn will not be crimped under compression. In this case, the misalignment of the warp yarns could happen with increasing the compression strain.

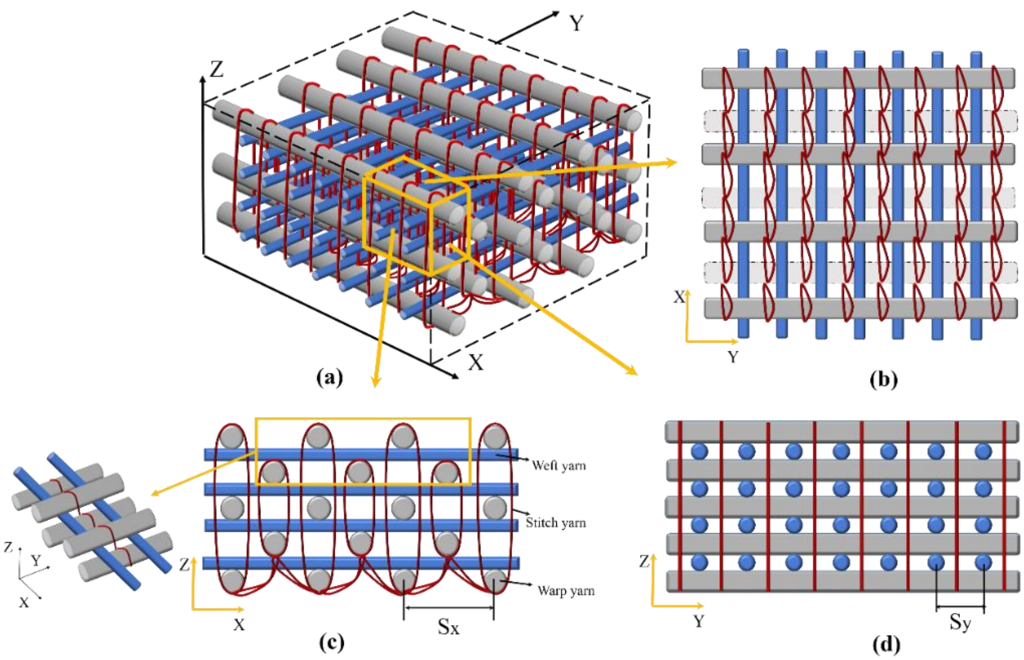

Figure 3- 1 3D auxetic textile structure (a) 3D view; (b) x-y plane; (c) x-z plane; (d) y-z plane

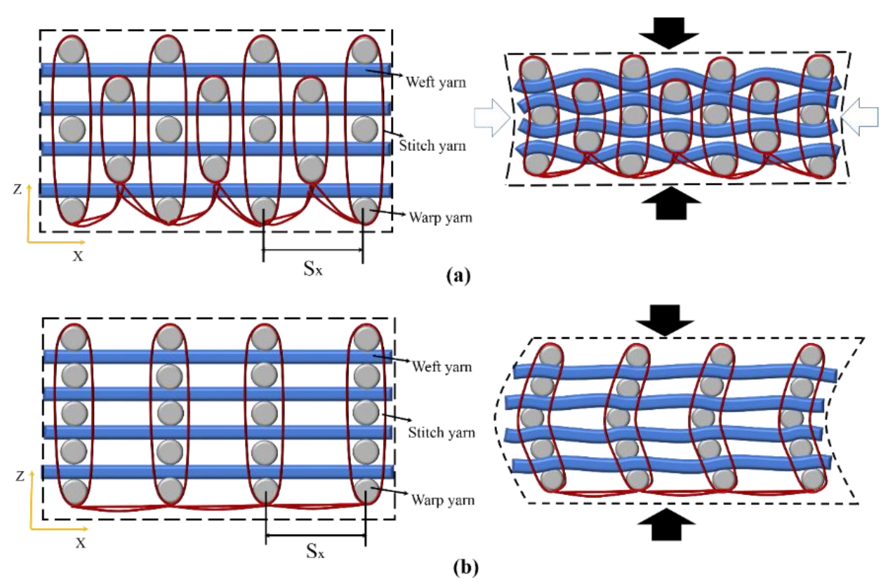

Figure 3- 2 Deformation of 3D textile structures under compression (a) Auxetic

structure; (b) Non-auxetic structure

Table 3- 1 The components and structural parameters of yarns

	Material	Diameter (mm)	Modulus (MPa)	Poisson’s ratio
Warp yarn	Rigid braided yarn made of polyamide fiber	4	32.98	0.18
		6	36.84	0.2
Weft yarn	Braided cotton yarn	2	42.12	0.2

3.2.2 The structural parameters of 3D auxetic textile structure

A customized mould made of stainless steel for fabrication of 3D auxetic textile structure was used to fabricate the 3D auxetic textile reinforced structure, as illustrated in Figure 3-3. Before fabricating the inner structure, there are two structural parameters that may affect the auxetic effect of 3D auxetic textile structures, namely the diameters of warp yarns and the arrangement density of weft yarns based on the customized mould.

As for the diameter of warp yarns, 4mm and 6mm rigid braided yarns are selected. There is no doubt that the diameter of warp yarns in the auxetic textile structures will affect the auxetic behaviors of 3D auxetic composites. It is predicted that the 3D auxetic textile structures with 6mm warp yarns will relatively achieve better auxetic effect.

As for the arrangement of weft yarns, as shown in Figure 3-4, half-arranged and full-arranged weft yarns are selected. For the half-arranged series, the weft yarns in each fabric plane are arranged one in and one out. While, for the full-arranged series, the weft yarns are arranged in each and every weft yarn layer without any elimination. As mentioned above, the weft yarn will get shrunk if compressed, resulting in auxetic effect of the textile structure in the weft directions. It is predicted that the 3D auxetic textile structure with half-arranged weft yarns will have higher NPR. Because, compared to the full-arranged ones, the half-arranged weft yarns are relatively easier to be compressed and crimped with the same compression strain.

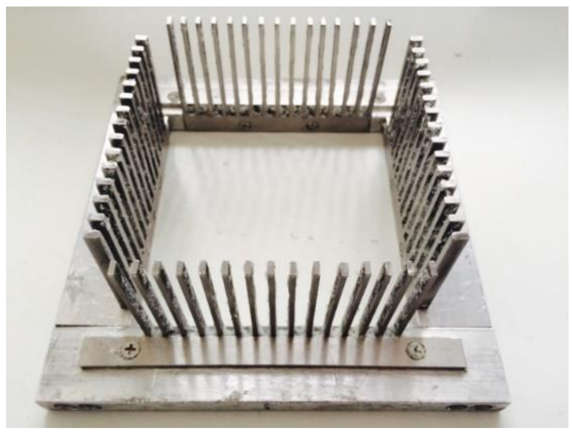

Figure 3- 3 The customized mould for fabrication of 3D auxetic textile structure

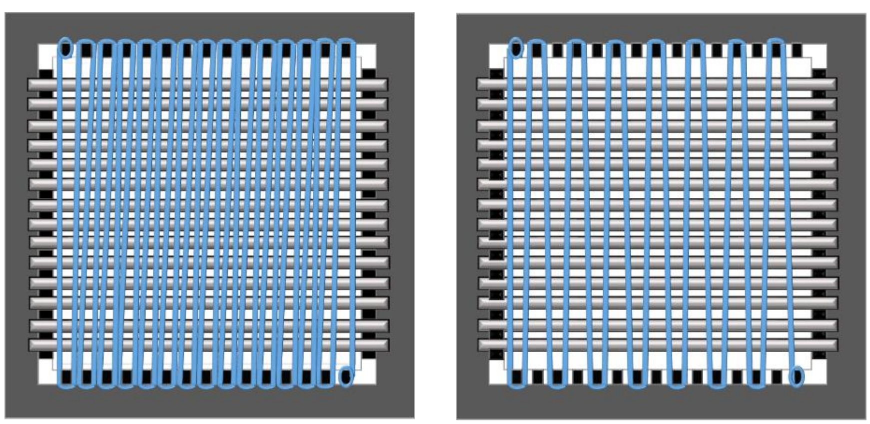

(a) (b)

Figure 3- 4 The arrangements of weft yarns on customized mould in x-y cross-section

(a) Full-arranged; (b) Half-arranged

3.2.3 Fabrication of 3D auxetic and non-auxetic textile structure

A prototype machine was built to fabricate the above designed 3D auxetic and non-auxetic textile structures [142]. As show in Figure 3-5, the process includes two steps: The first step is to place the weft and warp yarns in a mold made of stainless steel as mentioned above to form multilayer orthogonal auxetic textile structures. The second step is to stitch the warp yarns and weft yarns together to form a 3D integrated textile structure by using the similar manufacturing process as the previous research work by Ge and Hu[20] as shown in Figure 3-6. A produced 3D auxetic textile structure fixed together with the stainless steel mold is illustrated in Figure 3-7.

The fabrication process of the 3D non-auxetic textile structures remains the same as the auxetic ones. The difference in the fabrication of auxetic and non-auxetic structures is the result of different placement of the warp yarns in the mold. To facilitate the comparison, the space between two adjacent weft yarns (weft yarn spacing S_y) and that between two adjacent warp yarns (warp yarn spacing S_x), as shown in Figure 3-1(c) and (d), were kept unchanged for both the auxetic structure and non-auxetic structure, respectively. Previous studies[20, 21] have shown that a high size difference between the warp yarns and weft yarns could achieve relatively higher auxetic effect of the auxetic structure. For this reason, warp yarns with a much larger diameter than that of the weft yarns were used for fabricating the auxetic textile structure.

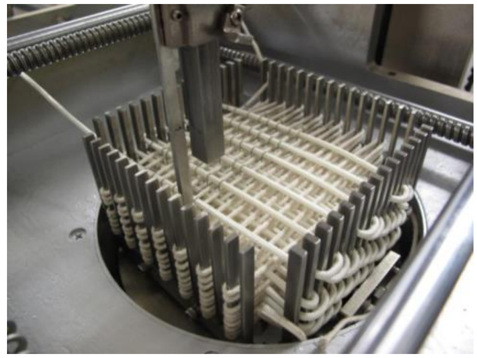

Figure 3- 5 Fabrication of 3D auxetic textile structure on a prototype machine.

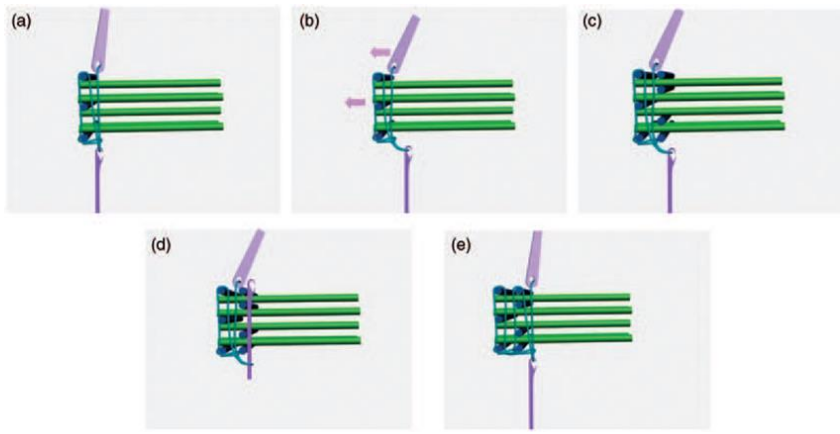

Figure 3- 6 Fabrication process of 3D textile structure [10]

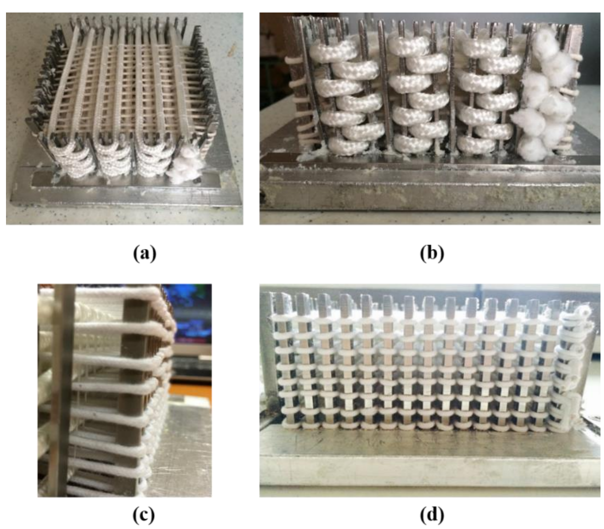

Figure 3- 7 The produced 3D auxetic textile structure fixed together with the stainless

steel mould (a) Overview; (b) The warp yarns in x-z cross-section; (c) The stitch yarns in z direction; (d) The weft yarns in y-z cross-section

3.2.4 Summary of produced 3D textile structures

There are mainly two categories of 3D textile structures: auxetic and non-auxetic. In this study, the diameter of stitching yarn used is 0.5mm. To facilitate the comparison, the warp yarns spacing and the diameter of weft yarns remain unchanged for all the developed fabrics. The structural parameters of the 3D auxetic structures are summarized in Table 3-2. For auxetic textile structures, there are mainly four types of structures, among which the main differences are the diameters of warp yarns and the arrangement methods of weft yarns. For non-auxetic textile structures, two types are separated based on different diameters of warp yarns. All the above produced textile structures are prepared for the fabrication of 3D auxetic and non-auxetic composites.

Table 3- 2 The summary of produced 3D auxetic and non-auxetic textile structures

Structure type	Structure No.	Warp yarn			Weft yarn			Diameter of stitch yarn (mm)	Fabric structure thickness (mm)
		Diameter r1(mm)	Arrangement method	Spacing Sx (mm)	Diameter r2(mm)	Arrangement method	Spacing Sy (mm)		
Auxetic	A1	6	In the form of one in and one out	15	2	full-arranged	3.7	0.5	50
	A2	6	In the form of one in and one out	15	2	half-arranged	7.5	0.5	50
	A3	4	In the form of one in and one out	15	2	full-arranged	7.5	0.5	46
	A4	4	In the form of one in and one out	15	2	half-arranged	7.5	0.5	46
Non-auxetic	N1	6	In the vertical lines	15	2	half-arranged	7.5	0.5	51
	N2	4	In the vertical lines	15	2	half-arranged	7.5	0.5	47

3.3 Fabrication of composites

3.3.1 Preparation of fabrication process

The 3D auxetic and non-auxetic textile structures are designed for composite reinforcement. The selected chemical solutions is uniformly mixed with two chemical constitutes PU resin composition and MDI (isocyanate), The PU resin composition contains ingredients including polyether polyol, catalysts and blowing agents. The general technical indicators of Cst-1076A/B PU foam are listed in Table 3-3. All chemical solutions were achieved of analytical grade and used without further distillation. Moreover, to facilitate the manufacturing process of 3D auxetic textile composites, a customized mould made of Polytetrafluoroethene (PTFE) is adopted, as show in Figure 3-8.

Table 3- 3 General technical indicators of Cst-1076 A/B PU foam

	A	B
Composition	Polyether polyol	Isocyanate
Colour	Ivory	Blackened brown
Blending Ratio	100	30-40
Foaming Ratio (%)	15-20	
Foam Density (kg/m^3)	32-35	
Tensile Strength (/k pa)	60-118	
Tear Strength (/N/cm)	2.8-8.6	
Rebound Rate (%)	26-60	

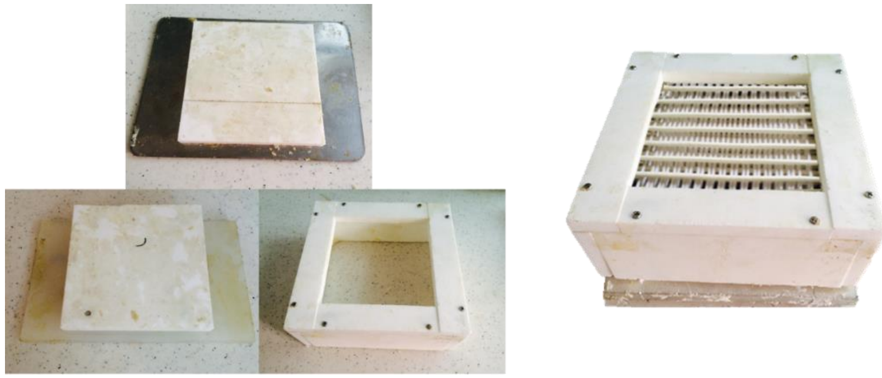

(a) (b)

Figure 3- 8 The customized PTFE mould for fabricating the 3D auxetic textile composites (a) Parts of the mould; (b) With the 3D auxetic textile structure

3.3.2 The structural parameters of 3D auxetic textile composites

Compressible polyurethane (PU) foam consisting of A and B two chemical constitutes was used as matrix in the fabrication of 3D auxetic textile composites. The proportion of A/B is a critical factor that affects the auxetic effect of 3D auxetic textile composites. Before fabricating the 3D auxetic textile composites, it is necessary to evaluate whether the proportion of A/B PU foams as composite matrix would affect the auxetic effect. As mentioned above, the chemical solution consists of two chemical constitutes A and B, here A is PU resin compositions and B is MDI (isocyanate). The pure PU foam is formed of the chemical solution by mixing A and B. The general mixing ratio of A/B is 100/30-40. So three different proportions (A: B) of PU foams of 3D auxetic textile composites were made and tested, namely 2:1, 3:1 and 4:1. Moreover, three types of pure PU foams were manufactured for comparisons with auxetic composites, which are named as E2:1, E3:1 and E4:1. Because the proportions of A and B may affect the elastic resilience of the pure PU foam samples.

3.3.3 Fabrication process of composites

Both auxetic and non-auxetic composites were fabricated using the 3D textile structures above fabricated as reinforced components and PU foam as matrix through a filling and foaming fabrication procedure. The fabrication process is shown in Figure 3-9. To keep all the weft yarns and warp yarns in a straight state, 3D textile structure fixed together with the customized rustless iron mold (Figure 3-9(a)) was first placed into the PTFE mold (Figure 3-9(b)). Then, the chemical solution was filled into the PTFE mold (Figure 3-9(c)) to form the PU foam (Cst-1076A/B) in the presence of a blowing agent. After filling, the mold was closed to let the foaming process to occur. After finishing the foaming process, the composite was de-molded from the mold and cut to the required size for the subsequent compression tests. Finally, mainly three categories of samples including 3D auxetic composites, 3D non-auxetic composite and pure PU foams were finally obtained. Some of the produced samples including the pure PU foam, the auxetic composites and non-auxetic composites are as described in Figure 3-10(a)-(c), respectively.

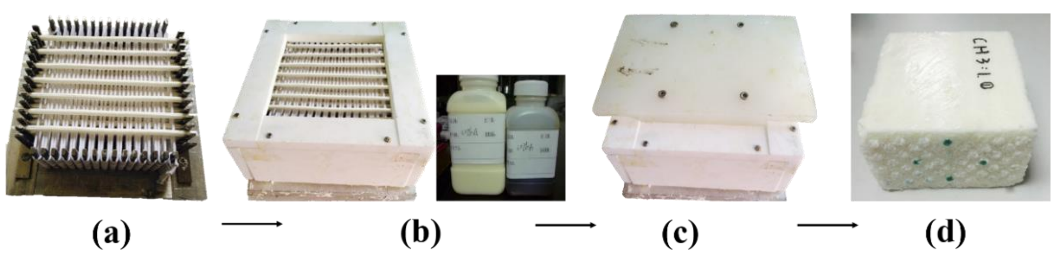

Figure 3- 9 Fabrication process of composites

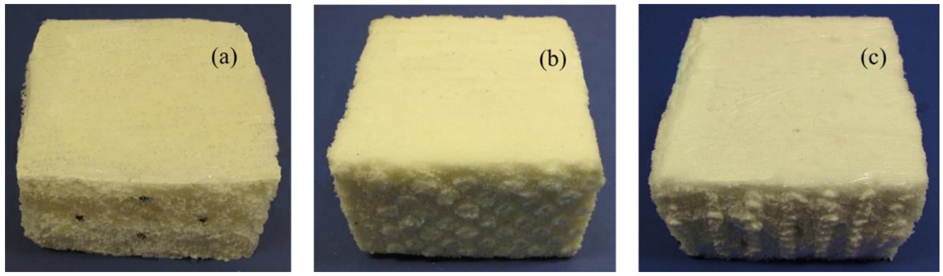

Figure 3- 10 Samples produced (a) pure PU foam; (b) auxetic composite; (c) non-auxetic composite

3.4 Summary of produced samples for compression experiments

In this study, it is necessary to evaluate the deformation behaviors of three categories of specimens, namely pure PU foams, 3D auxetic composites and non-auxetic composites. Three same samples were produced for each type of material and the average value was calculated. It should be noted that the thicknesses of produced samples are varied because of the different levels of PU foam expansion during the foaming procedure. The density of auxetic composites and non-auxetic composites is 0.27g/cm3 and 0.24g/cm3, respectively.

3.4.1 Pure PU foams

The pure PU foams were used to evaluate their deformation behaviors and compression behaviors based on different proportions of A/B PU foams, which are named as E2:1,E3:1 and E4:1. The average fabric thickness of pure PU foams is 62mm.

3.4.2 3D non-auxetic composites

As for non-auxetic composites, only the factor of diameter of warp yarns are taken into consideration. The arrangement of weft yarns is half-arranged and the proportion of A/B PU foams is 3:1. And the non-auxetic composites with 4mm warp yarns are named ZXH3:1, and the ones with 6mm are named ZCH3:1. Table 3-4 shows the details of non-auxetic composites fabricated with different diameter of warp yarns.

Table 3- 4 The details of non-auxetic composites fabricated with different diameter of warp yarns

Composite sample number	**Reinforced structure No.**	**Proportion of PU foams (A:B)**	**Average composite thickness (mm)**	**Average volume of composite (cm^3)**	**Average volume of embedded textile structures (cm^3)**	**Average percentage of yarns in composite (%)**
ZCH3:1	N1	3:1	6.6	739.24	184.69	24.99%
ZXH3:1	N2	3:1	6.6	764.82	99.44	13.00%

3.4.3 3D auxetic composites

Auxetic composites are used to investigate the compression properties based on different structural parameters including the diameters of warp yarns, the arrangement of weft yarns (full- or half- arranged based on the customized mould) and the proportions of PU foams (A: B are 2:1, 3:1 and 4:1, respectively). One factor is evaluated when the rest factors are kept unchanged. Table 3-4 shows the structural parameters of 3D auxetic textile reinforced composites. As shown in Table 3-5, four series of auxetic composites are classified based on the structural parameters, name CF, CH, XF and XH. CF series are the auxetic composites with 6mm warp yarns and full-arranged weft yarns, and CH are the ones with half-arranged weft yarns; XF series are the auxetic composites with

4mm warp yarns and full-arranged weft yarns, and XH are the ones with half-arranged weft yarns.

Table 3- 5 The structural parameters of 3D auxetic textile reinforced composites

Composite sample number	Reinforced structure number	Proportion of PU foams (A:B)	Average composite thickness (mm)	Average volume of composite (cm^3)	Average volume of embedded textile structures (cm^3)	Average percentage of yarns in composite (%)
CF2:1	A1	2:1	6.33	706.87	211.40	29.91
CF3:1	A1	3:1	6.3	709.79	213.10	30.02
CF4:1	A1	4:1	6.3	693.88	211.26	30.45
CH2:1	A2	2:1	5.57	623.93	174.78	28.01
CH3:1	A2	3:1	6.17	647.74	170.54	26.33
CH4:1	A2	4:1	6.23	676.03	172.34	25.49
XF2:1	A3	2:1	6.27	713.15	173.87	24.38
XF3:1	A3	3:1	6.6	724.49	171.15	23.62
XF4:1	A3	4:1	6.5	680.52	166.93	24.53
XH2:1	A4	2:1	6.23	681.45	125.09	18.36
XH3:1	A4	3:1	6.4	698.45	124.09	17.77
XH4:1	A4	4:1	6.43	675.64	122.23	18.09

3.5 Conclusions

This chapter has set out the methodological approach taken to the research reported in this thesis. It includes the design and fabrication process of the 3D auxetic and non-auxetic structures and composites. This chapter also has provided a broad overview of the design of the study, sample making. Four main series of auxetic composites are made for the following compression test. In the next chapter, the deformation and compression performance of produced 3D auxetic composites will be analyzed based on the compression test results.

CHAPTER 4 QUASI-STATIC COMPRESSION PROPERTIES OF 3D AUXETIC AND NON-AUXETIC COMPOSITES

4.1 Introduction

This chapter emphasizes on investigating the deformation behaviors and the compression performance of the produced samples in the quasi-static compression tests including pure PU foams, 3D auxetic and non-auxetic composites. The samples are tested on the Instron 5566 compression machine. The compression stress-strain relationship of the produced composites is achieved from the quasi-static compression test, in which compression load-displacement data was recorded by the tester. Then the deformation behaviors and compression properties of produced samples are analyzed based on different investigated structural parameters within same types of produced samples and comparisons are made between different types. The relationship of compression properties and the deformation behaviors of the samples in repeated compression tests are also revealed.

4.2 Quasi-static Compression Tests

4.2.1 Quasi-static Single Compression Tests

To evaluate the deformation and compression behaviors of the produced samples mentioned in the last chapter including the pure PU foam, auxetic and non-auxetic composites, and a series of uni-axial compression experiments were conducted. The tester was the Instron 5566 Universal Testing Machine (Instron Worldwide Headquarters, Norwood, Massachusetts, USA) equipped with two 150mm circular compression plates. The set-up of the compression testing system is described in Figure 4-1. All the compression tests were carried out at a compression speed of 30mm/min up to a 55% compression deformation of the original thickness of each sample. The maximum load of the testing device and the sample size were 10kN and 10cm x 10cm, respectively. Three same samples were produced for each type of material and the average value was calculated.

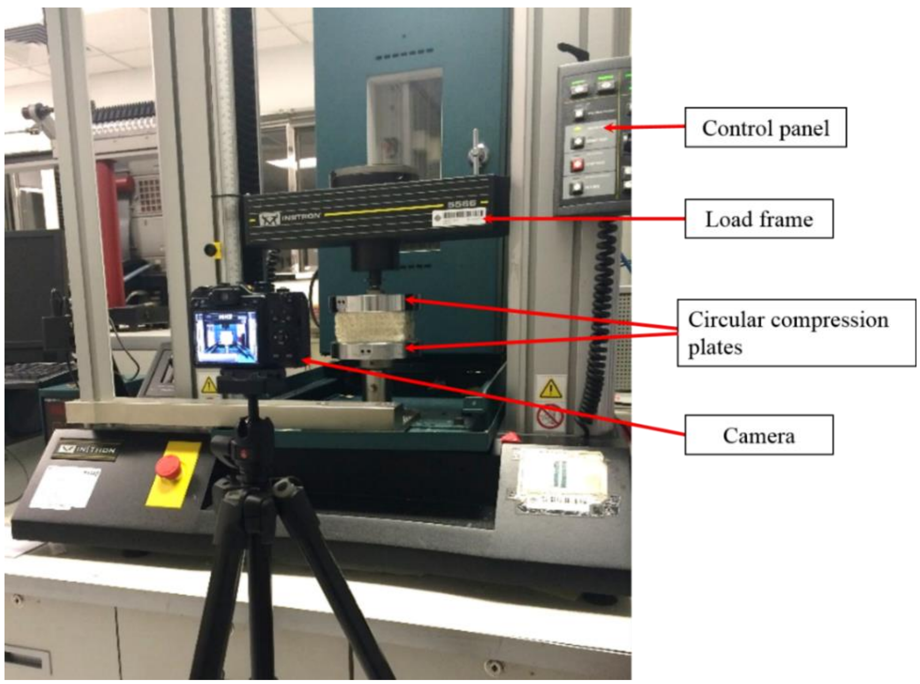

Figure 4- 1 Set-up of the quasi-static compression testing system

To measure the lateral and vertical change of sample, as presented in Figure 4-2, four black points were marked on the cross-section of the sample to facilitate recording of the deformation change during testing process. A camera Canon PowerShot G10 with time-lapse photograph function, which was kept the distance of 50 cm from the tested sample, was used to take pictures of the marked points. The initial distances between the marked points in both the horizontal and vertical directions were first measured before compression. As shown in Figure 4-2, H is the distance between the two marked points in the vertical loading direction and L is the distance between the two marked points in the horizontal direction. H_0 and L_0 are their initial values. The distances of the marked points were measured from the pictures taken by the camera during the compression process using a screen ruler. Based on the measured results, the compression strain ε_z and transversal strain ε_x could be calculated from Equation (1) and (2).

$$\varepsilon_z = \frac{\mathrm{H} - \mathrm{H}_0}{\mathrm{H}_0} \tag{1}$$

$$\varepsilon_x = \frac{\mathrm{L} - \mathrm{L}_0}{\mathrm{L}_0} \tag{2}$$

Finally, the PR ν could be calculated from Eq. (3).

$$v = -\frac{\varepsilon_x}{\varepsilon_z} \tag{3}$$

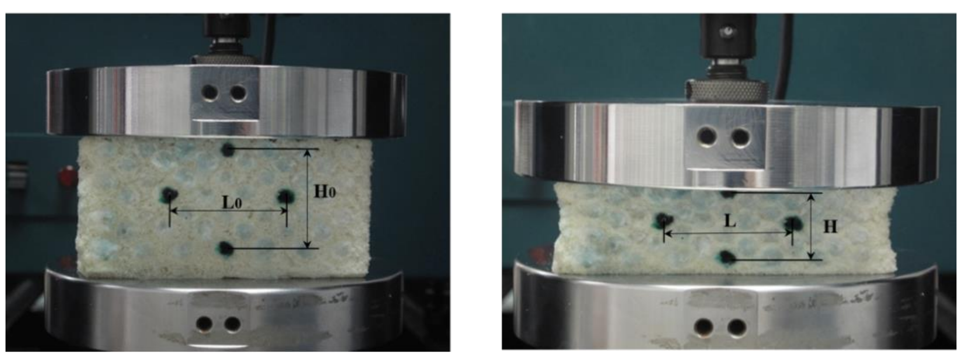

(a) (b)

Figure 4- 2 Points marked on produced auxetic composites (a) Undeformed; (b) Deformed

4.2.2 Quasi-static Single Repeating Compression Tests

One of the difficulties that the auxetic textile reinforced composites may face is the loss of NPR and mechanical properties under repeating compression conditions, which will influence its property when repeated uses. For purpose of deeper understanding how the produced 3D auxetic composite samples could maintain their auxetic behaviors and mechanical properties, a repeating compression test was also conducted. The compression cycles used were ten. A pre-load of 0.2N was applied at the start of each cycle. For each compression cycle, the composite was firstly compressed to a 55% deformation from its initial situation at the speed of 30 mm/min and remained at this status for 2 seconds, and released back to its original place with the same speed and stop for 5 seconds at this situation.

4.3 Deformation Behaviors in Quasi-static Compression Test

4.3.1 Deformation Behaviors of Pure PU foams

As mentioned above, pure PU foams are named as E2:1, E3:1 and E4:1 based on the proportion of A/B PU foam. Three samples for each types are made and the average PR values of each type are calculated and compared. The PR-compression strain curves of PU foams samples are presented in Figure 4-3. All the PU foams are conventional PU foams that show PPR. And the curves of three types of pure PU foams have similar rising tendency from 0% to 10% while the PPR value of E3:1 is relatively low. The E2:1 has the highest PPR value of 0.087 at the strain of 7%. From 10% to 18% of compression strain, the curve of E2:1begins decreasing, meanwhile the curves of E3:1 and E4:1 keep increasing and reach their maximum value of 0.096 and 0.074 at the strains of 13% and 18%, respectively. When the compression strain exceeds 18%, the curves of three types of foams gradually decline and reach their minimum values at the compression strain of 55% because the foams are compressed to a near-densified state. Compared with the PR-compression strain curves of three types of pure PU foams, the deformation behaviors of the pure PU foam with the proportion of 3:1 is relatively stable.

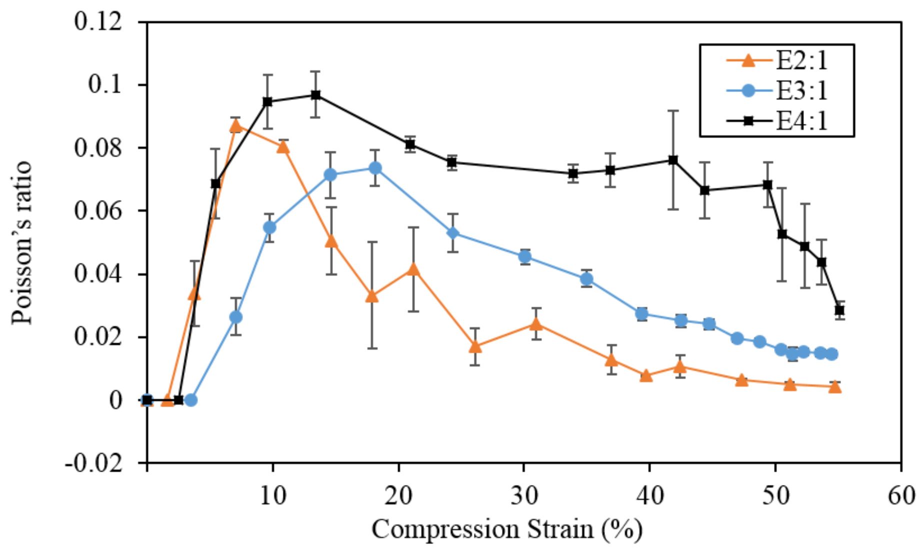

Figure 4- 3 The PR-compression strain curves of different proportions of pure PU foams

4.3.2 Deformation Behaviors of 3D Non-auxetic Composites

As mentioned above, two types of non-auxetic composites (ZCH3:1 and ZXH3:1) are fabricated and used for quasi-static compression tests. The values of PR for the non-auxetic composites as a function of compression strain are depicted in Figure 4-4. From compression strain 0%-5%, the PR of both types of non-auxetic composites almost approaches zero while the PR value of ZXH3:1 keep zero relatively longer until 13%. This effect mainly originates from the deformation of the PU foams that is filled in the peripheries of the reinforcements in the initial stage. For the self-made pure PU foam, it has the zero PR in the initial stage of compression due to its porous structure. In this stage, the compression mainly causes the decrease of voids sizes in the compression direction, and not in the transversal direction. As a result, the size of the pure foam in the transversal direction almost keeps unchanged.

As presented in Table 3-3, the percentage of yarns for composite reinforcement of ZCH3:1 is 24.99% which is much higher than that of ZXH3:1 (13.00%). Therefore, more void space could be filled with PU foams in ZXH3:1, thus it has zero PR with higher range of compression strain (~14%). However, with the compression strain increasing, the PU foam starts to be compact and the deformation of composites mainly comes from the textile reinforced structure. Non-auxetic composites with 6mm warp yarns (ZCH3:1) start undulate between 0.014 and 0.027. Moreover, sample with 4mm warp yarns (ZXH3:1) achieves its highest value of 0.029 at the compression strain of 25%. After 14% compression strain, the curves of both types of non-auxetic composites fluctuate between 0.009 and 0.03. Basically, the average PPR value of ZXH3:1 is higher than that of ZCH3:1. This effect mainly originate from the difference between the diameters of warp yarns, which are 6mm and 4mm, respectively.

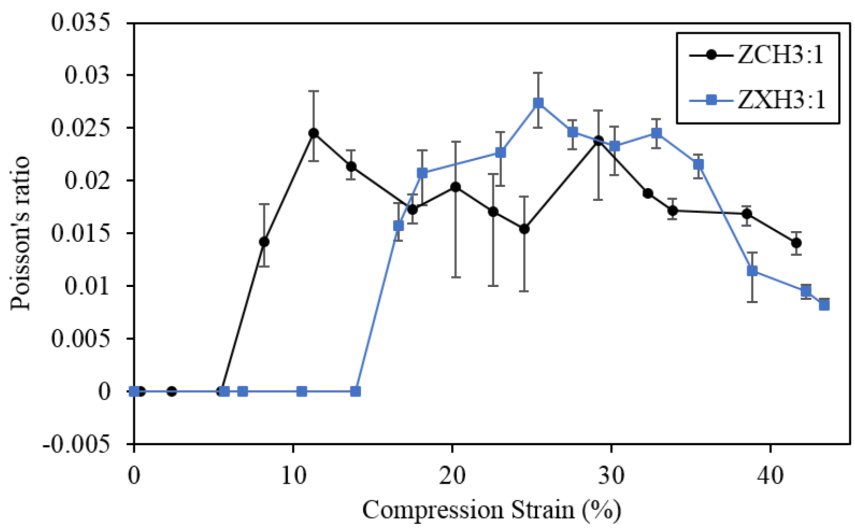

Figure 4- 4 The PR-compression strain curves of non-auxetic composites

4.3.3 Deformation Behaviors of 3D Auxetic Composites

The effects of different structural parameters, including diameter of warp yarns (6mm and 4mm), arrangement of weft yarns (full-arranged and half-arranged) and proportion of PU foams (A: B are 2:1, 3:1 and 4:1, respectively), on the deformation behaviors of the 3D auxetic textile composites were analyzed based on the PR-compression strain curves.

4.3.3.1 Auxetic Behaviors in Different Diameters of Warp Yarns

A group of auxetic composites produced with the same arrangements of weft yarns (half-arranged), the same proportion of PU foams in comparison (2:1, 3:1 and 4:1) but with different diameters of warp yarns (4mm and 6mm) are used to analyse the effect of diameters of warp yarns on the deformation behaviors of 3D auxetic textile composites. The PR-compression strain curves of these auxetic composites are illustrated in Figure 4-5. The auxetic composites with same full-arranged weft yarns and same proportion of

PU foams but different diameters of warp yarns are shown in Figure 4-5 (a) to (c), and those with half-arranged weft yarns are presented in Figure 4-5 (d) to (f). The following performance can be observed and summarized.

(1) For all the auxetic composites, the PR-compression strain curves tend to firstly rise between 0% and 30% of compression strain and then decrease with the increasing compression strain.

(2) It is observed that under the conditions that other structural parameters are kept same, compared with 4mm diameters of warp yarns, the produced samples with 6mm warp yarns have relatively higher NPR values. As explained above, for the auxetic composites, weft yarns will shrink under compression because of the void spaces created by elimination of the warp yarns. The auxetic composites with 6mm warp yarns are stiffer than those of 4mm, which will make weft yarns crimp more easily thus gaining higher NPR value.

(3) There is no doubt that the diameters of warp yarns in the auxetic textile structures will affect the deformation behaviors of 3D auxetic composites

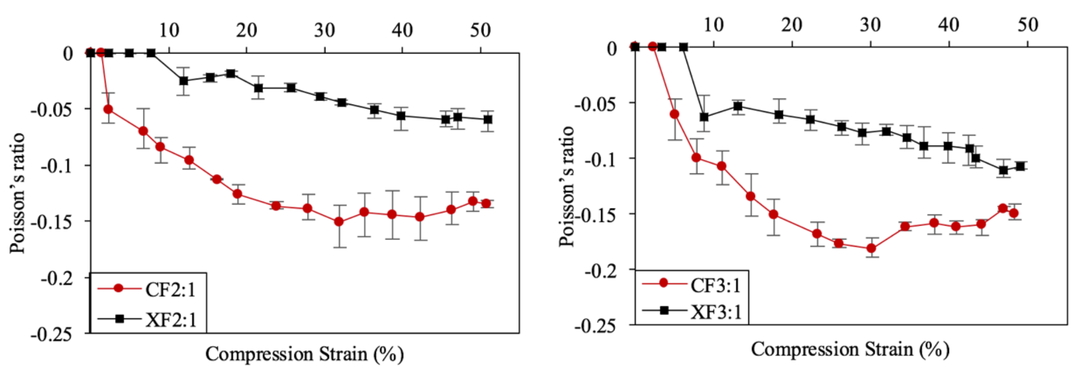

(a) (b)

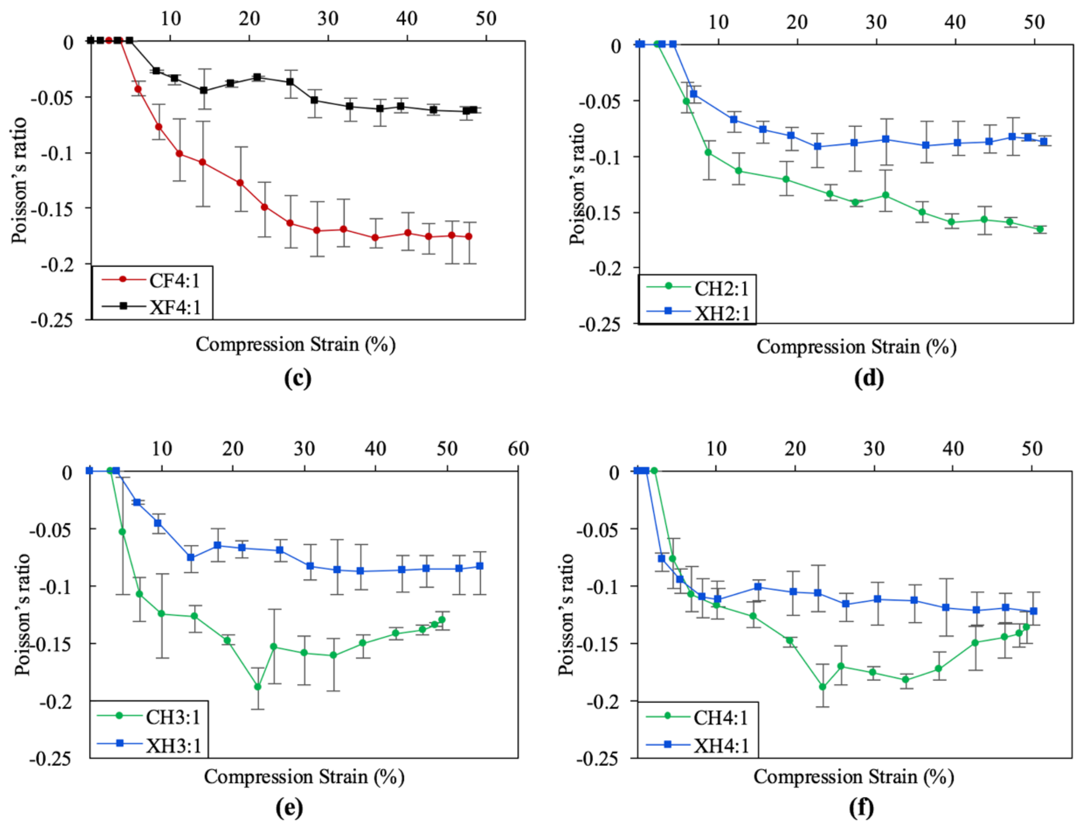

Figure 4-5 The PR-compression strain curves of different types of 3D textile auxetic composites based on varied diameters of warp yarns (a) CF 2:1 & XF 2:1; (b) CF 3:1 & XF 3:1; (c) CF 4:1 & XF 4:1; (d) CH 2:1 & XH 2:1; (e) CH 3:1 & XH3:1; (f) CH 4:1 & XH 4:1

4.3.3.2 Auxetic behaviors in Different Arrangement Density of Weft Yarns

A group of auxetic composites produced with the same proportion of PU foams in comparison (2:1, 3:1 and 4:1) and same diameters of warp yarns in comparison (4mm and 6mm) but with different arrangements of weft yarns (half-arranged and full arranged) are tested under compression. The results are used to analyse the effect of arrangements of weft yarns on the deformation behaviors of 3D auxetic textile composites. Figure 4-6 describes the y-z cross section of 3D auxetic textile composites with half- and full-arranged weft yarns. The PR- compression strain curves of these auxetic composites are illustrated in Figure 4-7. The auxetic composites with 6mm warp yarns and same proportion of PU foams but with different arrangements of weft yarns are shown in Figure 4-7 (a) to (c), respectively; and those with 4mm warp yarns are shown in Figure 4-7(d) to (f). The following performance can be observed and summarized.

(1) As presented in Figure 4-7(a) to (c), for the auxetic composites with 6mm warp yarns and same proportions of PU foams, the curves fluctuate with similar tendency, thus there are no significant influence for the arrangement density of weft yarns affecting auxetic effects. With increasing proportion of polyester polyol in PU foam, the foams become more elastic, and the auxetic composites present relatively higher NPR value.
(2) As presented in Figure 4-7(e), auxetic composites with 4mm warp yarns and 3:1 proportion also have similar tendency with above composites and no significant differences are found. As shown in Figure 4-7(d) and (f), auxetic composites with half-arranged weft yarns show higher NPR than those with full-arranged weft yarns. As explained above, the weft yarns will crimp by action of warp yarns under compression. The auxetic composites with full-arranged weft yarns may stiffer than half-arranged weft yarns when compressed.
(3) Overall, it is found that no significant effect for arrangement density of weft yarns in the auxetic textile structures will affect the deformation behaviors of 3D auxetic composites in the compression tests.

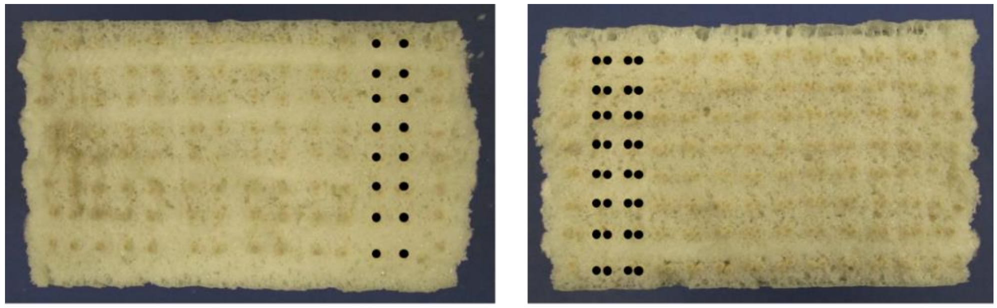

(a) (b)

Figure 4- 6 y-z cross section of 3D auxetic textile composites (a) with half-arranged weft yarns; (b) with full-arranged weft yarns

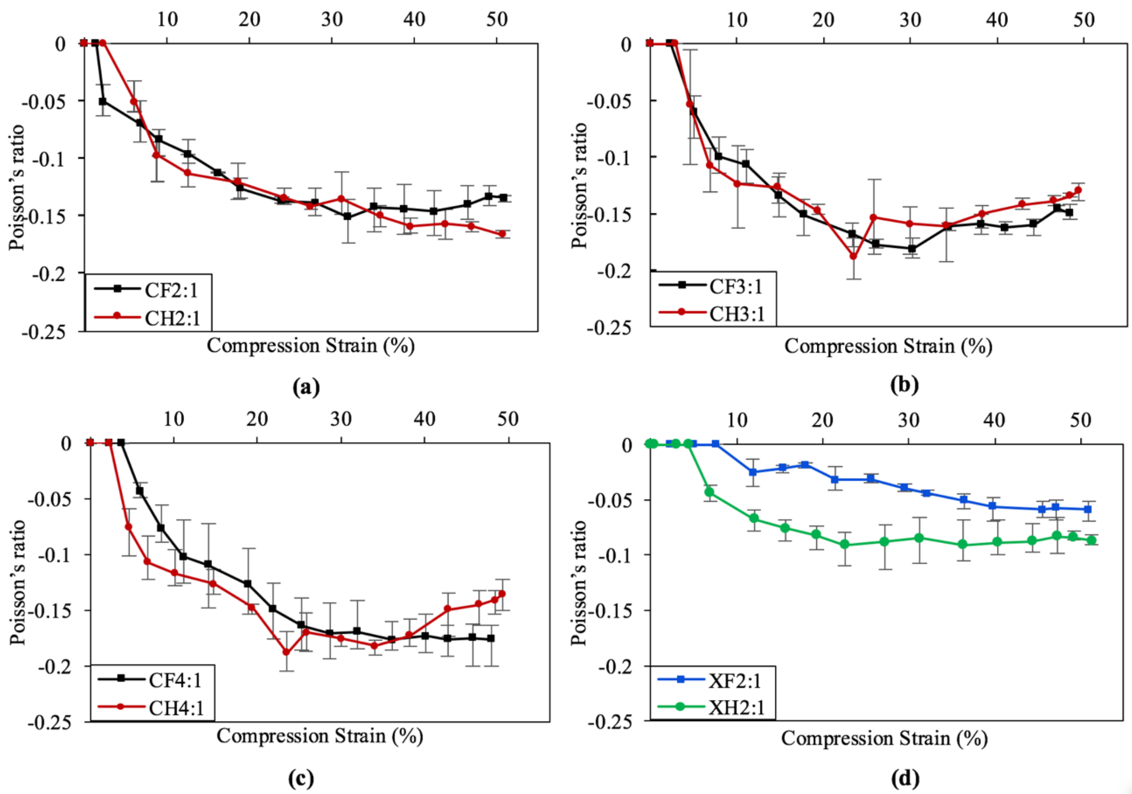

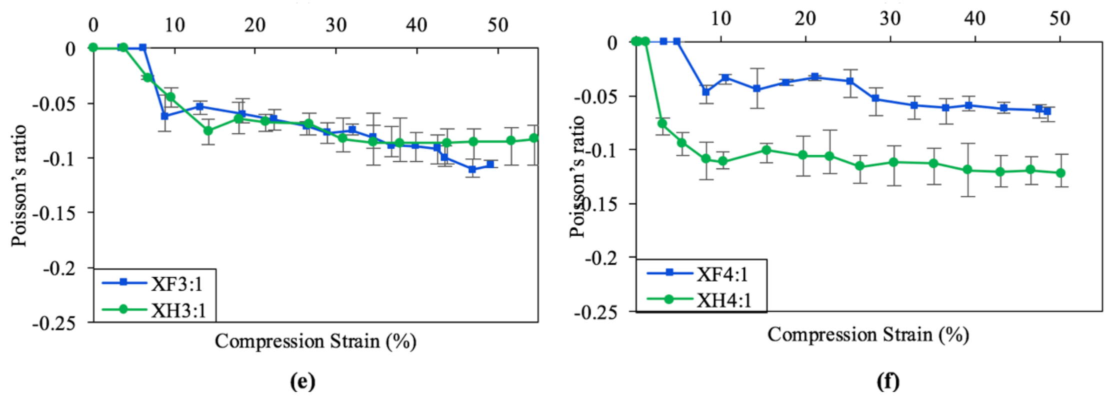

Figure 4- 7 The PR-compression strain curves of different series of 3D textile auxetic composites based on varied arrangement density of weft yarns (a) CF 2:1 & CH 2:1; (b) CF 3:1 & CH 3:1; (c) CF 4:1 & CH 4:1; (d) XF 2:1 & XH 2:1; (e) XF 3:1 & XH3:1; (f) XF 4:1 & XH 4:1

4.3.3.3 Auxetic behaviors in different proportions of A/B PU foams

A group of auxetic composites produced with same diameters of warp yarns in comparison (4mm and 6mm) and same arrangement of weft yarns (full- and half-arranged) but with different proportions of PU foams (A: B are 2:1, 3:1 and 4:1, respectively) are investigated under compression. The obtained results are used to analyse the effect of proportions of PU foams on the deformation behaviors of 3D auxetic textile composites. The PR- compression strain curves of these auxetic composites (CF, CH, XF and XH) are illustrated in Figure 4-8. The following performance can be observed and summarized.

(1) From Figure 4-8, the auxetic composites with 2:1 proportion have relatively lower NPR. Because the PU foams of auxetic composites with 2:1 proportion are stiffer than those with 3:1 and 4:1, which may require more compression stress with same

compression strain thus having relatively lower NPR.

(2) There are no significant differences between auxetic composites with 3:1 and 4:1. Figure 4-8 shows that they have similar tendency when other structural parameters change.

(3) Overall, there are no significant impact for proportions of PU foams will affect the deformation behaviors of 3D auxetic composites in the compression tests.

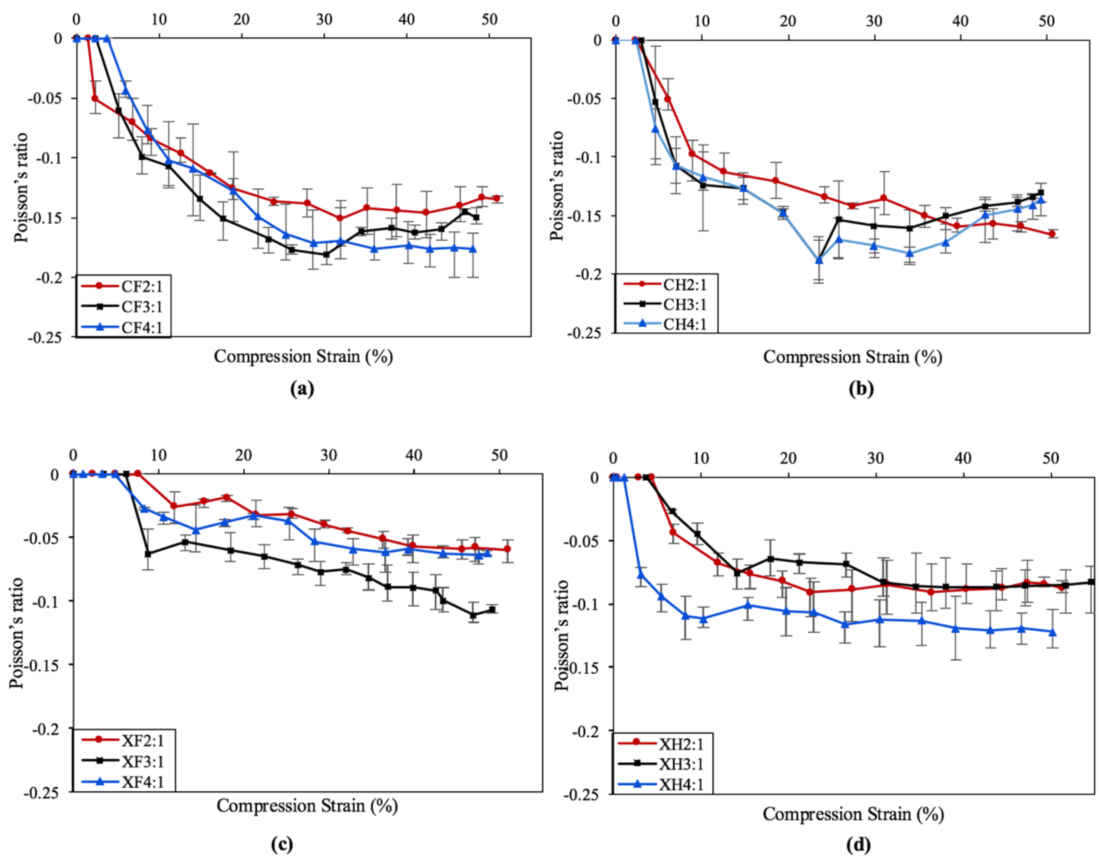

Figure 4- 8 The PR-compression strain curves of different series of 3D textile auxetic composites based on varied proportions of PU foams (a) Series CF; (b) Series CH; (c) Series XF; (d) Series XH

4.3.4 Comparisons of Deformation Behaviors

To compare different types of produced samples including pure PU foam, non-auxetic and auxetic composites. For auxetic and non-auxetic composites, we choose to pick up the samples with same proportions of 3:1 and half-arranged weft yarns but with different warp yarns. The PR versus compression strain calculated from the experimental result for all three types of materials, namely the pure PU foam (E3:1), the auxetic composites (CH3:1 and XH3:1) named as 4mm NPR and 6mm NPR and the non-auxetic composites (ZCH3:1 and ZXH3:1) named as 4mm PPR and 6mm PPR, are shown in Figure 4-9. The PR values of three types of materials are not constant with the increase of compression strain and that the quasi-zero PR effect exists for all three types of materials on the primary stage of compression process. For the pure PU foam, its PR value is zero from 0% to 5% of compression strain and reaches its peak value of 0.103 at the compression strain of 10%. After then, its PR starts to gradually decrease, but still above zero. For the non-auxetic composites, their PR keep zero from 0% to 9% of compression strain and then start to increase but the values do not exceed 0.026. For the auxetic composites, values of the curves remain zero from 0% to 5% of compression strain, and then become negative. It is also found that their NPR values increase with the growth of both the compression strain and diameter of the warp yarns. This quasi-zero PR effect has been confirmed in our previous study. For the self-made pure PU foam, it has the quasi-zero PR in the initial stage of compression due to its particular porous structure. In this stage, the compression mainly causes the decrease of voids sizes in the compression direction, and not in the transversal direction. Thus, the size of the pure foam in the transversal direction almost keeps unchanged. For the auxetic and non-auxetic composites, as the gaps between each layer of textile reinforcements and the peripheries of the reinforcements are filled with the PU foam. At the same time, the compressive modulus of PU foam is much lower than that of the braided cotton yarn and braided polyamide yarn, their deformation at the beginning of compression process is mainly caused by the deformation of the PU foam. As the pure PU foam has quasi-zero PR in the initial phase of compression process, the auxetic and non-auxetic composites have also quasi-zero PR in this stage. However, with the growth of the compression strain, the PU foam starts to be compact and the deformation of composites mainly comes from the textile-reinforced structure. As explained above, for the auxetic composites, the weft yarns will contract when compressed because of the void spaces created by elimination of the warp yarns. However, for the non-auxetic composites, the warp yarns are arranged in each and every layer without any elimination, which can support all the weft yarns to be kept in the straight state under compression. Therefore, the NPRs are obtained for the auxetic composites reinforced with 3D auxetic textile structure and the PPR are obtained for the non-auxetic composites reinforced with non-auxetic textile structure. The results clearly show that textile structure have a crucial role for the deformation behaviors of the composites.

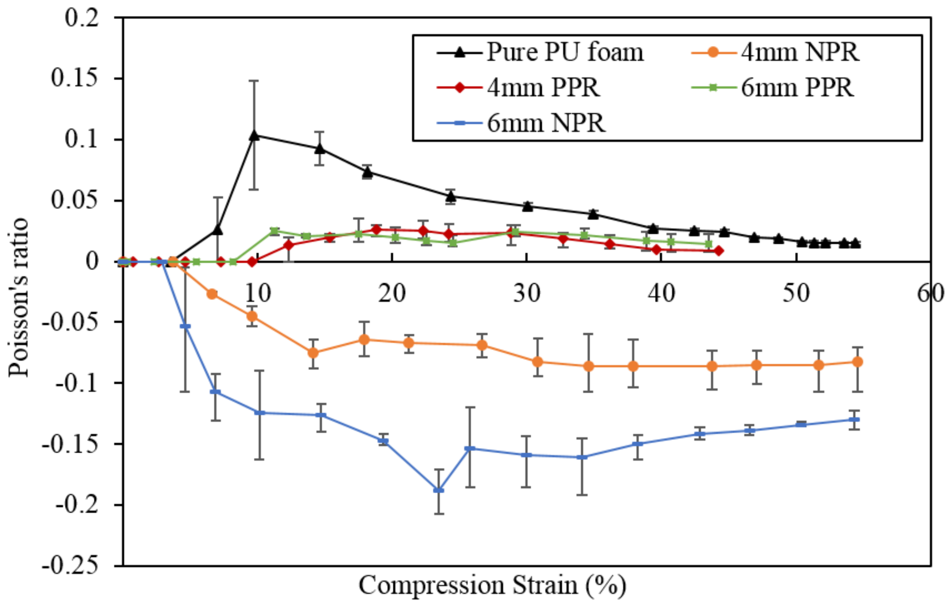

Figure 4- 9 PR-compression strain curves of pure PU foam, auxetic and non-auxetic composites

Figure 4-10 and Figure 4-11 illustrate the lateral deformations of auxetic composites and non-auxetic composites under compression. From Figure 4-10, it is obvious that the auxetic composite transversely crimps under vertically loading. This effect is caused by the crimping of the weft yarns in the x-z plane, as depicted in Figure 3-2(a). On going from (a) to (c) of Figure 4-10, with growth of the compression strain, the weft yarns tend to be more crimped, resulting in an increase of shrinkage of the composite, and thus the dimension along the x-direction is decreasing. However, on going from (c) to (d) of Figure 4-10, the NPR values remain stable and start to slightly decrease from 35% to 55% of compression strain because the void spaces of auxetic composites are gradually filled under compression. The value of L in (d) is less than the L_0 in (a) with the increasing compression strain, which suggests that the dimension along x-direction is increasing but remain decrease compared to its initial state. Moreover, an increase of the warp yarn diameter allows a larger displacement of the weft yarns in the compression direction, causing a higher shrinking of the composite at the same compression strain. Therefore, increasing the diameter of the warp yarns can contribute to an increase of auxetic behaviors of the composite.

However, for the non-auxetic composites, the influence of the yarn diameter on the PR is not very evident. As illustrated in Figure 3-2(b), as all warp yarns are arranged vertically in the loading direction, the weft yarns can keep a straight form under compression. As shown in Figure 4-11, at the lower compression strains under 9%, as the warp yarns which are arranged vertically well support the weft yarns and the weft yarns cannot be crimped, the PR of composites are quasi-zero. However, after the compression ratio exceeds 9%, on one hand, the cross-section of the warp yarns changes from the circular form to the elliptic form with increased compression stress. On the other hand, the warp yarns arranged in vertical lines start to lose their stability and the warp yarns located in the central layer shift towards the left or right side of the composite, causing an increase of composite size along the horizontal direction in x-z plane. As a result, the PR values become positive. It turns out that although the auxetic and non-auxetic composites consist of the same matrix materials and structural parameters, their deformation behaviors is significantly different due to varied arrangement methods of the warp yarns in the 3D textile reinforced structure. While the auxetic composites have NPRs with a very stable composite structure, the non-auxetic composites have zero and PPR with instable composite structure.

To know the experimental errors, the error bars are also inserted in Figure 4-9 for each

PPR value. In the initial stage of compression strain, the error range is relatively large for three types of materials. With compression of the PU foam, their PR values tend to become relatively stable. The largest standard deviations for composites 4mm NPR, 6mm NPR, 4mm PPR, 6 mm PPR and PU foam are 1.9%, 4.1%, 0.9%, 0.9% and 4.4% respectively, which all happened between 0% and 20% of compression strain except for 4mm NPR that happened at 33% of compression strain. For the pure PU foam, the error ranges are much higher at lower compression strain due to the non-uniform distributions of voids in its structure. However, as compression strain, the PU foam is getting compact and the error ranges decrease. For the non-auxetic composites, as the compression loads are mainly supported by the warp yarns and the variations in the measurement of the deformation of the cross section of the warp yarns is smaller, lower errors of the results are obtained. For the auxetic composites, they have a wider range of error than that of non-auxetic composites. Although the three samples of each type of auxetic composite are fabricated and tested in the same experimental condition. There are avoidable differences in their NPRs coming from factors such as voids in the self-fabricated PU foams, the gaps between the warp yarns and weft yarns in inner auxetic structures, the deformation process of inner 3D auxetic structures due to crimping of weft yarns under compression, etc.

Compared with the nodule-fibril (NF) model proposed by Alderson et al[23], the results obtained for the auxetic composites in this study have the similar trends, that is, the NPR values increase with the compression strain increasing in the beginning of compression process, because both structures have the similar deformation mechanisms as explained before. In the second and third stage of the NF model, the PR curve shows a steep increase to zero before achieving a plateau with positive values. Although the changes of PR from negative to zero and then even to positive have not been observed in the present study due to limitation of experimental condition, it is expected that the same phenomenon could be obtained if auxetic composites continue to be compressed to a much high compression strain.

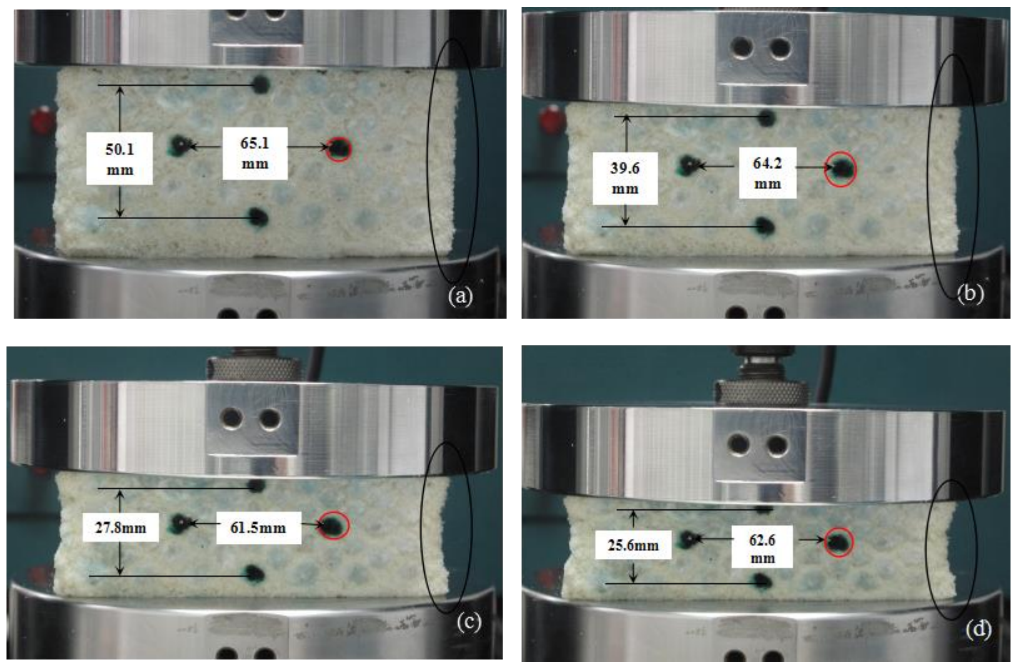

Figure 4- 10 Lateral deformation of auxetic composites under compression strain (a) 0%; (b) 13.450%; (c) 35.98%; (d) 54.36%

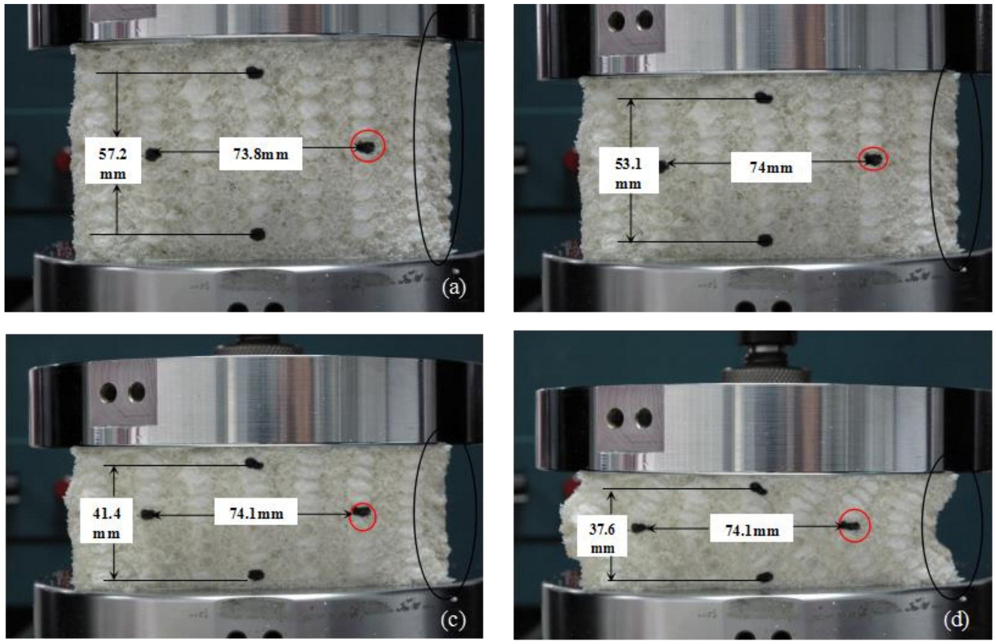

Figure 4- 11 Lateral deformation of non-auxetic composites under compression strain (a) 0%; (b) 12.60%; (c) 42.39%; (d) 45.57%

4.4 Compression Properties in Quasi-static Compression Test

4.4.1 Compression Properties of PU Foams and 3D Non-auxetic Composites

The compression stress-strain curves of the pure PU foams based on different proportion of A/B are shown in Figure 4-12. The curves of the foams are varied. The deformation of E2:1 is much higher than that of E3:1 followed by E4:1. The reason is that three types of pure PU foams have different proportions of A and B. As mentioned above, the proportions of A and B may affect the elastic resilience of the pure PU foam samples. If the proportion of A is lower, the pure PU foam will be stiffer. Therefore, E2:1 requires more compression stress than E3:1 and E4:1.

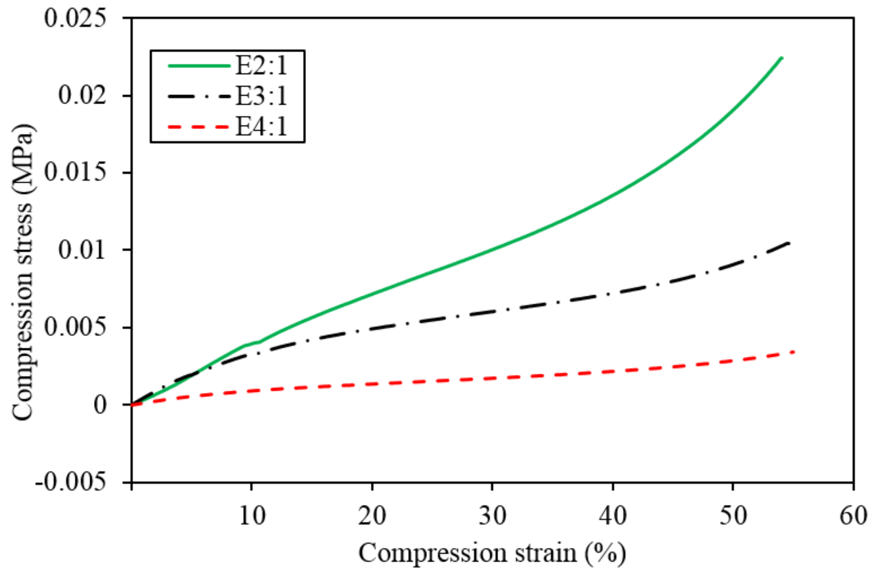

Figure 4- 12 The compression stress-strain curves of pure PU foams: E2:1, E3:1 and E4:1

4.4.2 Compression properties of 3D Non-auxetic Composites

Figure 4-13 shows the compression stress-strain curves of 3D non-auxetic composites: ZCH3:1 and ZXH3:1. The two types of non-auxetic composites are with the same weft yarn arrangement and proportion of A/B PU foam. Due to different diameters of warp yarns, ZCH3:1 with 6mm warp yarns is stiffer than ZXH3:1 with 4mm, resulting in higher compression stress with same compression strain. Therefore, the diameters of warp yarns affect the PR of non-auxetic composites.

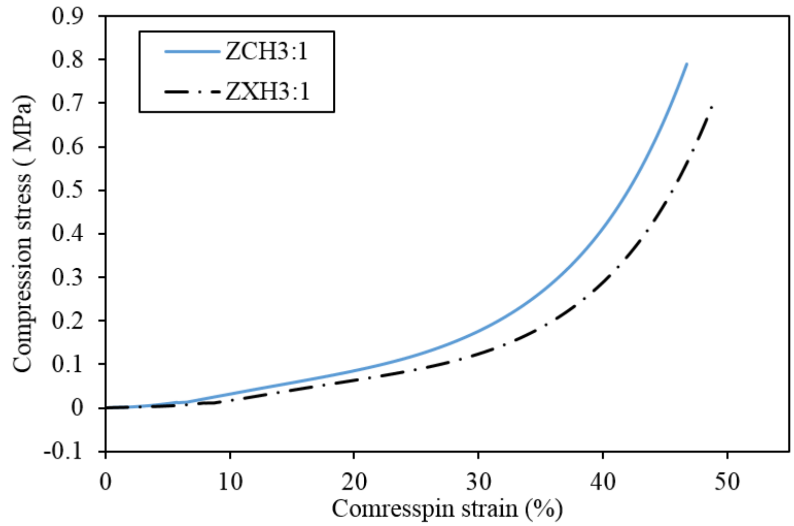

Figure 4- 13 The compression stress-strain curves of 3D non-auxetic composites: ZCH3:1 and ZXH3:1

4.4.3 Compression Properties of 3D auxetic Composites

4.4.3.1 Compression Properties in Different Diameters of Warp Yarns

Figure 4-14 shows the compression stress-strain curves of different series of 3D textile auxetic composites based on varied diameters of warp yarns. Figure 4-14(a)-(c) shows the auxetic composites with full-arranged weft yarns and same proportions of PU foams but with varied diameters of warp yarns, from which basically the auxetic composites with 6mm warp yarns have higher compression stress than those with 4mm warp yarns with the same compression strain. Figure 4-14(d)-(f) shows the auxetic composites with half-arranged weft yarns and same proportions of PU foams but with varied diameters of warp yarns, from which similar effect from Figure 4-12(a)-(c) can be observed. Therefore, for the auxetic composites with different diameters of warp yarns, ones with 6mm require relatively higher compression stress than those with 4mm.

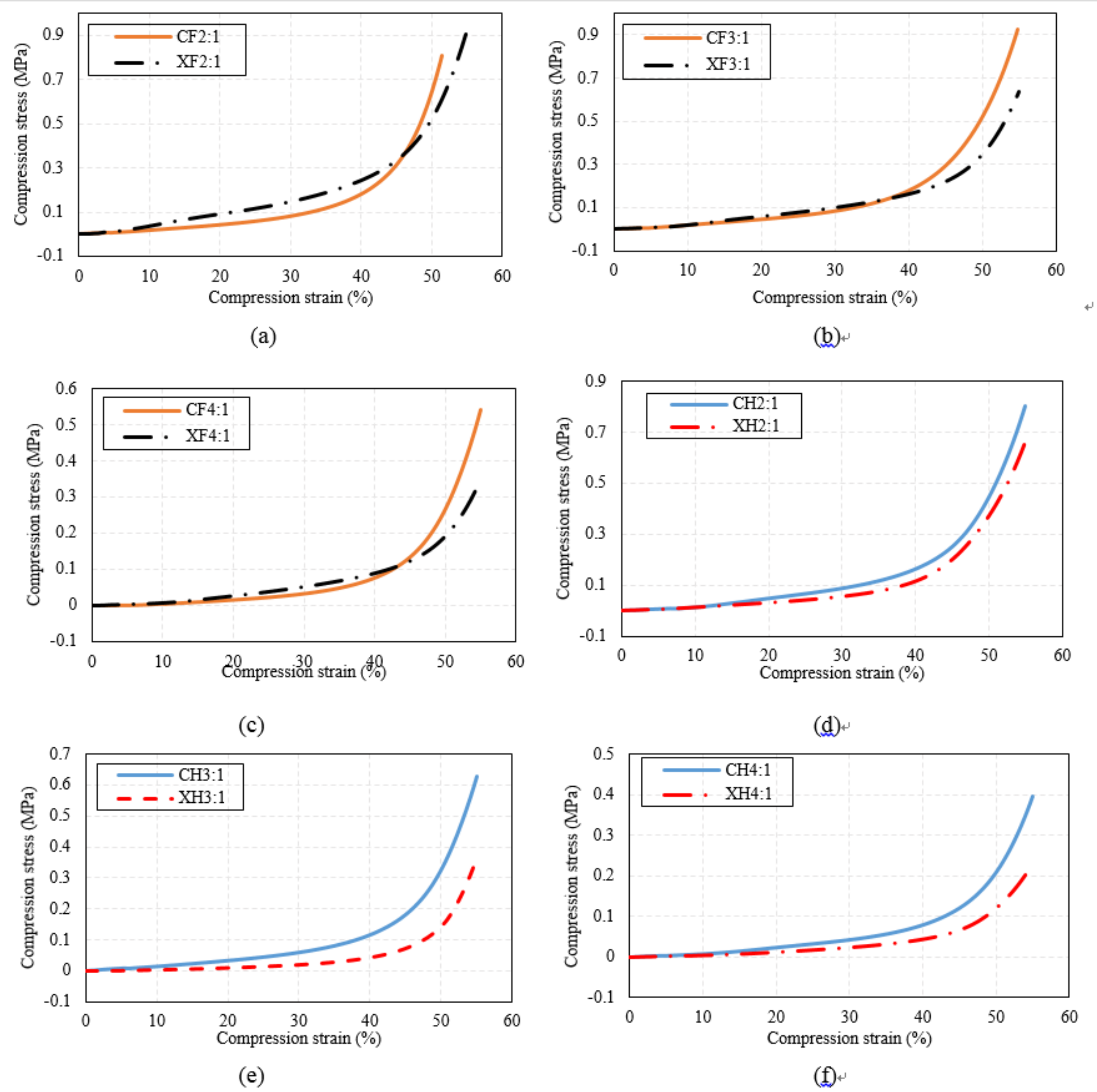

Figure 4- 14 The compression stress-strain curves of different series of 3D textile auxetic composites based on varied diameters of warp yarns (a) CF 2:1 & XF 2:1; (b) CF 3:1 & XF 3:1; (c) CF 4:1 & XF 4:1; (d) CH 2:1 & XH 2:1; (e) CH 3:1 & XH3:1; (f) CH 4:1 & XH 4:1

4.4.3.2 Compression properties in different arrangement of weft yarns

Figure 4-15 shows the compression stress-strain curves of 3D auxetic composites based on different arrangement of weft yarns. Figure 4-15(a) to (c) show the auxetic composites with 6mm warp yarns and same proportions of PU foams but with different arrangement of weft yarns, and Figure 4-15(d) to (f) shows those with 4mm warp yarns. From Figure 4-15, the auxetic composites with full-arranged weft yarns require relatively higher compression stress than those with half-arranged. As mentioned above, the weft yarns of auxetic composites will crimp by action of warp yarns under compression. So for the auxetic composites with different arrangement of weft yarns, ones with full-arranged require relatively higher compression stress than those with half-arranged.

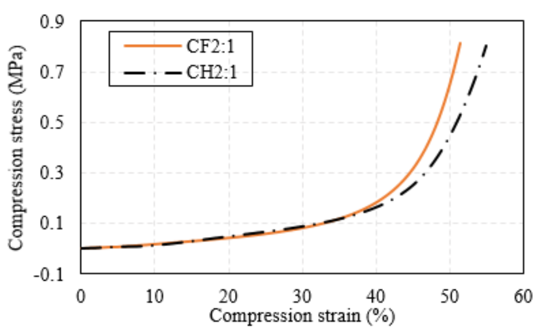

(a)

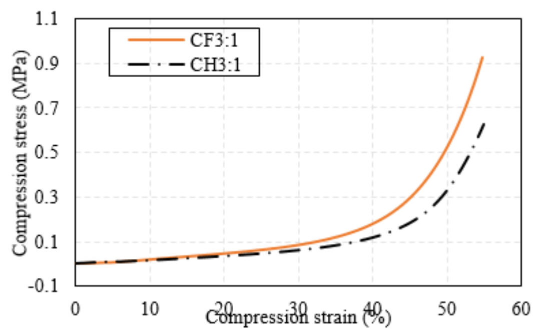

(b)

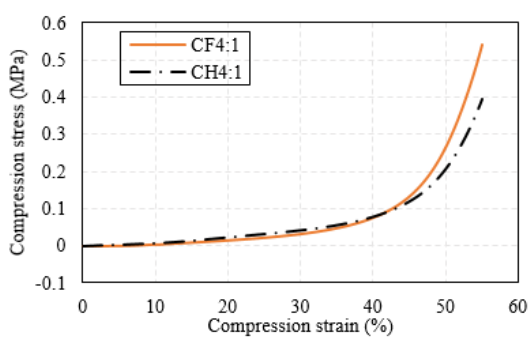

(c)

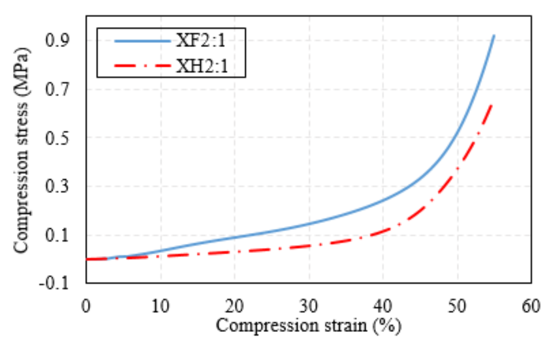

(d)

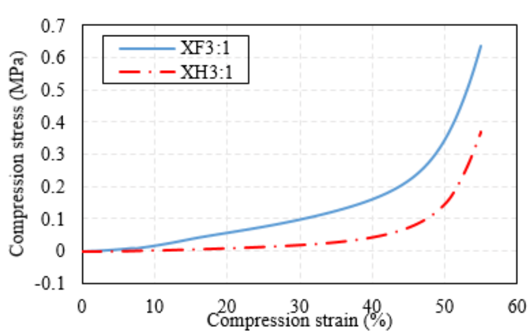

(e)

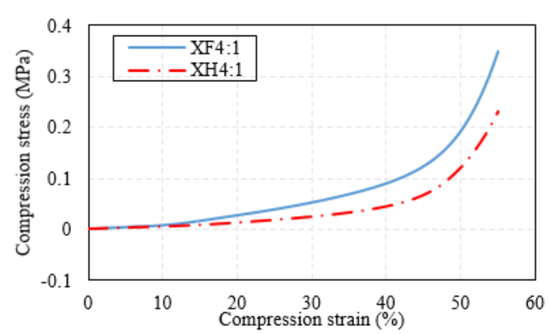

(f)

Figure 4- 15 The compression stress-strain curves of different series of 3D textile auxetic composites based on varied arrangements of weft yarns (a) CF 2:1 & CH 2:1; (b) CF 3:1 & CH 3:1; (c) CF 4:1 & CH 4:1; (d) XF 2:1 & XH 2:1; (e) XF 3:1 & XH3:1; (f) XF 4:1 & XH 4:1

4.4.3.3 Compression properties in different proportions of PU foams

Figure 4-16 shows the compression stress-strain curves of auxetic composites based on varied proportions of PU foams, from which it can be seen that the auxetic composites with the proportions of 2:1 have relatively higher compression stress than those of 3:1 followed by those of 4:1. As previously explained, the composites with 2:1 proportions are stiffer than those of 3:1 and 4:1. Therefore, if the proportion of A in PU foams is lower in auxetic composites, they will require higher compression stress with same compression strain.

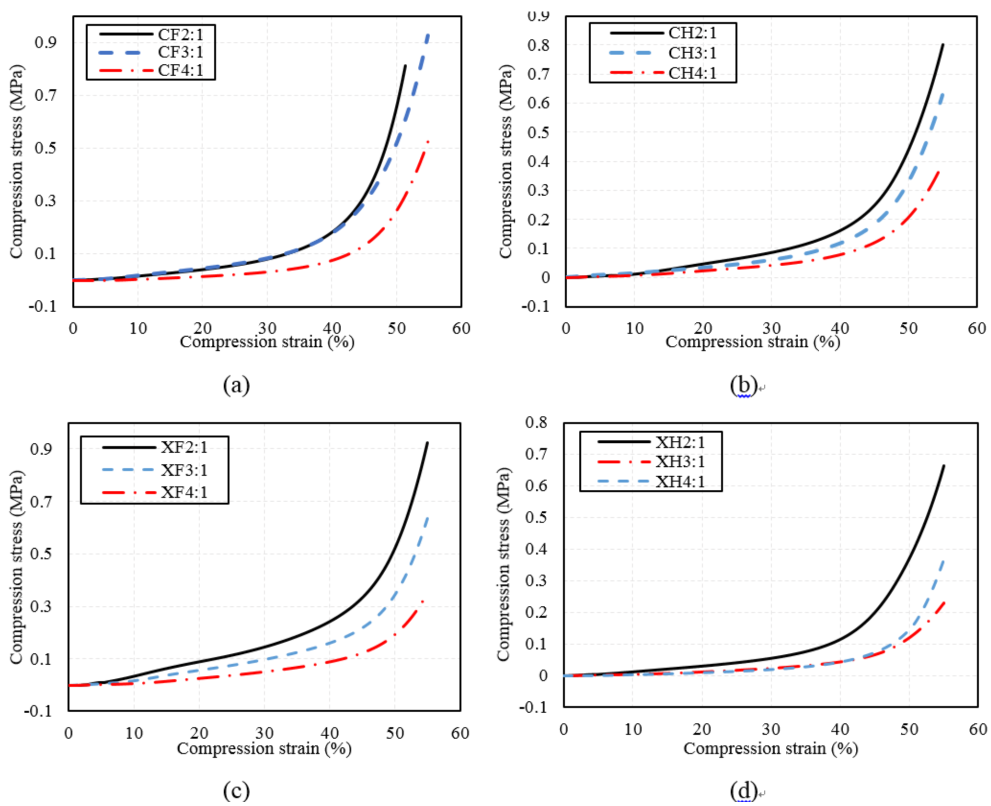

Figure 4- 16 The compression stress-strain curves of different series of 3D textile auxetic composites based on varied proportions of PU foams (a) Series CF; (b) Series CH; (c) Series XF; (d) Series XH

4.4.4 Comparisons of Compression Properties

The compression stress-strain curves of the pure PU foam, auxetic and non-auxetic composites, as depicted in Figure 4-17, exhibit different compression behaviors. As presented in Figure 4-17, the pure PU foam, which is used as the composite matrix, has the lowest compression value among the three types of materials. It has only a maximum value of $4.8\text{x}10^{-3}$MPa at the strain of 55%. Compared to composite materials, the pure PU foam behaves more flexible and has a larger deformation range. However, the easy deformation of the PU foam when compressed makes the auxetic composites easily shrunk in the lateral direction when compressed. As the arrangement method of warp yarns in the inner 3D auxetic textile structure allows the weft yarns to be easily shrunk in the x-z plane, the deformation of auxetic composites is much higher than that of non-auxetic composites under the same compression load, which indicates that the non-auxetic composites are much stiffer than the auxetic composites.

Compared to the compression behaviors of the non-auxetic and auxetic composites reported by Jiang and Hu et al.[24], the auxetic composites in this study have similar tendency, but the non-auxetic composites have different behaviors. The reason is that the materials used in two studies are different. Jiang used hollow ABS tubes as warp yarns that are more rigid and easier to be buckled under compression when they are arranged in a vertical line. However, in the current study, the braided yarns with lower bending modulus are used and their cross-sections are easy to be deformed under compression. Besides, the PU foam used in the previous study is much stiffer than the elastic compressible PU foam used in this study.

As illustrated in Figure 4-17, the compression stress-strain curves of auxetic composites can be generally divided into three phases according to the change of the slope of the curves. At the initial phase, a low slope is observed between the strain of 0% and 10% due to the compression of PU foam in gaps and outer layers and its ineffective constraint for the inner auxetic structure. When the composites are further compressed into the second phase ranging from 10% to 40%, the compression stress rise slightly and a quasi-plateau area is formed. The compression strain after 40% is the third phase. In this phase, the compression stress significantly goes up due to the compaction of the composite structure. Compared to the auxetic composites, the quasi-plateau region in the deformation of non-auxetic composites is not found. In this case, the deformation process could be divided into two stages. As presented in Figure 4-17, the first phase is a gradual growth of the compression stress from 0% to about 30% of compression strain, in which the change in the cross section of the warp yarns from the circular form to the elliptic form could be visually observed. The second stage starts from about 30% of compression strain. In this phase, the compression stress rapidly increase and the warp yarns tend to get misaligned under compression. Although the test compression strain was set up to 55%, the compression tests were stopped before 55% as the compressive loads reached the capacity of the testing device. As arranged vertically in the non-auxetic composite structures, the warp yarns play a critical part in standing load during the static compression procedure, which leads to a more dramatic growth of the compression stress and a lower deformation of non-auxetic composites. This arrangement method also makes non-auxetic composite stiffer than the auxetic composite.

As presented in Figure 4-17, it can be also found that the influence of warp yarn diameter on the compression behaviors of composites is much less important than their arrangement in the textile structures. For the auxetic composites, as the warp yarns are not arranged vertically, the compression loads result in bending of the weft yarns in the initial stage and quasi-plateau stage. Therefore, the influence of warp yarn diameter is very low. However, the influence of the warp yarn diameter for the non-auxetic composites is more evident as the warp yarns withstand the compression load due to their arrangement method in the form of the vertical lines. In this case, as the 6mm warp yarn is easier to get flattened than the 4mm warp yarn, the compression stress of the composite made of textile structure with 4mm warp yarn is higher than that of the composite made of textile structure with 6mm warp yarn within the same compression strain.

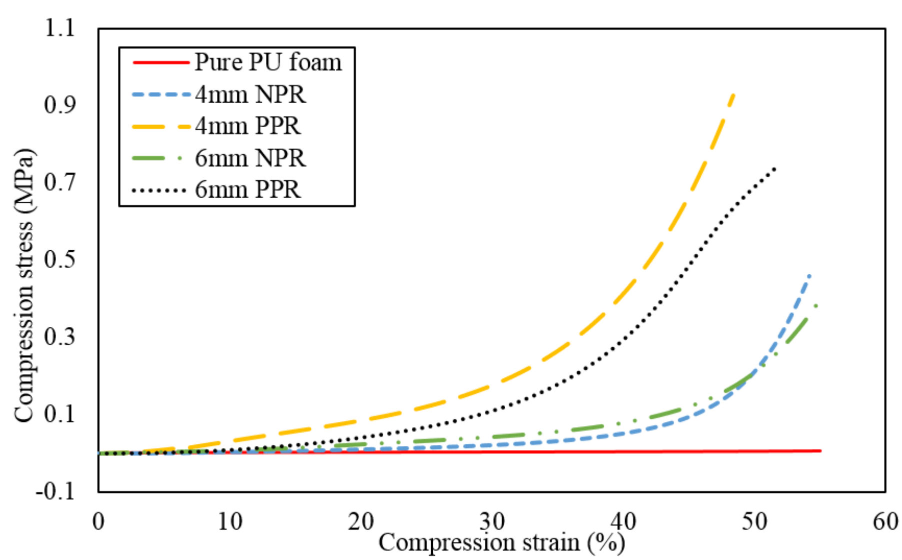

Figure 4- 17 Compression stress-strain curves of pure PU foam, auxetic and non-auxetic composites with 4mm and 6mm warp yarns

4.5 Repeated Quasi-static Compression Test

4.5.1 Deformation Behaviors in Repeated Quasi-static Compression Test

Figure 4-18 exhibits the variation of PR of auxetic composite 6mm NPR at different compression strains when subjected to repeated compression tests. It can be seen that the NPR values of the composite at all four compression strains decrease from the first compression cycle to the second one, but they turn to remain steady after the second compression cycle. The result suggests that the retention of the NPR effect of auxetic composites is critical. The solution to enhance the retention property of NPR of 3D textile composites might be to use foams with high elastic and recovery property to fabricate the matrix.

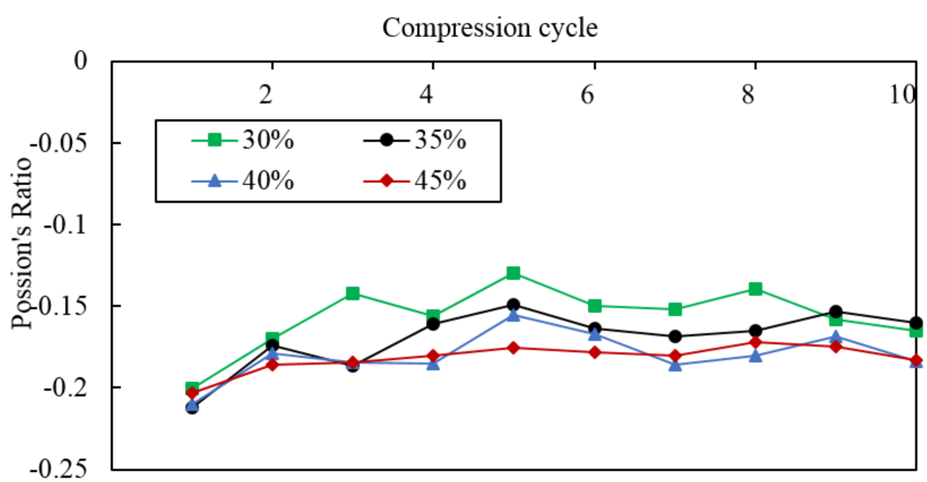

Figure 4- 18 Variation of PR under repeated compression condition

4.5.2 Compression Properties in Repeated Quasi-static Compression Test

Figure 4-19 presents the compression stress-strain curves of the 4mm and 6mm auxetic composites under the repeated compression testing condition. It can be seen that the decline of compression stress of the composites after the first compression cycle is evident. After the first compression cycle, the compression behaviors of the composites tends to be stabilized. The similar behaviors was observed for most of auxetic composites. The non-auxetic composites were not suitable for repeating compression test because the warp yarns would get misaligned when increasingly compressed. The retention of the compression behaviors mainly depends on the elastic recovery of the PU foam. Therefore, to get stable compression behaviors of auxetic composite under repeating compression, PU foam with high elastic recovery is required.

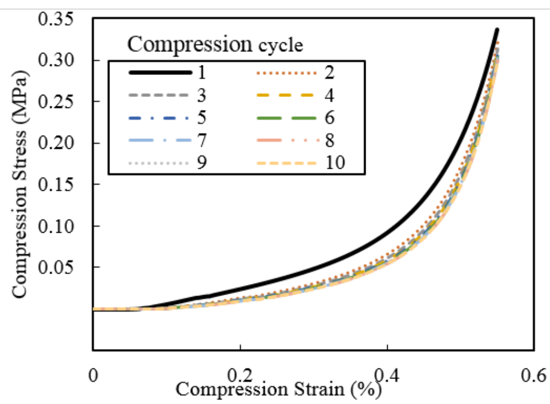

(a)

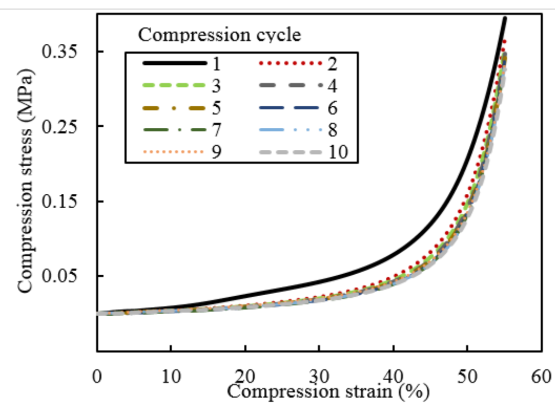

(b)

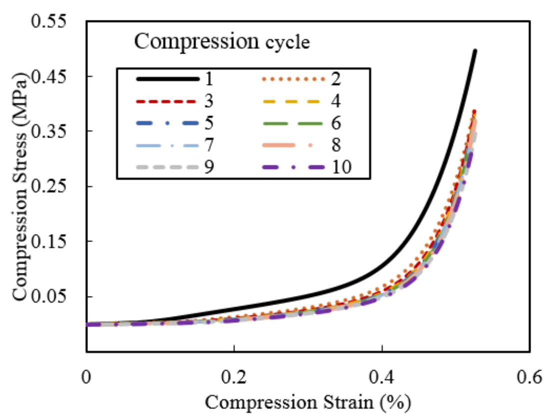

(c)

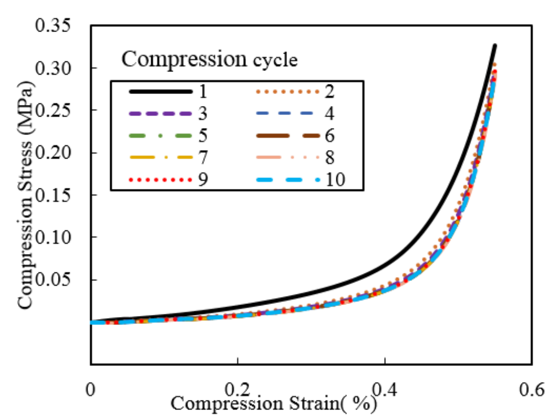

(d)

Figure 4- 19 Compression stress-strain curves of auxetic composites under repeating compression condition (a) 6mm NPR sample 1; (b) 6mm NPR sample 2; (c) 4mm NPR sample 1; (d) 4mm NPR sample 2

4.4 Conclusions

A series of produced samples including pure PU foams, 3D auxetic and non-auxetic composites were tested on compression testers. Both deformation behaviors and compression properties were measured and analyzed. The effects of different structural parameters, including diameter of warp yarns, arrangement of weft yarns and proportion of A/B PU foams, on the deformation behaviors of the 3D auxetic textile composites were analyzed based on the PR-compression strain curves. The deformation behaviors and compression properties of auxetic composites were also tested and evaluated.

CHAPTER 5 LOW-VELOCITY IMPACT PROPERTIES OF 3D AUXETIC AND NON-AUXETIC TEXTILE COMPOSITES

5.1 Introduction

In this paper, a further study on their mechanical properties under low velocity impact is presented. Both single-time and repeating impact tests were conducted under different impact energy ranging from 12.7 J to 25.5 J. Results showed that the 3D auxetic textile composite shows better impact protective performance than the 3D non-auxetic textile composite because of better transmitted force reduction and higher energy absorption capacity under single-time impact and higher structural stability under repeating impacts. Moreover, the stress hardening effect under impact was observed for the auxetic composite, which could enhance its impact protection properties with increasing of impact velocity

5.2 Low-velocity Impact Tests

5.2.1 Low-velocity Single Impact Tests

The low-velocity impact test equipment used was a drop-weight impact tester KD-3168-E provided by King Design Company in Taiwan. As shown in Figure 5-1, the impact tester used a drop striker with a 150mm circular flat surface at impact side. The total weight of the striker was 6.5kg. The drop striker was instrumented with an ISOTRON accelerometer (with a sensitivity of 9.929mV/g and a measured range of ±500g) to measure the acceleration. The transmitted force was measured by a load cell (with a sensitivity of 4.171mV/g) installed on a massive base with a weight of 1000kg. The sample was stuck on the anvil installed on the base. All the measurement signals were recorded by a high-speed data acquisition card NI6040E having recording frequency of 80kHz.

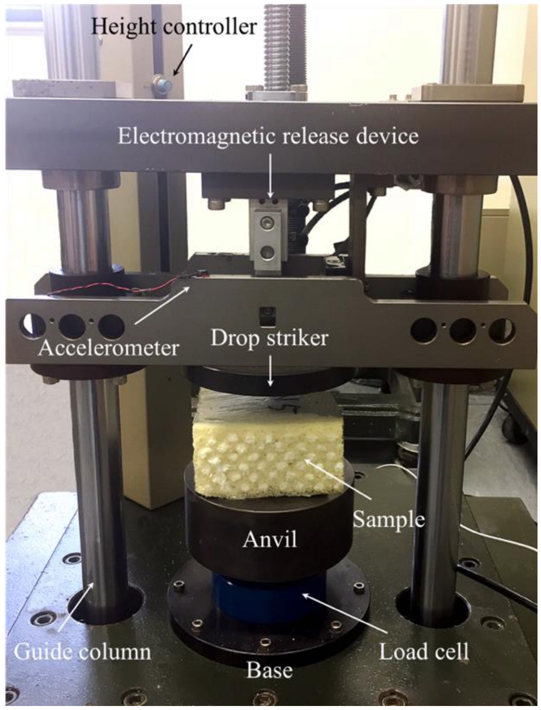

Figure 5- 1 Drop-weight impact tester

The impact tests were performed according to ASTM D 1596-97 (Standard Test Method for Dynamic Shock Cushioning Characteristics of Packaging Material). It is based on the drop-weight principle using a low-energy and a low-speed impact tester that can measure the changes in acceleration of the drop striker and the force transmitted from the top side to the bottom side of the specimen. The transmitted force is obtained directly from the load cell. Nevertheless, the contact force is proportional to the measured acceleration and can be calculated from Newton's second law. Because it is freely falling, the maximum velocity of the striker is determined by the drop height when the striker just falls onto the top surface of the sample. Using the maximum velocity of the striker as the initial value, the velocity of the striker can be calculated by integrating the acceleration of the striker after it has contacted the sample. Meanwhile, the impact displacement can be obtained by integrating this velocity of the striker, assuming the time is zero when the initial contact occurs. Due to the slightly difference in the thickness of each specimen, the impact strain and compression strain will be used for analysis and comparison. All specimens of 3D auxetic and non-auxetic composites are approximately 10cm × 10cm × 6cm. Before impact tests, all the tested specimens are preprocessed in an environment of 20℃ and 65% relative humidity. The auxetic and non-auxetic composites were first carried out under constant impact tests parameters with the same impact energy (19.1J) and impact velocity (1.98m/s) to test their stability. After that, both auxetic and non-auxetic composites were tested with varied impact energy (from 12.7J to 31.9J) to make a comparison on their impact protection properties. Meanwhile, the quasi-static compression was also tested on an Instron 5566 Universal Testing Machine at a speed of 30mm/min up to 55% deformation strain to measure their PR and assist to investigate the impact protection ability. The detail compression test conditions can be found in [148].

The transmitted force is generated from the load cell. And the contact force is proportional to the acceleration and can be calculated from Newton's second law:

$$F = ma \tag{1}$$

Where m is the mass of the drop striker (6.5kg) and a is the acceleration

The velocity and displacement of the strikers can be calculated by acceleration and time according to the following equations:

$$v = \sqrt{2gh} - \int a dt \tag{2}$$

$$s = \sqrt{2ght} - \int(\int adt)dt \tag{3}$$

Where v is the velocity, s is the displacement, a and t are acceleration and time, respectively. And h is the initial height of the striker. Due to the slightly different thicknesses of each specimen, the impact strain and compression strain will be used for analysis and comparison.

In order to investigate the energy absorption ability, it is necessary to define the Energy absorption capacity (E_a). The energy absorption can be calculated as followed:

$$Ea = \int_0^s F(x)ds \tag{4}$$

Where s is the displacement and F denotes the impact force

5.2.2 Low-velocity Repeated Impact Tests

One of interesting research areas of auxetic and non-auxetic composites is the mechanical properties and structure stability under repeated impact conditions, which will have influence in the impact behaviors during repeated uses. The peak transmitted force is a critical parameter to estimate the protective performance of composite materials. It is crucial to know how much peak contact force can be transmitted to the bottom side. To evaluate the structural stability under continuous impact, the repeating impact tests were conducted for both of the auxetic and non-auxetic composite with two impact energy levels (19.1J and 31.9J). Due to the time required for striker to go back to its initial impact height, the time interval between two impacts was 30s.

5.2.3 Treatment of the Acceleration and Transmitted Force Signals

In this work, fast Fourier transform with a low-pass filter was used for filtering the acceleration and transmitted force data of samples under impact tests. Figure 5-2 shows the contact acceleration time and transmitted force–time curves of a tested sample in both original and filtered form at a set cut-off frequency of 400 Hz. The cut-off frequency was determined according to MIL-STD-883F Method 2002.4, which indicates that a cut-off frequency of a half-sine waveform should be at least five times of the fundamental frequency of the shock pulse. As shown in Figure 5-3, this method also indicates that the pulse duration should be measured between the point at 10% of the peak acceleration during the rising time and the point at 10% of the peak acceleration during the decaying time. Meanwhile, the impact duration should be measured from the beginning to the end of the whole impact process. Taking a non-auxetic composite under 31.9 J impact energy as an example, as shown in Figure 5-2, the peak acceleration was 487 g; thus, its pulse duration was about 14.2 ms. In this case, the cut-off frequency should be higher than 352 Hz. To meet the standard requirement and to obtain a good presentation, 400 Hz was used for this sample. Also as shown in Figure 5-2, the data of the contact acceleration and transmitted force were filtered in such a way that noise was removed, but there was sufficient signal remained for the analysis of the curve features. It can be seen that the low-pass filter with this cut-off frequency is effective to eliminate the noise.

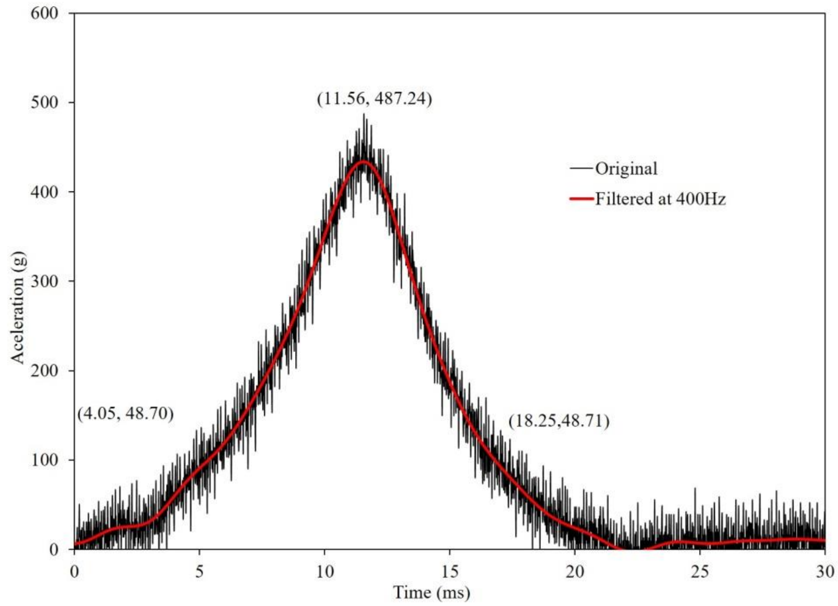

(a)

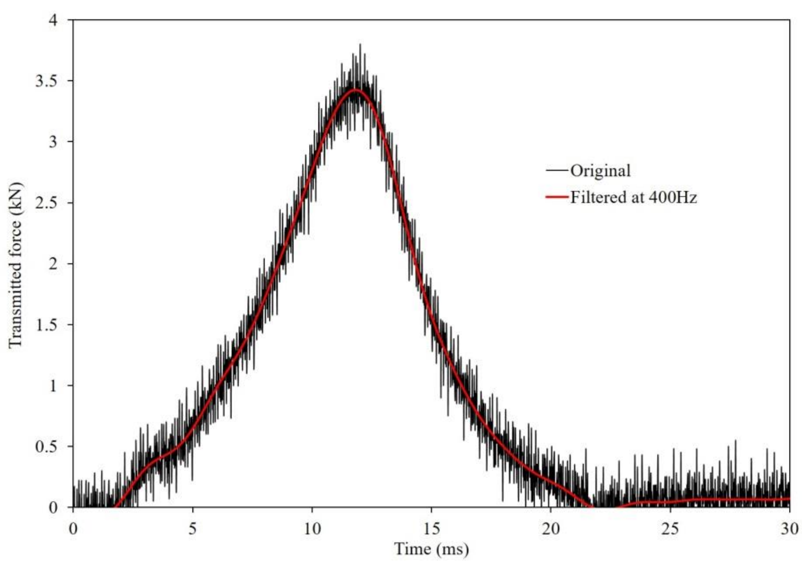

(b)

Figure 5- 2 Signals in original and after filtering for non-auxetic composites under 31.9J impact energy: (a) acceleration; (b) transmitted force.

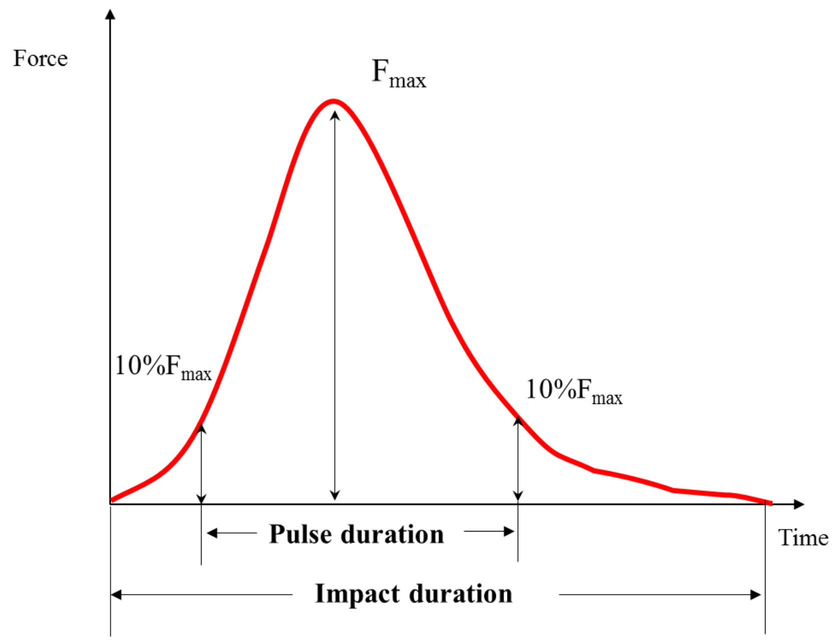

Figure 5- 3 Schematic demonstration of pulse duration and impact duration.

5.2.4 Summary of the Samples under Impact Tests

Based on the previous compression test, it is found that only the diameter of warp yarns is the effective structural parameters for auxetic effect. To further analyze the energy absorption ability of the developed composites, only four groups of samples (CH3:1, ZCH3:1, XH3:1 and ZXH3:1) were chose to be tested under low-velocity impact tests. The auxetic and non-auxetic composites with 6mm and 4mm warp yarns, respectively. To easily understand, the CH3:1, ZCH3:1, XH3:1 and ZXH3:1 were named as 6mm NPR, 6mm PPR, 4mm NPR, 4mm PPR, respectively.

5.3 Impact Process Analysis

Figure 5-4 depicts the representative force–time curves obtained from the low-velocity impact tests for the pure PU foam, the auxetic and non-auxetic textile composites at an impact energy of 19.1 J. Among three different materials, the pure PU foam has the highest peak contact and transmitted force, which are 3.62 and 2.74 kN, respectively. Under the same impact energy, the auxetic textile composite has relatively lower peak contact force and peak transmitted force than those of the non-auxetic textile composite. The peak contact force of the auxetic textile composite is 2.17 kN, which is lower than that of the non-auxetic textile composite (2.47 kN). And the peak transmitted forces of the auxetic and non-auxetic textile composites are 1.55 and 1.92 kN, respectively. Moreover, the impact duration for the PU foam, auxetic and non-auxetic textile composites is 23.3, 26.7 and 25.3 ms, respectively. According to the theorem of momentum, a longer impact duration will result in a lower acceleration and a lower dynamic force. The longer impact duration may help to reduce more force and absorb more energy. Thus, among three types of samples, the auxetic textile composite could help to store the impact energy and then release it over a longer time, resulting in a reduction in the contact force and transmitted force. In addition, compared to the contact force curves, the transmitted force curves are relatively smooth and stable. Thus, the auxetic textile composite shows better force reduction than the non-auxetic textile composite under low-velocity impact, indicating the auxetic textile composite has better impact protective performance than the non-auxetic textile composite.

From Figure 5-4, the force perturbation is also observed in the contact force curve of the auxetic textile composite. It can be seen that there is a sudden force drop (Area A) on the curve, indicating that the weft yarns located at the topside of the auxetic composite are bent by the adjacent warp yarns to cause a force reduction. When the PU foam at the topside is compacted by the bent weft yarns to a certain condition, the impact force begins to increase. As the impact process continues, the force drops occur again in Area

B and Area C, which are also caused by bending of weft yarns in the lower layers. It should be noted that the force drops can result in a reduction in the contact force peak. The contact force drops again after reaching the peak force (2.17 kN) and then rebounds. This trend could be attributing to the recovery ability of elastic PU foam as matrix and the load redistribution of the surviving auxetic composite until the impact load has been removed. For the non-auxetic textile composite, its contact force curve has a clear ascending and descending section, which exhibits the stiffening and softening process of the tested specimen. It can be found that there is a plateau (Area D) at the beginning of the impact loading. The main reason is that the PU foam matrix is compressed, but the yarns in the non-auxetic composite have not been compressed at the initial stage of impact. At this stage, the warp yarns are still kept aligned. With the accumulation of impact energy, the warp yarns lose their stability. In this case, the non-auxetic composite is deformed like a buckled bar. As the impact continues, the curve of the non-auxetic composite continues to rise to the peak contact force (2.47 kN) without fluctuation. As the warp yarns are arranged in the form of vertical lines in the non-auxetic textile composite, the warp yarns mainly bear the impact load, which lead to higher stiffness and higher contact peak force than the auxetic textile composite under the same impact energy.

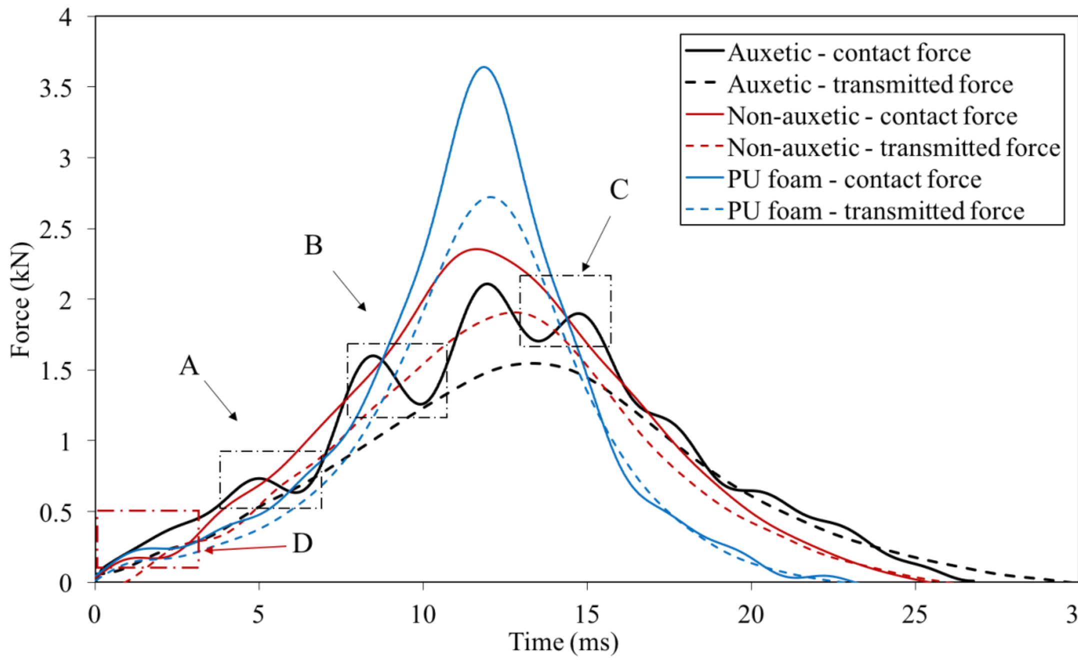

Figure 5- 4Contact force and transmitted force curves of PU foam, 3D auxetic and non-auxetic textile composites. Impact energy = 19.1 J.

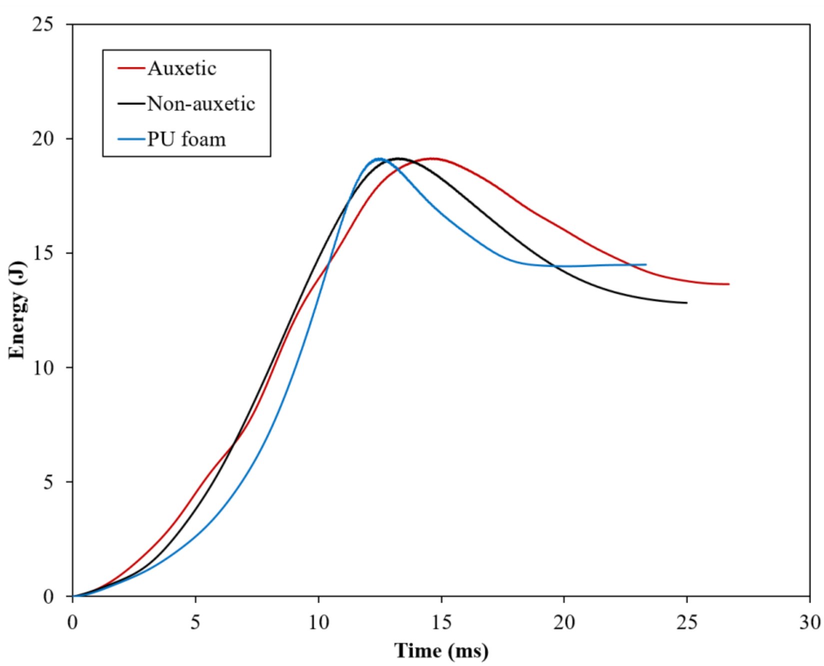

Figure 5- 5 Energy–time curves of PU foam, 3D auxetic and non-auxetic textile composites. Impact energy = 19.1 J.

Figure 5-5 shows the energy versus time curves of the PU foam, auxetic and non-auxetic textile composites when the impact energy is 19.1 J. It can be seen that the impact energy absorption of the auxetic textile composite can be divided into three distinct stages. In the first stage (0–5 ms), the value of absorbed energy is relatively low due to small deformation of the foam matrix and insignificant compression of auxetic textile structure. In the second stage (5–15 ms), the energy–time curve increases rapidly and reaches the peak value (19.1 J), representing the deformation of the reinforced auxetic textile structure and the increase in vertical displacement of the composite structure. At the last stage (from 15 ms to the end), the absorbed energy gradually decreases until the impact process finishes. The whole impact duration of auxetic composite is 26.7 ms. Figure 5-5 also shows that the absorbed energy of the auxetic composite is 14.3 J. For the non-auxetic textile composite, its energy–time curve has similar tendency as that of auxetic textile composite, but the curve of the non-auxetic textile composite reaches its peak value at 13.2 ms and then decreases until the impact ends. The energy absorbed by the non-auxetic textile composite is 12.8 J. The impact process duration of the non-auxetic textile composite is 25.3 ms. For the PU foam, its impact duration is 23.3 ms and its curve reaches the peak value at 12.5 ms. The energy absorbed by the PU foam is 14.5 J. The results show that under the same impact energy, the auxetic textile composite could absorb relatively more energy than the non-auxetic textile composite and PU foam during 15–22 ms of impact process.

Due to the limitation of the test equipment, it was hard to obtain the Poisson's ratio curve of the auxetic textile composite under flat plate impact tests. Therefore, adopting finite element (FE) method to simulate the Poisson's ratio of the composites under impact could be an alternative. According to our previous FE analysis on the 3D auxetic composite made of multilayer orthogonal reinforcement structure, the general variation trends of Poisson's ratio between the quasi-static compression test and the FE impact simulation are the same, but the negative Poisson's ratio value under the quasi-static compression test is higher than that of the FE impact simulation. This difference may come from the hysteresis of impact response. Under the quasi-static compression test, the stress wave is fully propagated among different materials in the composite due to a slow increase rate of compression load (2 mm/min). However, under the impact tests from an impact velocity of 1.50–2.67 m/s, the stress wave could not be transmitted to the distant end of the composite in time, thereby causing the hysteresis of shrinking of the composite in horizontal direction. In other words, the negative Poisson's ratio effect of the auxetic composite from the FE impact simulation is lower than that from the quasi-static compression. On the other hand, the increase in impact energy could lead to an increase in the maximum negative Poisson's ratio value of the composite since higher impact energy could cause higher compression strain. The FE analysis confirmed that the auxetic composite still retains auxetic characteristic under impact although the auxetic effect is lower than that of the auxetic composite under quasi-static compression.

5.4 Impact Compressive Behaviors Analysis

The contact stress–strain curves and energy absorption–strain curves of the pure PU foam, 3D auxetic and non-auxetic textile composites under the same impact energy (19.1 J) are shown in Figure 5-6 and Figure 5-7, respectively. For the comparisons, the compression stress–strain curves and energy absorption–strain curves of these materials under quasi-static compression are also presented in these two figures. Figure 5-6 shows that the mechanical behaviours of three types of materials under quasi-static compression are very different. Among three types of materials, the PU foam exhibits a flexible behavior and has the lowest compression stress. With embedding of textile structures in the PU foam matrix, the compression stress of the textile composites gets considerably enhanced. However, due to different arrangement of warp yarns in the textile structure, two types of textile composites behave differently. It can be seen that the auxetic textile composite deforms much easier than the non-auxetic textile composite due to easier bending deformation of weft yarns under compression of warp yarns. Therefore, the compression stress of the auxetic textile composite is much lower than that of the non-auxetic textile composite for the same compression strain. For the non-auxetic textile composite, as the warp yarns are arranged in the form of vertical lines, it can bear larger compression load than the auxetic composite under quasi-static compression. However, the difference in mechanical properties among three materials diminishes under the low-velocity impact. As shown in Figure 5-6 and Figure 5-7, under the low-velocity impact, although the effect of textile reinforcement is still evident as both the contact stress–strain curve and energy–strain curve of the PU foam are much lower than those of two textile composites, the difference between the auxetic and non-auxetic composites become not so evident as the contact stress–strain curves and energy–strain curves of these two composites get closed. Under the quasistatic compression, the energy absorption of the 3D auxetic textile composite is much lower that of the non-auxetic textile composite for the same strain. But under impact, the energy absorption curves of two types of textile composites are almost overlapped, which means that their difference is small. Under impact, the auxetic textile composite even has a little higher energy absorption than the non-auxetic textile composite due to higher deformation. As explained above, the auxetic composite still has negative Poisson's ratio effect under impact, but this effect is considerably reduced if compared with that of the auxetic composite under quasi-static compression. Therefore, the effect of negative Poisson's ratio on the impact behaviour of the textile composite is reduced, making the auxetic and non-auxetic textile composites have similar responses under impact. However, with the increase in impact energy, the maximum negative Poisson's ratio value of the auxetic composite increases according to the FE simulation. As a result, the effect of negative Poisson's ratio on impact properties will increase too. This phenomenon can be confirmed by Figure 5-8, in which the energy absorption of the auxetic textile composite increases faster than that of the non-auxetic textile composite with the increase in impact energy. The results suggest that under lower impact energy, the PU foam plays more important role than textile reinforcement. But with the increase in impact energy, the role of textile reinforcement becomes more important.

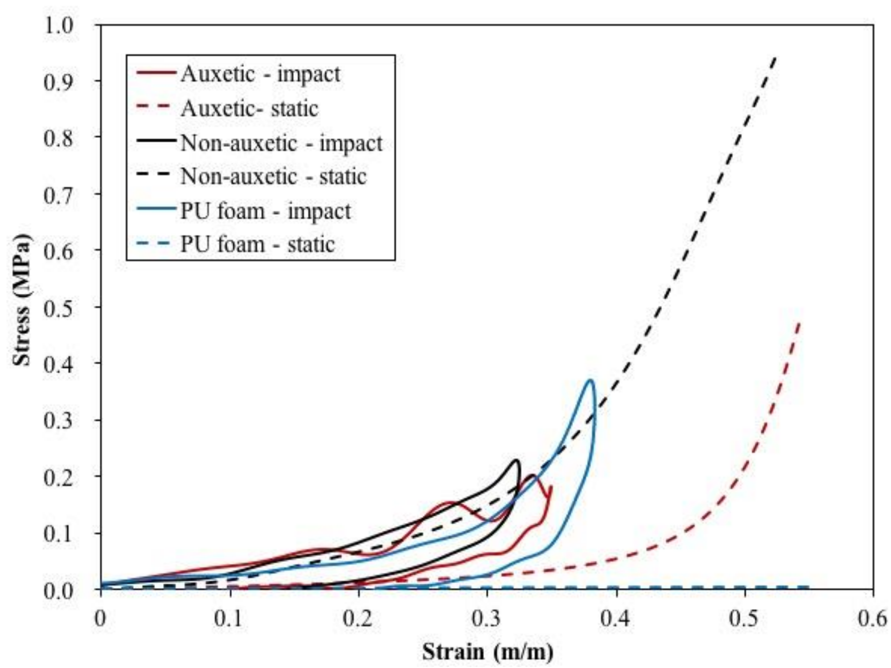

Figure 5- 6 Stress–strain curves of PU foam, 3D auxetic and non-auxetic textile

composites under quasi-static compression and impact tests.

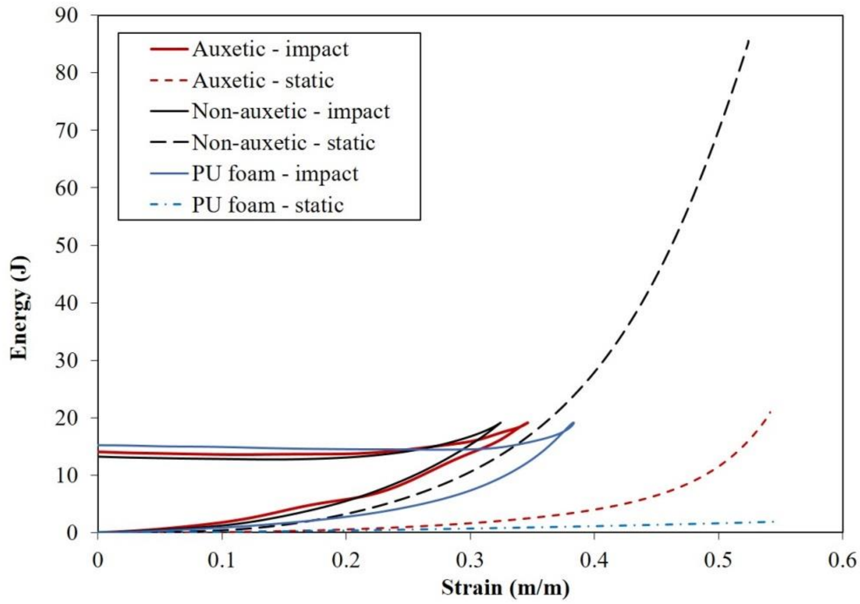

Figure 5- 7 Energy–strain curves of PU foam, 3D auxetic and non-auxetic textile composites under quasi-static compression and impact tests.

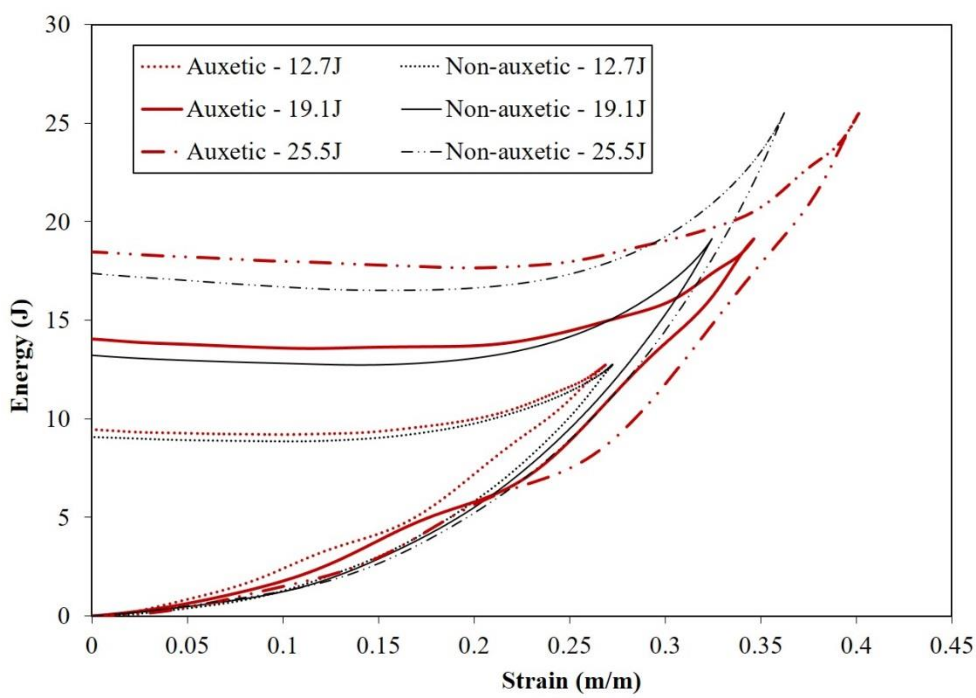

Figure 5- 8 Energy – strain curve of 4mm NPR and 4mm PPR under varied impact energy. The impact energy is 12.7J, 19.1J and 25.5J.

5.5 Effect of Initial Impact Energy

As mentioned above, the peak transmitted force is a critical parameter to determine the impact performance of composite materials. It is critical to evaluate how much peak contact force can be transmitted to the bottom side of composites. The dynamic impact tests were conducted for two cases were evaluated to investigate the impact energy absorption characteristics with varied initial impact energies as the exterior influencing factor. By controlling the heights of impact striker, the initial impact energy varies to be 12.7J, 15.9J, 19.1J, 22.3J, 25.5J, 28.7J, 31.9J respectively. This varies the initial impact height as 250-500mm. For each impact energy, the auxetic and non-auxetic composites were measured for three times and their average values are used to draw in Figure 5-9. The standard deviation of three measured values is calculated as the error bar to show the perturbation of the experimental data. The experimental results very clearly illustrate that as the initial impact energy goes up the maximum contact force of auxetic and non-auxetic composites increases significantly. It should be noted, the contact duration of low velocity impact test is long enough for the entire sample to respond [139], so the impact performance of tested specimens is governed by inner textile structures. And the maximum transmitted force of auxetic and non-auxetic composites shows a linear relationship with the increasing of impact energies. And the peak load under the same impact energy indicates the load buffering ability of the tested specimens [149].

Figure 5-9(a) and (b) illustrates the effect of impact energy on the peak contact force and transmitted force for both the 3D textile composites with 4mm and 6mm warp yarn respectively. Two groups of composites with different diameters of warp yarns exhibit different trends. As depicted in Figure 5-9(a), it is found that both the peak contact and transmitted force increase almost linearly with the growth of the impact energy. This is reasonable because the increase of the initial impact energy can increase the deformation of the composite structure, which results in an increase in peak forces. Under all impact energies, the results show that both the peak contact force and transmitted force of 4mm NPR are lower than those of 4mm PPR, which indicate that the auxetic textile composite with 4mm warp yarns has better impact protective performance in a range of impact energy. It is also discovered that the gap in peak force between 4mm NPR and 4mm PPR is getting larger with the increase of impact energy. As the increasing speed of the peak contact and transmitted force for 4mm PPR is higher than that of 4mm NPR, the impact protection capacity of the auxetic composite is getting better than that of the non-auxetic composite when the impact energy increases. As illustrated in Figure 5-9(b), the peak loads of 6mm PPR are higher than those of 6mm NPR under the same impact energy. And the gap of contact force tends to enlarge from 12.1J to 22.3J and narrow until 31.9J. Under 31.9J impact energy, the transmitted and contact force of 6mm NPR and 6mm PPR remains similar value. In this stage, the inner auxetic structure has moved to the densification stage by crimp of weft yarns, and then the warp yarns start to be compressed to be in a vertical line like the non-auxetic textile structure. Thus, 6mm NPR becomes stiff and the warp yarns would bear the impact loading.

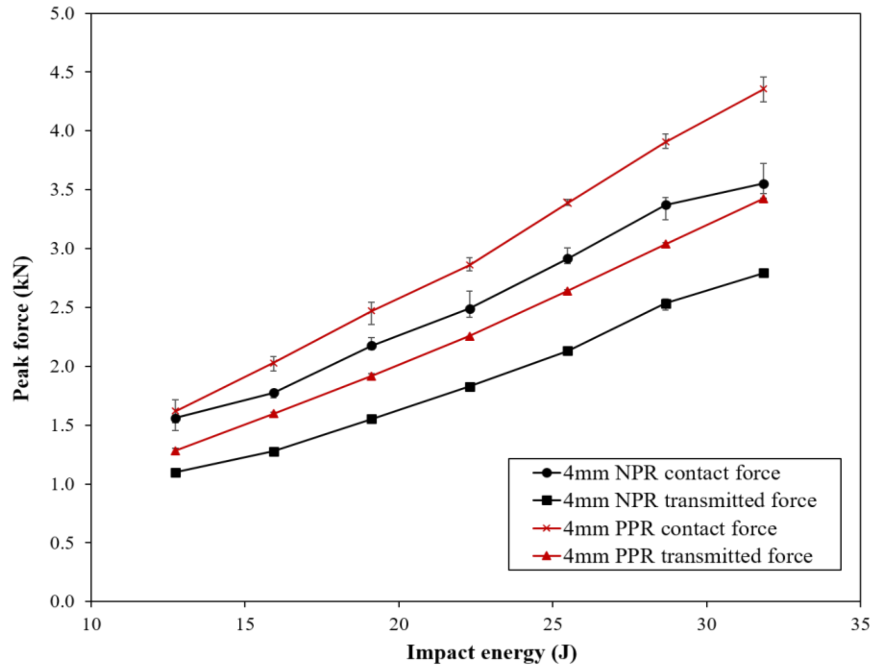

(a)

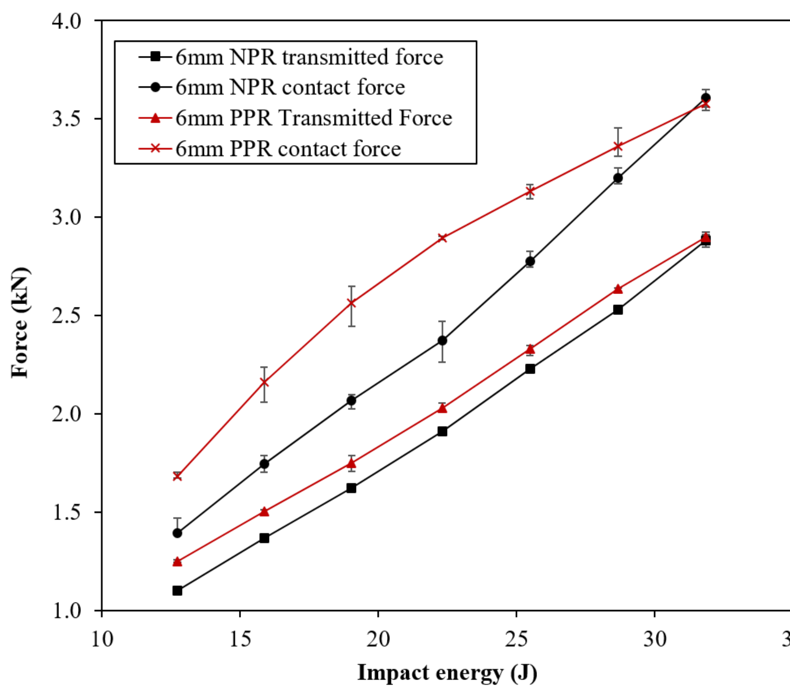

(b)

Figure 5- 9 Force – impact energy curves of (a) 4mm NPR and PPR; (b) 6mm NPR and PPR under different impact energy

In order to better description of the experimental results, the key impact parameters including peak load, absorbed energy, impact velocity and peak force reduced for auxetic and non-auxetic composites are summarized in Table 5-1. Here, each value is the average number of three tested specimens. In addition, Figure 5-10 indicates that the transmitting rate of auxetic and non-auxetic composites under varied initial impact energies. The textile composites with varied diameters of warp yarns present different trends. As for 4mm NPR and 4mm PPR, the auxetic composites generally provide lower transmitting rate compared with non-auxetic composites under same impact energy ranging from 12.7J to 28.7J, which may be due to NPR effect of auxetic composites. While under 31.7J impact energy, the transmitting rate of 4mm NPR and 4mm PPR keeps general same value (around 78.6%). The main reason is that the reinforced auxetic textile structures are compressed to a critical state, where the warp yarns cannot be dragged inward to improve the NPR effect. Due to the limitation of NPR effect of auxetic composite, the force reduction reaches critical value when the 4mm NPR is compressed to its critical state. In this work, the critical compression strain is about 30% by considering the quasi-static compression results. Considering the impact velocity, the critical strain must be larger than 30%. However, for low-velocity impact, the critical strain may be slightly larger than 30%. Thus, in this work, the transmitting rate is dramatically increasing, when the impact energy is more than 30J. However, transmitting rate of 6mm NPR and 6mm PPR shows different tendency. The auxetic composites with 6mm warp yarns provide higher transmitting rate compared with that of non-auxetic composites. In addition, the transmitting rate of 6mm NPR is much higher than that of 4mm NPR It indicates that the larger diameters of warp yarns in the inner textile structure may not significantly affect the transmitting rate of auxetic composites. Experimental findings on 3D auxetic and non-auxetic composites reveal that auxetic composites with 4mm warp yarns are necessarily advantageous over non-auxetic ones under low velocity impact under low level of impact energies.

Table 5- 1 The impact parameters of auxetic and non-auxetic composites under varied impact energies

	Impact height (mm)	Impact Energy (J)	Peak trassmitted force	Peak contact force (kN)	Velocity(m/s)	Displacement(m)	Peak force ratio (%)	Peak force reduced (%)
6mm NPR	200	12.74	1.10	1.40	1.98	0.025	78.74	21.26
	250	15.87	1.37	1.74	2.21	0.027	78.42	21.58
	300	19.03	1.62	2.07	2.43	0.028	78.58	21.42
	350	22.31	1.91	2.37	2.62	0.031	80.61	19.39
	400	25.48	2.23	2.78	2.80	0.031	80.18	19.82
	450	28.67	2.53	3.20	2.97	0.032	79.02	20.98
	500	31.84	2.88	3.61	3.13	0.033	79.84	20.16
6mm PPR	200	12.74	1.25	1.68	1.98	0.023	74.34	25.66
	250	15.87	1.50	2.16	2.21	0.025	69.49	30.51
	300	19.03	1.75	2.56	2.43	0.027	68.29	31.71
	350	22.31	2.03	2.90	2.62	0.028	70.13	29.87
	400	25.48	2.33	3.13	2.80	0.032	74.33	25.67
	450	28.67	2.64	3.36	2.97	0.034	78.38	21.62
	500	31.84	2.90	3.58	3.13	0.035	81.02	18.98
4mm NPR	200	12.7	1.10	1.54	1.98	17.0	71.34	28.66
	250	15.9	1.28	1.73	2.21	21.9	73.79	26.21
	300	19.1	1.55	2.17	2.43	23.4	71.73	28.27
	350	22.3	1.83	2.50	2.62	25.8	73.16	26.84
	400	25.5	2.13	2.95	2.80	27.2	72.20	27.80
	450	28.7	2.54	3.39	2.97	29.5	74.73	25.27
	500	31.9	2.79	3.55	3.13	26.6	78.56	21.44
4mm PPR	200	12.7	1.28	1.62	1.98	18.6	79.27	20.73
	250	15.9	1.60	2.03	2.21	22.4	78.76	21.24
	300	19.1	1.92	2.47	2.43	22.5	77.64	22.36
	350	22.3	2.26	2.86	2.62	24.3	78.84	21.16
	400	25.5	2.64	3.39	2.80	24.6	77.99	22.01
	450	28.7	3.04	3.90	2.97	29.0	77.77	22.23
	500	31.9	3.43	4.36	3.13	28.8	78.62	21.38

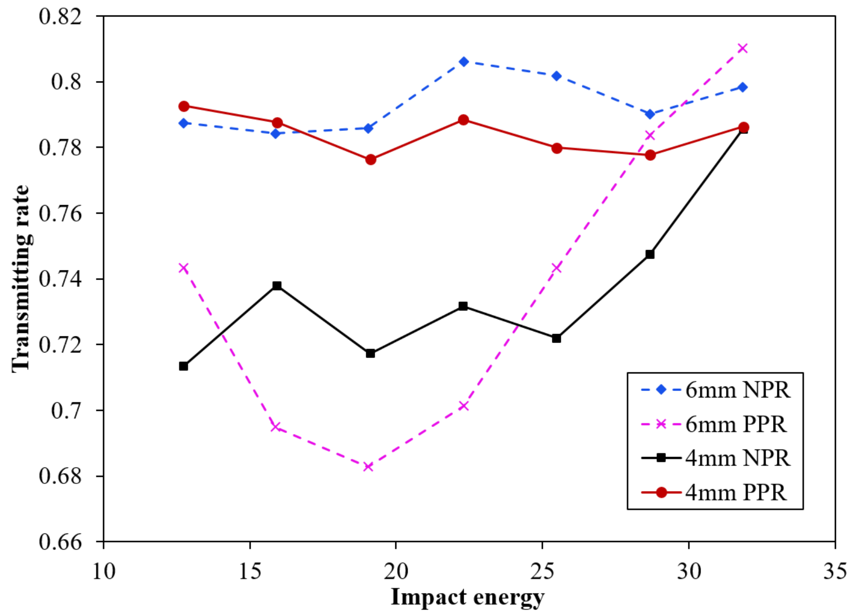

Figure 5- 10 The transmitting rate- impact energy curves of auxetic and non-auxetic composites

5.6 Impact Compressive Behaviors under Repeating Impact

One of interesting research areas of auxetic and non-auxetic composites is the mechanical properties and structure stability under repeated impact conditions, which will have influence in the impact behaviors during repeated uses. The peak transmitted force is a significant parameter to evaluate the impact behaviors of composite materials. It is critical to investigate how much peak contact force can be transmitted to the bottom surface. To investigate the structural stability under continuous impact, a repeated impact testing was conducted for two impact energy levels (19.1J and 31.9J) on both auxetic and non-auxetic composites. The obtained peak contact force and transmitted force for each impact is presented in Figure 5-11.

Figure 5-11(a) illustrates the peak contact and transmitted force of 4mm NPR and 4mm

PPR under repeating impacts at two given impact energy levels (19.1J and 31.9J). It can be found that the maximum contact force of 4mm NPR remains nearly the same under repeated impact while the maximum contact force of 4mm PPR fluctuates especially at lower impact energy. The differences of the peak contact forces between 4mm NPR and PPR enlarged when the impact energy increased from 19.1J to 31.9J. And 4mm NPR shows relatively lower transmitted force under the same impact energy. This result appear to show that the recovery ability of auxetic composites with 4mm warp yarns under repeating impact load is relatively more stable than those of non-auxetic composites. The maximum contact force of 4mm NPR is lower than that of 4mm PPR under the same impact energy and when the impact energy goes up from 19.1J to 31.9J, the difference on maximum contact force between 4mm NPR and PPR is getting larger. Form Figure 5-11(a), the same trend was captured for the maximum transmitted force. The results also show that the peak transmitted force tends to be stabilized after the first impact under higher impact energy. As these textile composites are self-fabricated with PU foam as matrix, irregular voids exist in the composite structure. Under each impact, irregular voids may result in different compacting states, causing the variation of the peak contact force. At higher impact energy level, as the composite structure is easier to be compacted, the difference in compacted state at the end of each impact decreases. Therefore, the variation of the peak contact force decreases. As mentioned before, the warp yarns in the 3D non-auxetic textile structure are arranged in the way of vertical lines. This arrangement results in relatively low stability of 4mm PPR as the misalignment of the non-auxetic textile structure would happen under each impact, causing the buckling of the composite structure. And the buckling may lead to a non-recovering deformation. Therefore, the 3D auxetic textile composite with 4mm warp yarns should have better structural stability than the 3D non-auxetic composite under repeating impacts. Figure 5-11(b) presents the peak force of auxetic and non-auxetic composites with 6mm warp yarns, named as 6mm NPR and PPR. It can be seen that 6mm NPR and PPR exhibit similar trends with 4mm NPR and PPR. Under impact energy 31.9J, 6mm PPR shows relatively higher contact and transmitted force than that of 4mm PPR. And 6mm NPR exhibits lower transmitted force than that of 4mm NPR. The main reason is the different diameter of warp yarns thus resulting in different deformation behaviors of inner textile structure as mentioned above. Actually, the retention of the impact performance mainly depends on the elastic recovery of the PU foam matrix. Therefore, high elastic recovery PU foam is required to obtain stable impact behaviors of auxetic composite under repeated impact loading.

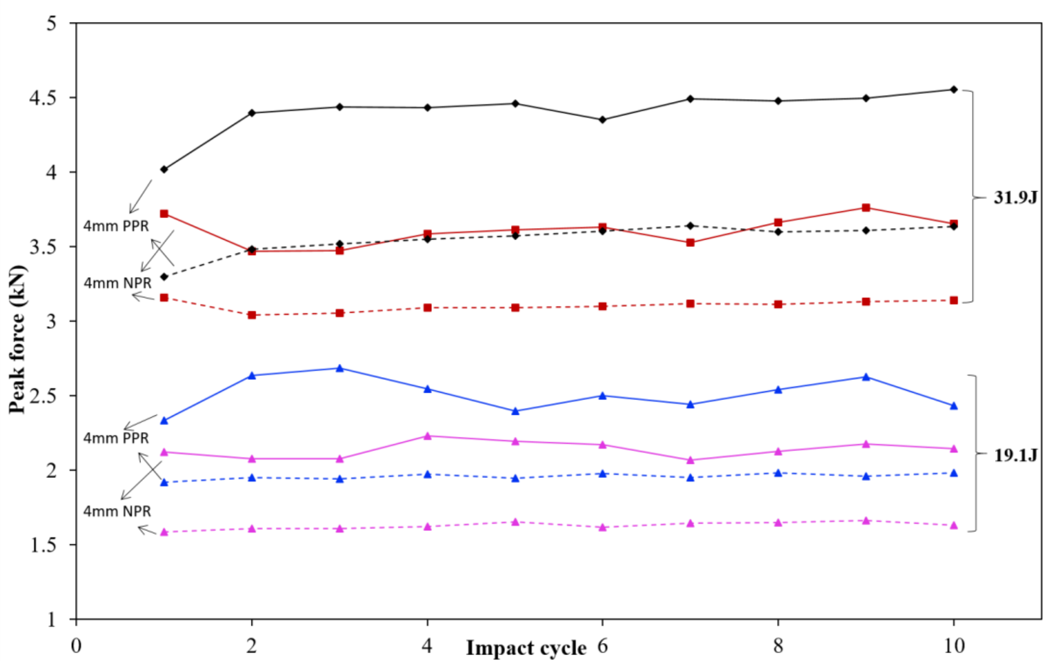

(a)

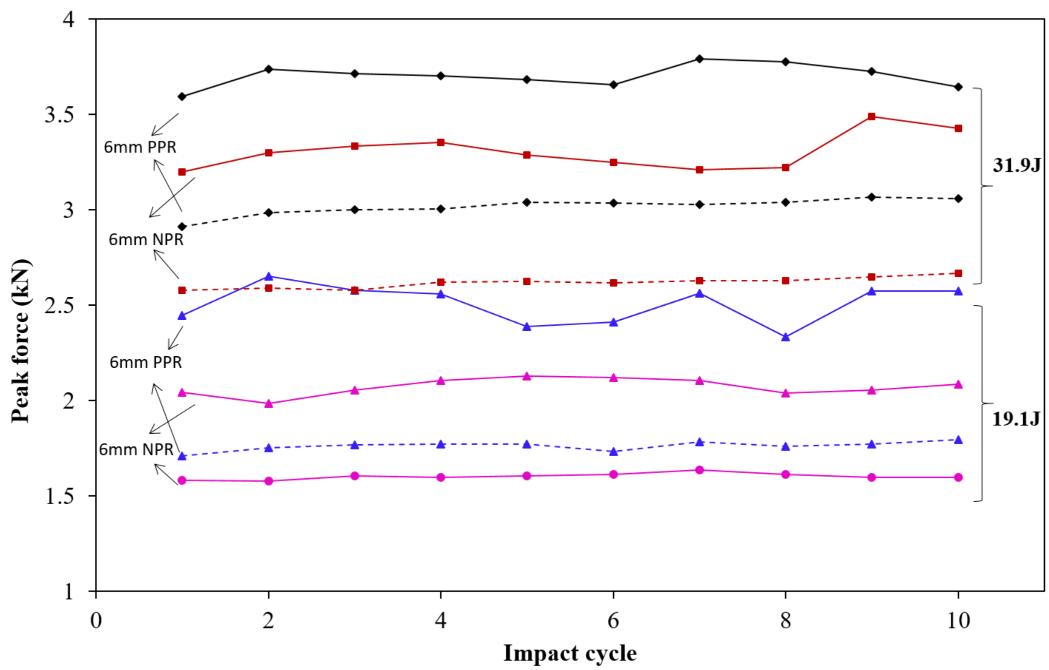

(b)

Figure 5- 11 Peak contact force (solid lines) and peak transmitted force (dash lines) of (a)4mm NPR and PPR; (b) 6mm NPR and PPR under repeating impact loading. The impact energy is 19.1J and 31.9J.

5.7 Conclusions

An experiment has been carried out to compare the performance of 3D auxetic composites and non-auxetic composites, by subjecting the specimens to single and repeating low-velocity impact drop tests. In order to compare impact response of the auxetic and non-auxetic composites, a number of single impact teste were performed under various impact energies from 12.7J to 31.9J. The results of this study deepen the understanding of 3D auxetic textile reinforced composites against with non-auxetic ones under low-velocity impact loading, which will assist in the development of applications for 3D auxetic textile composites. This work has shown further potential applications for auxetic composites to be applied under low-velocity impact.

CHAPTER 6 CONCLUSION AND FUTURE WORK

6.1 Conclusions

This study is concerned with the development of 3D auxetic textile reinforced composites, including design and fabrication of the novel textile reinforced composites, evaluation of their deformation behaviors and compression properties, identification of the relationships between the structural parameters of the composites and auxetic behaviors. The experimental investigations form a basis for the further study of 3D auxetic composites.

6.1.1 Composites Design and Manufacture

A novel kind of auxetic composite was fabricated by 3D auxetic textile structure as reinforcement and conventional PU foam as matrix via an filling and foaming procedure. Four different types of 3D auxetic textile reinforced composites were successfully made based on different parameter structures. The developed method is effective for making 3D auxetic textile reinforced composites. To make comparisons, a series of produced samples including pure PU foams and 3D non-auxetic composites were also design and fabricated for quasi-static compression tests. It is possible to obtain auxetic effect in a 3D textile structure if a suitable yarn arrangement method is adopted. Auxetic composites can be easily produced using 3D auxetic textile structure as reinforcement and conventional PU foam as matrix.

6.1.2 Deformation Behaviors and Compression Properties of 3D

Auxetic and Non-Auxetic Textile Reinforced Composites under Quasi-static Compression

The deformation behaviors and compression properties of 3D auxetic textile reinforced composites under compression were investigated and compared with pure PU foam and non-auxetic composites made with the same matrix materials and structural parameters but with different warp yarn arrangement in the inner textile structures. The specific work that has been done is summarized as followed:

1. For the deformation behaviors, the PR of the auxetic composite structures are not constant. They change with the compression strain and warp yarn diameter. The increase of the compression strain and warp yarn diameter can cause an increase of NPR values. Pure PU foam, auxetic composites and non-auxetic composites all have zero PR in the initial stage of compression strain when compressed. While the non-auxetic composites and pure PU foams show PPR under compression tests. Moreover, for the structural parameters, the compression experimental study showed that the diameter of warp yarns is an effective factor, and that the 3D auxetic composites with 6mm warp yarns have better auxetic effect.
2. For the compression properties, the auxetic and non-auxetic composites exhibit varied deformation mechanism due to different arrangements of warp yarns in 3D textile structure. While the auxetic composite exhibits more like a damping material with a lower range of compression stress, the non-auxetic composite behaves stiffer with a higher range of compression stress.
3. For the repeated compression tests, the deformation behaviors and compression properties of the 3D auxetic composites tend to be stabilized after the first

compression cycle under repeated compression testing condition.

6.1.3 Low-velocity Impact properties of 3D Auxetic and Non-auxetic Textile Reinforced Composites

Low velocity impact performance of 3D auxetic textile composites were systematically investigated and compared with those of the non-auxetic composites that was made of the same constituent materials and structural parameters. Based on the experimental results and analysis, the following conclusions could be drawn:

1. The 3D auxetic textile composite exhibits better impact protective performance than that of non-auxetic textile composite due to lower transmitted peak force and higher energy absorption.
2. The deformation mechanism of the textile composites under impact and quasi-static compression are very different. Under quasi-static compression, the auxetic textile composite behaves much softer and has lower energy absorption than the non-auxetic textile composite. However, under impact test, the difference in mechanical behaviors between the auxetic and non-auxetic textile composites becomes smaller due to impact hardening effect. The auxetic composite can absorb more energy than the non-auxetic composite with increase of impact energy. The 3D auxetic textile composite has better impact protective performance than the 3D non-auxetic textile composite because of better transmitted force reduction and higher energy absorption capacity under single-time impact and higher structural stability under repeating impacts. Moreover, the stress hardening effect under impact was observed for the auxetic composite, which could enhance its impact protection properties with

increasing of impact velocity.

3. The auxetic composite has stable impact behaviors under repeating impact tests. The results of this study demonstrate the potential application of textile composites made of 3D auxetic textile structure as reinforcement for impact protection under low velocity impact loading. For the structure design to be optimized and impact performance to be enhanced, further theoretical study is required to better understand their mechanical behaviors under low-velocity impact.

6.2 Contributions

This study systematically investigated 3D auxetic textile reinforced composite. In this study, the novel fabrication method and process of 3D auxetic textile reinforced was presented. Through the experiment work, the relationship between the deformation mechanism and compression properties of the 3D auxetic composites were found, and the compression properties of 3D auxetic composites were revealed. Moreover, the results of this study deepen the understanding of 3D auxetic textile reinforced composites against with non-auxetic ones under low-velocity impact loading, which will assist in the development of applications for 3D auxetic textile composites. This work has shown further potential applications for auxetic composites to be applied under low-velocity impact. In summary, this study brings a deeper understanding of 3D auxetic textile reinforced composites based on the previous study and provides a guidance for making 3D auxetic composites using non-auxetic materials.

6.3 Recommendations for Future Work

3D auxetic textile reinforced composites are a novel kind of composite with 3D auxetic textile structure as reinforcement and conventional PU foam as matrix. After evaluating the deformation behaviors and mechanical performance under quasi-static compression and low-velocity impact, compared to 3D non-auxetic composites, 3D auxetic textile reinforced composites exhibit excellent characteristics on the energy absorption under impact and repeated use. However, there are a lot of space to improve their performance. Some recommendations are suggested for further improvement as follows:

1. The developed 3D auxetic textile reinforced composites are all in a relatively small size because of the restriction of the laboratory conditions. Further research could be focused on investigate whether the size will have effect on the 3D auxetic textile reinforced composites and help to enhance their deformation behaviors.
2. The developed 3D auxetic textile reinforced composites have not been made yet into any product to explore the real application of the auxetic composites. Thus, the future study may lie on the industrial applications of 3D auxetic textile reinforced composites.
3. Higher impact energy than 31.84J is proposed to impact on the fabricated composites for evaluating the energy absorption capacity. And the interface between the foam and reinforcements are suggested to evaluate and analyse for the purpose of increasing the contact area.
4. The achieved NPR values are not very high enough. There will be further development to achieve high auxetic effect so that the mechanical performance under compression will be improved. The results of this study demonstrate the potential application of 3D auxetic textile structure as reinforcements for auxetic composites under impact loading. For the structure design to be optimized and

impact performance to be enhanced, further theoretical study and development of the 3D auxetic composites is required to better understand their benefits under low-velocity impact loading.

REFERENCE

1. Alderson, K.L., et al., *How to make auxetic fiber reinforced composites.* Physica Status Solidi B-Basic Solid State Physics, 2005. **242**(3): p. 509-518.
2. Lim, T.C., A. Alderson, and K.L. Alderson, *Experimental studies on the impact properties of auxetic materials.* physica status solidi (b), 2014. **251**(2): p. 307-313.
3. Evans, K.E., et al., *Molecular Network Design.* Nature, 1991. **353**(6340): p. 124-124.
4. Lakes, R., *Advances in negative Poisson's ratio materials.* Advanced Materials, 1993. **5**(4): p. 293-296.
5. Lakes, R.S., *Foam Structure with a Negative Poisson's Ratio.* Science, 1987. **235**: p. 1038-1040.
6. Almgren, R.F., *An isotropic three-dimensional structure with Poisson's ratio =−1.* Journal of Elasticity, 1985. **15**(4): p. 427-430.
7. Wojciechowski, K.W., *Constant Thermodynamic Tension Monte-Carlo Studies of Elastic Properties of a Two-Dimensional System of Hard Cyclic Hexamers.* Molecular Physics, 1987. **61**(5): p. 1247-1258.
8. Liu, Y.P. and H. Hu, *A review on auxetic structures and polymeric materials.* Scientific Research and Essays, 2010. **5**(10): p. 1052-1063.
9. Mir, M., et al., *Review of Mechanics and Applications of Auxetic Structures.* Advances in Materials Science and Engineering, 2014. **2014**: p. 1-17.
10. Strek, T., et al., *Finite element analysis of auxetic plate deformation.* Journal of Non-Crystalline Solids, 2008. **354**(35-39): p. 4475-4480.

11. Evans, K.E., J.P. Donoghue, and K.L. Alderson, *The design, matching and manufacture of auxetic carbon fiber laminates.* Journal of Composite Materials, 2004. **38**(2): p. 95-106.

12. Herakovich, C.T., *Composite laminate with Nagiave through-thickness Poisson's Ratios.* Journal of Composite Materials, 1984. **18**(5): p. 447-455.

13. Peel, L.D., *Exploration of high and negative Poisson's ratio elastomer-matrix laminates.* Physica Status Solidi B-Basic Solid State Physics, 2007. **244**(3): p. 988-1003.

14. Chen, C.P. and R.S. Lakes, *Viscoelastic Behaviors of Composite-Materials with Conventional-Poisson-Ratio or Negative-Poisson-Ratio Foam as One-Phase.* Journal of Materials Science, 1993. **28**(16): p. 4288-4298.

15. Zhang, R.G., H.L. Yeh, and H.Y. Yeh, *A preliminary study of negative Poisson's ratio of laminated fiber reinforced composites.* Journal of Reinforced Plastics and Composites, 1998. **17**(18): p. 1651-1664.

16. Hadi Harkati, E., et al., *Modelling the influence of the orientation and fiber reinforcement on the Negative Poisson's ratio in composite laminates.* physica status solidi (b), 2007. **244**(3): p. 883-892.

17. Clarke, J.F., et al., *Negative Poisson's ratios in angle-ply laminates: theory and experiment.* Composites 1994, 1994. **25**(9): p. 863-868.

18. Evans, K.E., M.A. Nkansah, and I.J. Hutchinson, *Modeling Negative Poisson Ratio Effects in Network-Embedded Composites.* Acta Metallurgica Et Materialia, 1992. **40**(9): p. 2463-2469.

19. Miller, W., et al., *The manufacture and characterisation of a novel, low modulus, negative Poisson's ratio composite.* Composites Science and Technology, 2009.

69(5): p. 651-655.

20. Ge, Z. and H. Hu, *Innovative three-dimensional fabric structure with negative Poisson's ratio for composite reinforcement.* Textile Research Journal, 2012. **83**(5): p. 543-550.

21. Ge, Z., H. Hu, and Y. Liu, *Numerical analysis of deformation behaviors of a 3D textile structure with negative Poisson's ratio under compression.* Textile Research Journal, 2014. **85**(5): p. 548-557.

22. Ge, Z.Y., H. Hu, and Y.P. Liu, *A finite element analysis of a 3D auxetic textile structure for composite reinforcement.* Smart Materials and Structures, 2013. **22**(8): p. 084005.

23. Alderson, A. and K.E. Evans, *Modelling concurrent deformation mechanisms in auxetic microporous polymers.* Journal of Materials Science, 1997. **32**(11): p. 2797-2809.

24. Jiang, L.L., B.H. Gu, and H. Hu, *Auxetic composite made with multilayer orthogonal structural reinforcement.* Composite Structures, 2016. **135**: p. 23-29.

25. Ge, Z. and H. Hu, *A theoretical analysis of deformation behaviors of an innovative 3D auxetic textile structure.* The Journal of The Textile Institute, 2014. **106**(1): p. 101-109.

26. Prawoto, Y., *Seeing auxetic materials from the mechanics point of view: A structural review on the negative Poisson's ratio.* Computational Materials Science, 2012. **58**: p. 140-153.

27. Alderson, A. and K.L. Alderson, *Auxetic materials.* Proceedings of the Institution of Mechanical Engineers Part G-Journal of Aerospace Engineering, 2007. **221**(G4): p. 565-575.

28. Gibson, L.J., et al., *The Mechanics of Two-Dimensional Cellular Materials.* Proceedings of the Royal Society of London Series a-Mathematical Physical and Engineering Sciences, 1982. **382**(1782): p. 25-42.

29. Masters, I. and K. Evans, *Models for the elastic deformation of honeycombs.* Composite structures, 1996. **35**(4): p. 403-422.

30. Theocaris, P.S., G.E. Stavroulakis, and P.D. Panagiotopoulos, *Negative Poisson's ratios in composites with star-shaped inclusions: a numerical homogenization approach.* Ingenieur-Archiv, 1997. **67**(4): p. 274-286.

31. Grima, J.N., A. Alderson, and K.E. Evans, *Auxetic behaviors from, rotating rigid units.* Physica Status Solidi B-Basic Solid State Physics, 2005. **242**(3): p. 561-575.

32. Subramani, P., et al., *Development and characterization of novel auxetic structures based on re-entrant hexagon design produced from braided composites.* Composites Part B: Engineering, 2016. **93**: p. 132-142.

33. Wei, G., *Negative and conventional Poisson's ratios of polymeric networks with special microstructures.* The Journal of Chemical Physics, 1992. **96**(4): p. 3226-3233.

34. Chan, N. and K.E. Evans, *Microscopic examination of the microstructure and deformation of conventional and auxetic foams.* journal of Materials Science, 1997. **32**: p. 5725-5736.

35. Shokri Rad, M., Y. Prawoto, and Z. Ahmad, *Analytical solution and finite element approach to the 3D re-entrant structures of auxetic materials.* Mechanics of Materials, 2014. **74**: p. 76-87.

36. Yang, L., et al., *Mechanical properties of 3D re-entrant honeycomb auxetic*

structures realized via additive manufacturing. International Journal of Solids and Structures, 2015. **69-70**: p. 475-490.

37. Yang, L., et al., *Compressive properties of Ti–6Al–4V auxetic mesh structures made by electron beam melting.* Acta Materialia, 2012. **60**(8): p. 3370-3379.

38. Yang, L., et al., *Modeling of uniaxial compression in a 3D periodic re-entrant lattice structure.* Journal of Materials Science, 2012. **48**(4): p. 1413-1422.

39. Grima, J.N., A. Alderson, and K.E. Evans, *Negative Poisson's ratios from rotating rectangles.* Computational Methods in Science and Technology, 2004. **10**(2): p. 137-145.

40. Grima, J.N. and K.E. Evans, *Auxetic behaviors from rotating triangles.* Journal of Materials Science, 2006. **41**(10): p. 3193-3196.

41. Grima, J.N., et al., *Auxetic behaviors from rotating semi-rigid units.* physica status solidi (b), 2007. **244**(3): p. 866-882.

42. Grima, J.N. and K.E. Evans, *Auxetic behaviors from rotating squares.* Journal of Materials Science Letters, 2000. **19**(17): p. 1563-1565.

43. Grima, J.N. and K.E. Evans, *Self expanding molecular networks.* Chemical Communications, 2000(16): p. 1531-1532.

44. Alderson, A. and K.E. Evans, *Rotation and dilation deformation mechanisms for auxetic behaviors in the α-cristobalite tetrahedral framework structure.* Physics and Chemistry of Minerals, 2001. **28**(10): p. 711-718.

45. Nazaré, F. and A. Alderson, *Models for the prediction of Poisson's ratio in the 'α-cristobalite' tetrahedral framework.* physica status solidi (b), 2015. **252**(7): p. 1465-1478.

46. Yeganeh-Haeri, A., D.J. Weidner, and J.B. Parise, *Elasticity of a-cristobalite: a*

silicon dioxide with a negative Poisson's ratio. Science, 1992. **257**(5070): p. 650-652.

47. Bückmann, T., et al., *On three-dimensional dilational elastic metamaterials.* New Journal of Physics, 2014. **16**(3): p. 033032.

48. Prall, D. and R.S. Lakes, *Properties of a chiral honeycomb with a poisson's ratio of — 1.* International Journal of Mechanical Sciences, 1997. **39**(3): p. 305,309-307,314.

49. Novak, N., M. Vesenjak, and Z. Ren, *Auxetic Cellular Materials - a Review.* Strojniški vestnik – Journal of Mechanical Engineering, 2016. **62**(9): p. 485-493.

50. Wojciechowski, K.W., *Non-chiral, molecular model of negative poisson ratio in two dimensions.* Journal of Physics A: Mathematical and General, 2003. **36**(47): p. 11765-11778.

51. Grima, J.N., R. Gatt, and P.-S. Farrugia, *On the properties of auxetic meta-tetrachiral structures.* physica status solidi (b), 2008. **245**(3): p. 511-520.

52. Spadoni, A., et al., *Phononic properties of hexagonal chiral lattices.* Wave Motion, 2009. **46**(7): p. 435-450.

53. Spadoni, A. and M. Ruzzene, *Elasto-static micropolar behaviors of a chiral auxetic lattice.* Journal of the Mechanics and Physics of Solids, 2012. **60**(1): p. 156-171.

54. Pozniak, A.A. and K.W. Wojciechowski, *Poisson's ratio of rectangular anti-chiral structures with size dispersion of circular nodes.* physica status solidi (b), 2014. **251**(2): p. 367-374.

55. Ha, C.S., M.E. Plesha, and R.S. Lakes, *Chiral three-dimensional lattices with tunable Poisson's ratio.* Smart Materials and Structures, 2016. **25**(5): p. 054005.

56. Lu, Z., et al., *Elastic properties of two novel auxetic 3D cellular structures.* International Journal of Solids and Structures, 2017.

57. Alderson, A. and K. Evans, *Microstructural modelling of auxetic microporous polymers.* Journal of materials science, 1995. **30**(13): p. 3319-3332.

58. Alderson, K.L., A. Fitzgerald, and K.E. Evans, *The strain dependent indentation resilience of auxetic microporous polyethylene.* Journal of Materials Science, 2000. **35**(16): p. 4039-4047.

59. Lim, T.-C. and R. Acharya, *An hexagonal array of fourfold interconnected hexagonal nodules for modeling auxetic microporous polymers: a comparison of 2D and 3D models.* Journal of materials science, 2009. **44**(16): p. 4491-4494.

60. Gaspar, N., et al., *A generalised three-dimensional tethered-nodule model for auxetic materials.* Journal of Materials Science, 2010. **46**(2): p. 372-384.

61. Larsen, U.D., O. Signund, and S. Bouwsta, *Design and fabrication of compliant micromechanisms and structures with negative Poisson's ratio.* Microelectromechanical Systems, Journal of, 1997. **6**(2): p. 99-106.

62. Ma, Z.-D., et al., *Functionally-graded NPR (negative Poisson's ratio) material for a blast-protective deflector*. 2010, MICHIGAN UNIV ANN ARBOR.

63. Zhang, W., et al., *The Nonlinear Compressive Response and Deformation of an Auxetic Cellular Structure under In-Plane Loading.* Advances in Mechanical Engineering, 2014. **7**(1): p. 214681-214681.

64. Lim, T.-C., *A 3D auxetic material based on intersecting double arrowheads.* physica status solidi (b), 2016. **253**(7): p. 1252-1260.

65. Smith, C.W., J.N. Grima, and K.E. Evans, *A novel mechanism for generating auxetic behaviors in reticulated foams missing rib foam.* Acta Materialia, 2000.

48(17): p. 4349-4356.

66. Gaspar, N., et al., *Novel honeycombs with auxetic behaviors.* Acta Materialia, 2005. **53**(8): p. 2439-2445.

67. Subramani, P., et al., *Development of novel auxetic structures based on braided composites.* Materials & Design, 2014. **61**: p. 286-295.

68. He, C., et al., *Toward molecular auxetics: Main chain liquid crystalline polymers consisting of laterally attached para-quaterphenyls.* physica status solidi (b), 2005. **242**(3): p. 576-584.

69. He, C.B., P.W. Liu, and A.C. Griffin, *Toward negative Poisson ratio polymers through molecular design.* Macromolecules, 1998. **31**(9): p. 3145-3147.

70. Bertoldi, K., et al., *Mechanics of deformation-triggered pattern transformations and superelastic behaviors in periodic elastomeric structures.* Journal of the Mechanics and Physics of Solids, 2008. **56**(8): p. 2642-2668.

71. Bertoldi, K., et al., *Negative Poisson's ratio behaviors induced by an elastic instability.* Adv Mater, 2010. **22**(3): p. 361-6.

72. Mullin, T., et al., *Pattern transformation triggered by deformation.* Phys Rev Lett, 2007. **99**(8): p. 084301.

73. Shim, J., et al., *Buckling-induced encapsulation of structured elastic shells under pressure.* Proceedings of the National Academy of Sciences of the United States of America, 2012. **109**(16): p. 5978-5983.

74. Yanping, L., et al., *Negative Poisson's Ratio Weft-knitted Fabrics.* Textile Research Journal, 2009. **80**(9): p. 856-863.

75. Schwerdtfeger, J., et al., *Auxetic cellular structures through selective electron-beam melting.* physica status solidi (b), 2010. **247**(2): p. 269-272.

76. Liaqat, M., et al., *The development of novel auxetic woven structure for impact applications.* The Journal of The Textile Institute, 2016: p. 1-7.

77. Ugbolue, S.C., et al., *The formation and performance of auxetic textiles. Part II: geometry and structural properties.* Journal of the Textile Institute, 2011. **102**(5): p. 424-433.

78. Feng, Y., *The Formation and Performance of Auxetic Warp Knit Structures: A Thesis in Textile Technology*. 2010, PhD Thesis, University of Massachusetts, Dartmouth.

79. Ugbolue, S.C., et al., *The formation and performance of auxetic textiles. Part I: theoretical and technical considerations.* Journal of the Textile Institute, 2010. **101**(7): p. 660-667.

80. Hong, H., W. Zhengyue, and L. Su, *Development of auxetic fabrics using flat knitting technology.* Textile Research Journal, 2011. **81**(14): p. 1493-1502.

81. Wang, Z.Y. and H. Hu, *3D auxetic warp-knitted spacer fabrics.* Physica Status Solidi B-Basic Solid State Physics, 2014. **251**(2): p. 281-288.

82. Wang, Z.Y., H. Hu, and X.L. Xiao, *Deformation behaviors of three-dimensional auxetic spacer fabrics.* Textile Research Journal, 2014. **84**(13): p. 1361-1372.

83. Hu, H., *3D negative Poisson's ratio spacer fabrics and relevant fabrication method*. 2012.

84. Chan, N. and K. Evans, *Microscopic examination of the microstructure and deformation of conventional and auxetic foams.* Journal of Materials Science, 1997. **32**(21): p. 5725-5736.

85. Lakes, R., *Foam structures with a negative Poisson's ratio.* Science, 1987. **235**(4792): p. 1038-1040.

86. Friis, E.A., R.S. Lakes, and J.B. Park, *Negative Poisson's ratio polymeric and metallic foams.* J. Mat. Sci., 1988. **23**(12): p. 4406-4414.

87. Choi, J.B. and R.S. Lakes, *Non-linear properties of polymer cellular materials with a negative Poisson's ratio.* Journal of Materials Science, 1992. **27**(17): p. 4678-4684.

88. Lakes, R., *Re-entrant transformation methods in closed cell foams.* Cell. Polym, 1996. **15**: p. 229-249.

89. Chan, N. and K.E. Evans, *Fabrication methods for auxetic foams.* Journal of Materials Science, 1997. **32**(22): p. 5945-5953.

90. Smith, C.W., J. Grima, and K. Evans, *A novel mechanism for generating auxetic behaviors in reticulated foams: missing rib foam model.* Acta materialia, 2000. **48**(17): p. 4349-4356.

91. Brandel, B. and R. Lakes, *Negative Poisson's ratio polyethylene foams.* Journal of Materials Science, 2001. **36**(24): p. 5885-5893.

92. Scarpa, F., et al., *Auxetic compliant flexible PU foams: static and dynamic properties.* physica status solidi (b), 2005. **242**(3): p. 681-694.

93. Scarpa, F., et al., *Dynamic crushing of auxetic open-cell polyurethane foam.* Proceedings of the Institution of Mechanical Engineers Part C-Journal of Mechanical Engineering Science, 2002. **216**(12): p. 1153-1156.

94. Grima, J.N., et al., *Negative Poisson's ratios in cellular foam materials.* Materials Science and Engineering: A, 2006. **423**(1): p. 214-218.

95. Bezazi, A. and F. Scarpa, *Mechanical behaviors of conventional and negative Poisson's ratio thermoplastic polyurethane foams under compressive cyclic loading.* International Journal of fatigue, 2007. **29**(5): p. 922-930.

96. Critchley, R., et al., *The Preparation of Auxetic Foams by Three-Dimensional Printing and Their Characteristics.(Report).* Advanced Engineering Materials, 2013. **15**(10): p. 980.

97. Evans, K., *Tensile network microstructures exhibiting negative Poisson's ratios.* Journal of Physics D: Applied Physics, 1989. **22**(12): p. 1870.

98. Caddock, B.D. and K.E. Evans, *Microporous materials with negative Poisson's ratios. I. Microstructure and mechanical properties.* J. Phys. D: Appl. Phys., 1989. **22**: p. 1877-1882.

99. Evans, K.E. and B.D. Caddock, *Microporous materials with negative Poisson's ratios: II. Mechanisms and interpretation.* Journal of Physics D: Applied Physics, 1989. **22**: p. 1883-1887.

100. Alderson, K. and K. Evans, *The fabrication of microporous polyethylene having a negative Poisson's ratio.* Polymer, 1992. **33**(20): p. 4435-4438.

101. Alderson, K. and K. Evans, *Strain-dependent behaviors of microporous polyethylene with a negative Poisson's ratio.* Journal of materials science, 1993. **28**(15): p. 4092-4098.

102. Alderson, K., et al., *Novel fabrication route for auxetic polyethylene. Part 1. Processing and microstructure.* Polymer Engineering & Science, 2005. **45**(4): p. 568-578.

103. Webber, R., K. Alderson, and K. Evans, *A novel fabrication route for auxetic polyethylene, part 2: mechanical properties.* Polymer engineering and science, 2008. **48**(7): p. 1351.

104. Alderson, K.L. and V.R. Simkins, *Auxetic filamentary materials*. U.S. Patent No 7,247,265, 2007.

105. Howell, B., P. Prendergast, and L. Hansen, *Examination of acoustic behaviors of negative poisson's ratio materials.* Applied Acoustics, 1994. **43**(2): p. 141-148.

106. Lakes, R.S. and K. Elms, *Indentability of conventional and negative Poisson's ratio foams.* Journal of Composite Materials, 1993. **27**(12): p. 1193-1202.

107. Sanami, M., et al., *Auxetic Materials for Sports Applications.* Procedia Engineering, 2014. **72**: p. 453-458.

108. Evans, K.E. and A. Alderson, *Auxetic materials: Functional materials and structures from lateral thinking!* Advanced Materials, 2000. **12**(9): p. 617-+.

109. Milton, G.W., *Composite material with Possion's ratio close to -1.* Journal of the Mechanics and Physics of Solids, 1992. **40**(5): p. 1105-1137.

110. Wei, G. and S. Edwards, *Auxeticity windows for composites.* Physica A: Statistical mechanics and its Applications, 1998. **258**(1): p. 5-10.

111. Hou, X., H. Hu, and V. Silberschmidt, *A novel concept to develop composite structures with isotropic negative Poisson's ratio: effects of random inclusions.* Composites Science and Technology, 2012. **72**(15): p. 1848-1854.

112. Alderson, K.L., et al., *Auxetic polypropylene fibers Part 1 - Manufacture and characterisation.* Plastics Rubber and Composites, 2002. **31**(8): p. 344-349.

113. Simkins, V.R., et al., *Single fiber pullout tests on auxetic polymeric fibers.* Journal of Materials Science, 2005. **40**(16): p. 4355-4364.

114. Alderson, K.L. and V.R. Simkins, *Auxetic materials*. 2005, Google Patents.

115. Ravirala, N., et al., *Negative Poisson's ratio polyester fibers.* Textile Research Journal, 2006. **76**(7): p. 540-546.

116. Alderson, A. and K. Alderson, *Expanding materials and applications: exploiting auxetic textiles.* Technical textiles international, 2005. **777**: p. 29-34.

117. Ravirala, N., et al., *Expanding the range of auxetic polymeric products using a novel melt-spinning route.* physica status solidi (b), 2005. **242**(3): p. 653-664.

118. Miller, W., et al., *A negative Poisson's ratio carbon fiber composite using a negative Poisson's ratio yarn reinforcement.* Composites Science and Technology, 2012. **72**(7): p. 761-766.

119. Sloan, M.R., J.R. Wright, and K.E. Evans, *The helical auxetic yarn – A novel structure for composites and textiles geometry, manufacture and mechanical properties.* Mechanics of Materials, 2011. **43**(9): p. 476-486.

120. Bhattacharya, S., et al., *The variation in Poisson's ratio caused by interactions between core and wrap in helical composite auxetic yarns.* Composites Science and Technology, 2014. **102**: p. 87-93.

121. Ge, Z., H. Hu, and S. Liu, *A novel plied yarn structure with negative Poisson's ratio.* The Journal of The Textile Institute, 2015. **107**(5): p. 578-588.

122. Hine, P., R. Duckett, and I. Ward, *Negative Poisson's ratios in angle-ply laminates.* Journal of materials science letters, 1997. **16**(7): p. 541-544.

123. Al-Khalil, M.F.S., *Strength of Filament Wound Structures under Complex Stresses*. 1990, University of Manchester.

124. Jayanty, S., J. Crowe, and L. Berhan, *Auxetic fiber networks and their composites.* Physica Status Solidi B-Basic Solid State Physics, 2011. **248**(1): p. 73-81.

125. MIKI, M. and Y. MUROTSU, *The peculiar behaviors of the Poisson's ratio of laminated fibrous composites.* JSME international journal. Ser. 1, Solid mechanics, strength of materials, 1989. **32**(1): p. 67-72.

126. Donoghue, J.P., *Negative Poisson's ration effects on the mechanical performance*

of composite laminates. 1995, PhD Thesis. University of Liverpool.

127. Jiang, L. and H. Hu, *Low-velocity impact response of multilayer orthogonal structural composite with auxetic effect.* Composite Structures, 2016.

128. Ko, F.K., *Three-dimensional fabrics for composites.* Elsevier Science Publishers, Textile Structural Composites, 1989: p. 129-171.

129. Mouritz, A., et al., *Review of applications for advanced three-dimensional fiber textile composites.* Composites Part A: applied science and manufacturing, 1999. **30**(12): p. 1445-1461.

130. Hu, H., et al., *Mechanical properties of composite materials made of 3D stitched woven-knitted preforms.* Journal of Composite Materials, 2010. **44**(14): p. 1753-1767.

131. Liu, Q., *Literature review: materials with negative Poisson's ratios and potential applications to aerospace and defence*. 2006, DTIC Document. No. DSTO-GD-0472.

132. Chan, N. and K.E. Evans, *The mechanical properties of conventional and auxetic foams. part I compression and tensile.* Journal of Cellular Plastics, 1999. **35**.

133. Chan, N. and K.E. Evans, *The mechanical properties of conventional and auxetic foams. part II shear.* Journal of Cellular Plastics, 1999. **35**.

134. Wei, Y., et al., *Review on auxetic material.* Journal of Materials Science, 2004. **39**: p. 3269-3279.

135. Evans, K.E., *Tailoring a negative Poisson's ratio.* Chem. Ind., 1990: p. 654.

136. Choi, J.B. and R.S. Lakes, *Fracture toughness of re-entrant foam materials with a negative Poisson's ratio: Experiment and analysis.* International Journal of Fracture, 1996. **80**(1): p. 73-83.

137. Scarpa, F., *Auxetic materials for bioprostheses.* IEEE Signal Processing Magazine, 2008. **25**(5): p. 125-126.

138. Scarpa, F., W.A. Bullough, and P. Lumley, *Trends in acoustic properties of iron particle seeded auxetic polyurethane foam.* Proceedings of the Institution of Mechanical Engineers Part C-Journal of Mechanical Engineering Science, 2004. **218**(2): p. 241-244.

139. Richardson, M. and M. Wisheart, *Review of low-velocity impact properties of composite materials.* Composites Part A: Applied Science and Manufacturing, 1996. **27**(12): p. 1123-1131.

140. Atas, C., et al., *An experimental investigation on the low velocity impact response of composite plates repaired by VARIM and hand lay-up processes.* Composite Structures, 2011. **93**(3): p. 1178-1186.

141. Alderson, K., et al., *Auxetic warp knit textile structures.* Physica Status Solidi B-Basic Solid State Physics, 2012. **249**(7): p. 1322-1329.

142. Hu, H. and Z.K. Zhang, *A 3D auxetic fabric manufacturing device and method*, S.I.P.O.o. China, Editor. 2015. Chinese invention. patent, no. 20120192738.3

143. Hook, P., *Uses of auxetic fibers*. 2011, Auxetic Limited, Devon: U.S.

144. A., G., *Pyrolytic materials for thermal protection systems.* Aerospace Engineering, 1963. **22**(1): p. 126-137.

145. Nakamura, M., *Fundamental Properties of Intermetallic Compounds.* Mrs Bulletin, 1995. **20**(8): p. 33-39.

146. Baker, C.E., *Auxetic spinal implants: consideration of negative Poisson's ratio in the design of an artificial intervertebral disc*, 2011. PhD Thesis. *University of Toledo*.

147. Burriesci, G. and G. Bergamasco, *Annuloplasty prosthesis with an auxetic structure*. 2011: US Patent. U.S. Patent No 8,034,103, 2011.

148. Zhou, L., L. Jiang, and H. Hu, *Auxetic composites made of 3D textile structure and polyurethane foam.* physica status solidi (b), 2016: p. 1-11.

149. Zhang, D., et al., *A comparative study on low-velocity impact response of fabric composite laminates.* Materials & Design, 2013. **50**: p. 750-756.